Journal of Mathematical Biology (2026) 92:42
https://doi.org/10.1007/s00285-026-02360-y

Mathematical Biology

Spatiotemporal cholera dynamics with antibiotic resistance and vaccination via demographic-epidemic data in Zimbabwe

Peng Wu[1] · Shuai Zhang[1] · Xiunan Wang[2] · Hao Wang[3]

Received: 1 June 2025 / Revised: 28 January 2026 / Accepted: 29 January 2026

Abstract

The diffusion of cholera epidemics and the emergence of drug-resistant strains pose significant challenges to cholera control and treatment, emphasizing the need for more effective interventions. By establishing a reaction-diffusion model of cholera with vaccination and two strains (wild and drug-resistant), we study the spatiotemporal dynamics of cholera transmission in this paper. In a spatially heterogeneous case, we derive R_0 and establish a threshold result: the disease-free steady state is globally stable if $R_0 < 1$, and the disease persists if $R_0 > 1$. In addition, we prove the global stability of the endemic equilibrium by constructing a Lyapunov functional in a spatially homogeneous case. Our model is successfully validated by the cholera data in Zimbabwe via Markov Chain Monte Carlo (MCMC). Using COMSOL Multiphysics software, we display the spatial transmission of cholera in the two-dimensional geographic map via demographic data in Zimbabwe. This offers a novel perspective for investigating the spatiotemporal dynamics of cholera transmission. Our findings indicate that restricted local population diffusion may contribute to the persistence and localized transmission of cholera in certain regions of Zimbabwe. Simulations fur-

Peng Wu and Shuai Zhang contributed equally to this work.

✉ Hao Wang
hao8@ualberta.ca

Peng Wu
pengwu89@hdu.edu.cn

Shuai Zhang
13230350410@163.com

Xiunan Wang
xiunan-wang@utc.edu

[1] School of Sciences, Hangzhou Dianzi University, Hangzhou 310018, China

[2] Department of Mathematics, University of Tennessee at Chattanooga, Chattanooga TN 37403, USA

[3] Department of Mathematical and Statistical Science, University of Alberta, Edmonton AB T6G 2G1, Canada

Published online: 02 March 2026

ther indicate that vaccination can serve as an effective intervention under such spatial dynamics.

Keywords Cholera · reaction-diffusion model · spatiotemporal dynamics · Markov Chain Monte Carlo (MCMC) · demographic-epidemic data

Mathematics Subject Classification 92D30 · 35A01 · 65M60

1 Introduction

Cholera, a highly infectious disease caused by the *Vibrio cholerae*, poses a significant threat to global health, particularly in areas with inadequate hygiene and limited access to clean water. If treatment is not timely, cholera can rapidly progress to life-threatening acute secretory diarrhea, resulting in extremely high mortality rates Wang and Wang (2019); Faruque et al. (1998). Since the first recorded epidemic in 1817 Harris et al. (2010), cholera has caused widespread suffering and loss of life. The ongoing seventh pandemic, which began in 1961, continues to fuel outbreaks worldwide, with an estimated 2.86 million infections and 95,000 deaths annually. Tragically, approximately 1.3 billion people are still exposed to the risk of being infected Sampath et al. (2021). In recent years, we have witnessed a resurgence of cholera pandemics, underscoring the urgent need for effective control measures. The 2008-2009 Zimbabwe outbreak saw nearly 100,000 reported cases Mukandavire et al. (2011), while Haiti experienced a devastating epidemic from 2010-2012, with nearly 545,000 reported infections Tuite et al. (2011). Furthermore, Yemen grappled with an outbreak in 2017-2018, reporting 1,115,378 cases and 2,310 deaths Carfora and Torcicollo (2022). Currently, the combination of antibiotics and rehydration therapy is an effective method for reducing the severity of cholera. However, this strategy also fuels the rise of drug resistance, presenting a significant obstacle to cholera control efforts Chatterjee et al. (2020). The majority of clinical isolates of *Vibrio cholerae* exhibit resistance to most routinely used antibiotics Tuite et al. (2019). *Vibrio cholerae* expresses membrane-integrated protein complexes, such as the RND family efflux pump systems, which actively export antibiotics out of the cell, reducing intracellular drug concentrations and thereby preventing antibiotic-induced damage Kunkle et al. (2017). This molecular mechanism enables the bacteria to survive antibiotic exposure. Meanwhile, the widespread use of antibiotics creates selective pressure that promotes the survival and spread of resistant strains, accelerating the evolution of antibiotic resistance. This alarming trend necessitates the exploration of alternative strategies, such as vaccines, to restrict the transmission of cholera and mitigate the dangerous rise of drug resistance Chatterjee et al. (2020). However, oral vaccines have shown reduced immunogenicity in certain individuals, possibly due to the need to overcome natural mucosal barriers that hinder effective antigen stimulation and immune activation. Studies indicate that factors such as malnutrition, micronutrient deficiencies, microbial imbalance, and structural or functional damage to the mucosa may impair mucosal immunity, leading to weaker responses to oral vaccines and reduced protective efficacy Qadri et al. (2013).

Mathematical modeling has been extensively used to study disease transmission dynamics. Capasso and Paveri-Fontana (1979) proposed the first model for a cholera outbreak along the Mediterranean coast, later expanded upon by Codeço (2001) to incorporate a class of susceptible individuals and posit water as the sole transmission route. Joh et al. (2009) and Kong et al. (2014) formulated and analyzed an iSIR model for indirectly transmitted infectious diseases with an immunological threshold. They studied the dynamics of the diseases caused by pathogenic microorganisms such as bacteria, viruses, and parasites. Their works suggest that it might be better to focus on bacterial control in the reservoir rather than on human behaviors and infrastructure. Luo et al. (2017) presented a cholera model to investigate the seasonal forcing and exponential threshold incidence in cholera dynamics. Li et al. (2023) proposed an age-structured dengue transmission model that accounts for both symptomatic and asymptomatic infections. Brauer et al. (2013) developed a PDE cholera model linking the infection age of individuals with the biological age of the pathogen. Under vaccination conditions, Cai et al. (2020) proposed a cholera model incorporating vaccination age and focused on investigating its impact. However, spatial heterogeneity is a non-negligible aspect of epidemiological modeling. Shu et al. (2021) introduced a nonlocal time-delayed cholera model within a spatially heterogeneous environment. Wang et al. (2016) proposed a reaction-convection-diffusion model showing that diffusion and convection have a significant impact on the transmission of cholera. Wang and Wu (2023) proposed a reaction-diffusion model with space-dependent parameters and bacterial hyperinfectivity, indicating that restricting the movement of susceptible individuals can lead to the mitigation of cholera epidemics, while disregarding hyperinfectivity will result in an underestimation of infection risks. Wang et al. (2024) formulated a generalized cholera model with nonlocal time delay to study the impact of bacterial hyperinfectivity on cholera epidemics in a spatially heterogeneous environment.

In this paper, we establish a reaction-diffusion model of cholera with vaccination and two strains to study the comprehensive impact of spatial heterogeneity, two strains, and vaccination on cholera transmission via available data from Zimbabwe. Furthermore, we use COMSOL Multiphysics software to visualize the spatiotemporal transmission via demographic data in Zimbabwe. The remainder of this paper is structured as follows: Section 2 establishes the reaction-diffusion model of cholera. In Section 3, we derive the basic reproduction number R_0 and prove its role as a threshold for disease persistence or extinction. In Section 4, we prove the endemic equilibrium is globally asymptotically stable in a homogeneous case. Numerical simulations are conducted based on real cholera data from Zimbabwe in Section 5. Finally, Section 6 provides a summary.

2 Model formulation

In order to study the spatiotemporal transmission of cholera, we establish a reaction-diffusion model based on the biological characteristics of the disease, incorporating spatial heterogeneity, two strains, and vaccination.

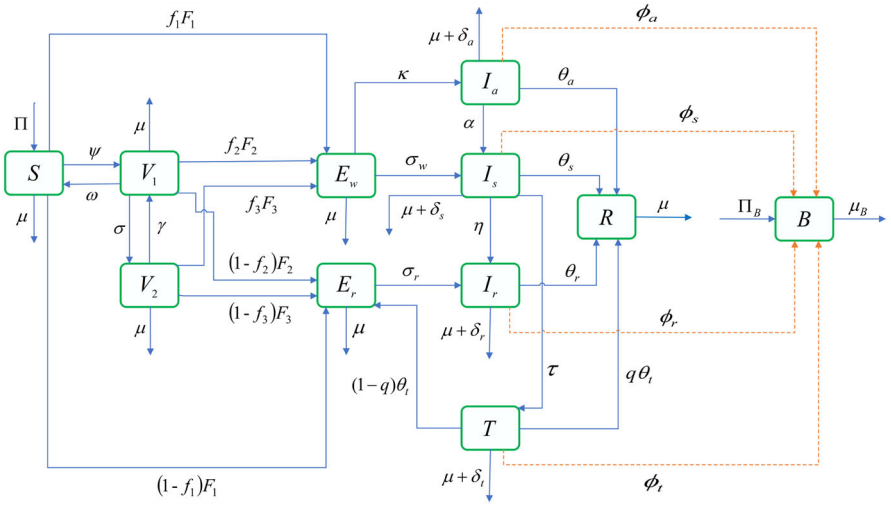

Fig. 1 Schematic diagram of the transmission of cholera.

All compartments in the model are defined as distribution functions dependent on both time t and spatial location x. Drawing upon the compartmental classification method from Safi et al. (2013), we organize the model variables as follows: susceptible individuals, consisting of unvaccinated individuals $S(t,x)$ and vaccinated individuals, who are further divided into those who have received the first dose $V_1(t,x)$ and those who have completed the full two-dose regimen $V_2(t,x)$. This classification follows the vaccination schedule as reported in United Nations Children's Fund (2024). After individuals are infected with *Vibrio cholerae*, they enter an incubation period, during which clinical symptoms have not yet appeared and the pathogen has not yet begun to be released into the environment. Based on this biological characteristic, we call such individuals exposed individuals, which are divided into two categories: $E_w(t,x)$ for those exposed to the wild strain, and $E_r(t,x)$ for those exposed to the drug-resistant strain. Following exposure, the infection progresses, and individuals start shedding *Vibrio cholerae*. We call individuals who can shed *Vibrio cholerae* bacteria-shedding individuals. These individuals include asymptomatic individuals $I_a(t,x)$, symptomatic individuals with the wild strain $I_s(t,x)$, and symptomatic individuals with the drug-resistant strain $I_r(t,x)$. Treated individuals $T(t,x)$ also continue to shed bacteria. Recovered individuals are denoted by $R(t,x)$, while the concentration of *Vibrio cholerae* in the environment is represented by $B(t,x)$.

We begin our presentation of the cholera model with a schematic diagram (see Fig. 1) that outlines the model structure and compartment interactions. Subsequently, we present a detailed description of the model, grounded in the biological characteristics and transmission of cholera.

(1) **Susceptible individuals**: In the model, $S(t,x)$ are fully susceptible to cholera. After receiving the first dose of vaccine, they transition to $V_1(t,x)$ at a rate $\psi(x)$, with reduced susceptibility quantified by $r_1(x)$. At a rate $\sigma(x)$, the second dose of

vaccine moves individuals from $V_1(t,x)$ to $V_2(t,x)$, with further reduced susceptibility quantified by $r_2(x)$. Vaccines do not provide lifelong immunity, and the immunity they induce will expire: individuals in $V_2(t,x)$ return to $V_1(t,x)$ at a rate $\gamma(x)$, and those in $V_1(t,x)$ return to $S(t,x)$ at a rate $\omega(x)$. This mechanism describes the stepwise acquisition and gradual loss of vaccine-induced immunity.

Cholera is mainly transmitted through ingestion of water or food contaminated with *Vibrio cholerae*, and direct person-to-person transmission is rare. Therefore, we assume that infection occurs entirely through contact with the environmental bacterial concentration $B(t,x)$. The force of infection is formulated using general incidence functions: $F_1(x, S(t,x), B(t,x))$, $F_2(x, V_1(t,x), B(t,x))$, $F_3(x, V_2(t,x), B(t,x))$. The model also includes $\Pi(x)$ and $\mu(x)$, which represent the birth or new individual input of unvaccinated individuals $S(t,x)$, and the natural mortality rate, respectively.

(2) **Exposed individuals**: Unvaccinated individuals $S(t,x)$, along with vaccinated individuals $V_1(t,x)$ and $V_2(t,x)$, come into contact with the environmental pathogen concentration $B(t,x)$ and become infected with the wild strain, entering $E_w(t,x)$ at rates proportional to $f_1(x)$, $f_2(x)$, and $f_3(x)$, respectively. Conversely, they become infected with the drug-resistant strain and enter $E_r(t,x)$ at rates $1-f_1(x)$, $1-f_2(x)$, and $1-f_3(x)$, respectively. Individuals in $E_w(t,x)$ subsequently progress either to the asymptomatic individuals $I_a(t,x)$ at a rate $\kappa(x)$, or to the symptomatic individuals with the wild strain $I_s(t,x)$ at a rate $\sigma_w(x)$. In addition to new infections, $E_r(t,x)$ also receives individuals from $T(t,x)$. Treated individuals $T(t,x)$ recover at a rate $\theta_t(x)$, with a proportion $q(x)$ successfully recovering, while the remaining proportion $1-q(x)$, representing those who fail to recover, transition to $E_r(t,x)$ at a rate $(1-q(x))\theta_t(x)$. Individuals in $E_r(t,x)$ eventually progress to the symptomatic individuals with the drug-resistant strain $I_r(t,x)$ at a rate $\sigma_r(x)$. Neither $E_w(t,x)$ nor $E_r(t,x)$ includes disease-induced mortality; death only occurs due to natural mortality at a rate $\mu(x)$.

(3) **Bacteria-shedding individuals**: The asymptomatic individuals $I_a(t,x)$ progre ss from exposed individuals $E_w(t,x)$ at a rate $\kappa(x)$. Individuals in $I_a(t,x)$ naturally die at a rate $\mu(x)$ or die from disease at a rate $\delta_a(x)$. Additionally, $I_a(t,x)$ can recover naturally at a rate $\theta_a(x)$, or transition to symptomatic individuals with the wild strain $I_s(t,x)$ at a rate $\alpha(x)$. The increase in $I_s(t,x)$ also includes the progression of exposed individuals $E_w(t,x)$ at a rate $\sigma_w(x)$. $I_s(t,x)$ can become the treated individuals $T(t,x)$ at a rate $\tau(x)$ or transition to symptomatic individuals with the drug-resistant strain $I_r(t,x)$ at a rate $\eta(x)$. Moreover, symptomatic individuals with the wild strain can recover naturally at a rate $\theta_s(x)$, with natural mortality and disease-induced mortality rates of $\mu(x)$ and $\delta_s(x)$, respectively. $I_r(t,x)$ mainly arise from two sources: first, from symptomatic individuals with the wild strain $I_s(t,x)$ at a rate $\eta(x)$, and second, from drug-resistant exposed individuals $E_r(t,x)$ at a rate $\sigma_r(x)$, progressing to symptomatic individuals with the drug-resistant strain. These individuals can recover at a rate $\theta_r(x)$, or die from natural causes at a rate $\mu(x)$ or from cholera at a rate $\delta_r(x)$. Currently, infected individuals typically receive antibiotic therapy upon the manifestation of clinical symptoms Mandal et al. (2011). However, resistance to a broad range of antibiotics, including β-lactams, quinolones, aminoglycosides, tetracyclines, sulphamethoxazole-trimethoprim (SXT), polymyxins, and macrolides.

Tuite et al. (2019) indicates that individuals in $I_r(t,x)$ do not receive effective treatment. Individuals in $T(t,x)$ can become $E_r(t,x)$ due to treatment failure at a rate $(1-q(x))\theta_t(x)$. $T(t,x)$ can also successfully recover after treatment and become the recovered individuals $R(t,x)$ at a rate $q(x)\theta_t(x)$. Treated individuals also experience natural mortality at a rate $\mu(x)$ and disease-induced mortality at a rate $\delta_t(x)$.

(4) **Concentration of *Vibrio cholerae***: After the incubation period, individuals begin shedding *Vibrio cholerae* into the environment. In the model, the amount of bacteria shed is represented by $\phi_a(x)I_a(t,x)$, $\phi_s(x)I_s(t,x)$, $\phi_r(x)I_r(t,x)$, and $\phi_t(x)T(t,x)$, where $\phi_a(x)$, $\phi_s(x)$, $\phi_r(x)$, and $\phi_t(x)$ are the contribution rates. The environmental concentration of *Vibrio cholerae* increases through natural proliferation at a rate $\Pi_B(x)$ and decreases due to natural loss at a rate $\mu_B(x)$.

(5) **Recovered individuals**: Recovered individuals $R(t,x)$ are assumed to acquire complete immunity upon recovery and cannot be reinfected. Individuals enter the recovered class through natural recovery or treatment, represented by the terms $\theta_a(x)I_a(t,x)+\theta_s(x)I_s(t,x)+\theta_r(x)I_r(t,x)+q(x)\theta_t(x)T(t,x)$. The only outflow from this compartment is due to natural death at rate $\mu(x)$.

Cholera is a waterborne disease, with transmission influenced by both the spatial movement of individuals and the diffusion of *Vibrio cholerae* in aquatic environments, particularly through river systems. To capture this feature, we employ the diffusion term $\nabla\cdot(d(x)\nabla u)$, where $d(x)$ is a spatially varying diffusion coefficient.

Throughout the paper, we make the assumption as follows:

Assumption 2.1 **(P1)** All parameters of model (2.1) are spatially heterogeneous and positive.

(P2) $F_1(x,S(t,x),B(t,x))$, $F_2(x,V_1(t,x),B(t,x))$, and $F_3(x,V_2(t,x),B(t,x)) \in C^2(\Omega\times\mathbb{R}_+\times\mathbb{R}_+)$; $F_1(x,S(t,x),B(t,x))$, $F_2(x,V_1(t,x),B(t,x))$, and $F_3(x,V_2(t,x),B(t,x))$ are bounded as $B\to\infty$; $F_1(x,S(t,x),B(t,x))=0$, $F_2(x,V_1(t,x),B(t,x))=0$, and $F_3(x,V_2(t,x),B(t,x))=0$ if and only if $SB=0$, $V_1B=0$, and $V_2B=0$, respectively.

(P3) $\partial_B F_1(x,S(t,x),B(t,x))$, $\partial_B F_2(x,V_1(t,x),B(t,x))$, and $\partial_B F_3(x,V_2(t,x),B(t,x))$ are positive, if $SB>0$, $V_1B>0$, and $V_2B>0$, respectively; $\partial_B F_1(x,S(t,x),0)$, $\partial_B F_2(x,V_1(t,x),0)$, and $\partial_B F_3(x,V_2(t,x),0)$ are positive, if $S>0$, $V_1>0$, and $V_2>0$, respectively; $\partial_B F_1(x,S(t,x),B(t,x))\to 0$, $\partial_B F_2(x,V_1(t,x),B(t,x))\to 0$, and $\partial_B F_3(x,V_2(t,x),B(t,x))\to 0$ as $B\to\infty$.

(P4) $\partial_B^2 F_1(x,S(t,x),B(t,x))<0$, $\partial_B^2 F_2(x,V_1(t,x),B(t,x))<0$, and $\partial_B^2 F_3(x,V_2(t,x),B(t,x))<0$, if $SB\geq 0$, $V_1B\geq 0$, and $V_2B\geq 0$, respectively.

(P5) Following Safi et al. (2013); Song and Xu (2022), we assume that $\Pi_B(x)<\mu_B(x)$ throught this paper.

(P6) According to Safi et al. (2013); Song and Xu (2022), we assume that asymptomatic individuals infected with the drug-resistant strain are not considered in the model.

Assumption 2.1 (P2–P4) implies that the infection rate is zero only when either susceptible individuals or *Vibrio cholerae* are absent, underscoring the necessity of both for transmission. While the infection rate increases with bacterial concentration, this rise slows at higher levels due to limits like contact efficiency or uptake capacity.

Table 1 The biological meaning of parameters of model (2.1)

Parameters	Biological meaning	Parameters	Biological meaning
$\Pi(x)$	Recruitment rate of unvaccinated susceptibles	$\omega(x)$	First dose vaccine failure rate
$\gamma(x)$	Second dose vaccine failure rate	$\psi(x)$	First dose vaccination coverage rate
$\sigma(x)$	Second dose vaccination coverage rate	$r_1(x)$	Contact efficiency of V_1
$r_2(x)$	Contact efficiency of V_2	$f_1(x)$	Proportion of S newly infected with the wild strain
$f_2(x)$	Proportion of V_1 newly infected with the wild strain	$f_3(x)$	Proportion of V_2 newly infected with the wild strain
$q(x)$	Proportion of recovered treated individuals	$\kappa(x)$	Progression rate from E_w to I_a
$\alpha(x)$	Conversion rate from I_a to I_s	$\sigma_w(x)$	Progression rate from E_w to I_s
$\sigma_r(x)$	Progression rate from E_r to I_r	$\theta_a(x)$	Recovery rate of I_a
$\theta_s(x)$	Recovery rate of I_s	$\theta_r(x)$	Recovery rate of I_r
$\theta_t(x)$	Treatment progression rate	$\tau(x)$	Treatment rate of I_s
$\eta(x)$	Conversion rate from I_s to I_r	$\delta_a(x)$	Disease-induced death rate of I_a
$\delta_s(x)$	Disease-induced death rate of I_s	$\delta_r(x)$	Disease-induced death rate of I_r
$\delta_t(x)$	Disease-induced death rate of T	$\phi_a(x)$	Contribution rate of I_a to B
$\phi_s(x)$	Contribution rate of I_s to B	$\phi_r(x)$	Contribution rate of I_r to B
$\phi_t(x)$	Contribution rate of T to B	$\mu(x)$	Natural death rate of humans
$\mu_B(x)$	Rate of natural loss of B	$\Pi_B(x)$	Growth rate of B

Moreover, as bacterial concentration rises, the incremental infection rate increase per unit of bacteria diminishes, reflecting diminishing marginal effects.

Notation 2.2 Examples of infection functions satisfying Assumption 2.1 (P2-P4):

(1) $F_i(x, u(t,x), B(t,x)) = \beta_i(x)u(t,x)B(t,x)/(K_i(x) + B(t,x))$ (semi–saturated incidence function) Safi et al. (2013).

(2) $F_i(x, u(t,x), B(t,x)) = \beta_i(x)u(t,x)B(t,x)/\left[(1+k_{i1}(x)B(t,x)+k_{i2}(x)u(t,x))\right]$ (Beddington–DeAngelis functional response) Dubey et al. (2015).

(3) $F_i(x, u(t,x), B(t,x)) = \beta_i(x)u(t,x)B(t,x)/\left[(1+k_{i1}(x)B(t,x))(1+k_{i2}(x)u(t,x))\right]$ (Crowley–Martin functional response) Upadhyay et al. (2019).

According to the above discussion, the proposed model is formulated as follows:

$$
\begin{cases}
\dfrac{\partial S(t,x)}{\partial t} = \nabla\cdot(d_1(x)\nabla S(t,x)) + \Pi(x) + \omega(x)V_1(t,x) - F_1(x,S(t,x),B(t,x)) \\
\qquad\qquad - (\psi(x)+\mu(x))S(t,x), \\
\dfrac{\partial V_1(t,x)}{\partial t} = \nabla\cdot(d_2(x)\nabla V_1(t,x)) + \psi(x)S(t,x) + \gamma(x)V_2(t,x) \\
\qquad\qquad - r_1(x)F_2(x,V_1(t,x),B(t,x)) - (\omega(x)+\sigma(x)+\mu(x))V_1(t,x), \\
\dfrac{\partial V_2(t,x)}{\partial t} = \nabla\cdot(d_3(x)\nabla V_2(t,x)) + \sigma(x)V_1(t,x) - r_2(x)F_3(x,V_2(t,x),B(t,x)) \\
\qquad\qquad - (\gamma(x)+\mu(x))V_2(t,x), \\
\dfrac{\partial E_w(t,x)}{\partial t} = \nabla\cdot(d_4(x)\nabla E_w(t,x)) + f_1(x)F_1(x,S(t,x),B(t,x)) \\
\qquad\qquad + f_2(x)r_1(x)F_2(x,V_1(t,x),B(t,x)) + f_3(x)r_2(x)F_3(x,V_2(t,x),B(t,x)) \\
\qquad\qquad - (\kappa(x)+\sigma_w(x)+\mu(x))E_w(t,x), \\
\dfrac{\partial E_r(t,x)}{\partial t} = \nabla\cdot(d_5(x)\nabla E_r(t,x)) + (1-f_1(x))F_1(S(t,x),B(t,x)) \\
\qquad\qquad + (1-f_2(x))r_1(x)F_2(V_1(t,x),B(t,x)) + (1-f_3(x))r_2(x)F_3(V_2(t,x), \\
\qquad\qquad B(t,x)) + (1-q(x))\theta_t(x)T(t,x) - (\sigma_r(x)+\mu(x))E_r(t,x), \\
\dfrac{\partial I_a(t,x)}{\partial t} = \nabla\cdot(d_6(x)\nabla I_a(t,x)) + \kappa(x)E_w(t,x) - (\alpha(x)+\theta_a(x)+\mu(x)+\delta_a(x))I_a(t,x), \\
\dfrac{\partial I_s(t,x)}{\partial t} = \nabla\cdot(d_7(x)\nabla I_s(t,x)) + \sigma_w(x)E_w(t,x) + \alpha(x)I_a(t,x) \\
\qquad\qquad - (\eta(x)+\theta_s(x)+\tau(x)+\mu(x)+\delta_s(x))I_s(t,x), \\
\dfrac{\partial I_r(t,x)}{\partial t} = \nabla\cdot(d_8(x)\nabla I_r(t,x)) + \sigma_r(x)E_r(t,x) + \eta(x)I_s(t,x) \\
\qquad\qquad - (\theta_r(x)+\mu(x)+\delta_r(x))I_r(t,x), \\
\dfrac{\partial T(t,x)}{\partial t} = \nabla\cdot(d_9(x)\nabla T(t,x)) + \tau(x)I_s(t,x) - (\mu(x)+\theta_t(x)+\delta_t(x))T(t,x), \\
\dfrac{\partial B(t,x)}{\partial t} = \nabla\cdot(d_{10}(x)\nabla B(t,x)) + \phi_a(x)I_a(t,x) + \phi_s(x)I_s(t,x) + \phi_r(x)I_r(t,x) \\
\qquad\qquad + \phi_t(x)T(t,x) + \Pi_B(x)B(t,x) - \mu_B(x)B(t,x), \\
\dfrac{\partial R(t,x)}{\partial t} = \nabla\cdot(d_{11}(x)\nabla R(t,x)) + \theta_a(x)I_a(t,x) + \theta_s(x)I_s(t,x) + \theta_r(x)I_r(t,x) \\
\qquad\qquad + q(x)\theta_t(x)T(t,x) - \mu(x)R(t,x),
\end{cases}
\tag{2.1}
$$

for $(t, x) \in (0, +\infty) \times \Omega$, where Ω is a bounded domain of $\mathbb{R}^n$ ($n \in \mathbb{Z}^+$) and $\partial\Omega$ is the smooth boundary of Ω. ∇ is the gradient operator. $d_i(x)$ is the diffusion rate related to location x, $i = 1, 2, \ldots, 11$. The biological meaning of the parameters of model (2.1) are given in Table 1. The initial and boundary conditions of model (2.1) are as follows:

$$\begin{cases} S(0,x) = S^0(x) \geq 0, V_1(0,x) = V_1^0(x) \geq 0, V_2(0,x) = V_2^0(x) \geq 0, \\ E_w(0,x) = E_w^0(x) \geq 0, E_r(0,x) = E_r^0(x) \geq 0, I_a(0,x) = I_a^0(x) \geq 0, \\ I_s(0,x) = I_s^0(x) \geq 0, I_r(0,x) = I_r^0(x) \geq 0, T(0,x) = T^0(x) \geq 0, \\ B(0,x) = B^0(x) \geq 0, R(0,x) = R^0(x) \geq 0, x \in \Omega, \\ \dfrac{\partial S(t,x)}{\partial \nu} = \dfrac{\partial V_1(t,x)}{\partial \nu} = \dfrac{\partial V_2(t,x)}{\partial \nu} = \dfrac{\partial E_w(t,x)}{\partial \nu} = \dfrac{\partial E_r(t,x)}{\partial \nu} = \dfrac{\partial I_a(t,x)}{\partial \nu} \\ = \dfrac{\partial I_s(t,x)}{\partial \nu} = \dfrac{\partial I_r(t,x)}{\partial \nu} = \dfrac{\partial T(t,x)}{\partial \nu} = \dfrac{\partial B(t,x)}{\partial \nu} = \dfrac{\partial R(t,x)}{\partial \nu} = 0, t > 0, x \in \partial\Omega, \end{cases} \tag{2.2}$$

where $S^0(\cdot) := S(0,\cdot)$, $V_1^0(\cdot) := V_1(0,\cdot)$, $V_2^0(\cdot) := V_2(0,\cdot)$, $E_w^0(\cdot) := E_w(0,\cdot)$, $E_r^0(\cdot) := E_r(0,\cdot)$, $I_a^0(\cdot) := I_a(0,\cdot)$, $I_s^0(\cdot) := I_s(0,\cdot)$, $I_r^0(\cdot) := I_r(0,\cdot)$, $T^0(\cdot) := T(0,\cdot)$, $B^0(\cdot) := B(0,\cdot)$, and $R^0(\cdot) := R(0,\cdot)$ are the smooth and non-zero functions, and ν is the outward unit normal vector on the boundary $\partial\Omega$.

Since $R(t, x)$ has no outgoing transitions to other compartments, it is decoupled from the system and omitted from the following parts. We have carried out a standard well-posedness analysis for model (2.1), rigorously establishing the global existence and uniqueness of solutions under biologically reasonable assumptions. The complete proof is provided in Appendix A.

3 The basic reproduction number

The basic reproduction number R_0 quantifies the average number of secondary infections generated by a single infected individual in a fully susceptible population. According to Ren et al. (2018), we derive the basic reproduction number R_0 using the next-generation operator method by linearizing the system at the disease-free steady state and considering only the compartments directly involved in infection and transmission. The spectral radius of the resulting next-generation operator defines R_0, which acts as a threshold for the transmission of the disease.

Model (2.1) admits a unique disease-free steady state denoted by $E_0 = (S_0(x), V_{10}(x), V_{20}(x), 0, 0, 0, 0, 0, 0, 0)$. By linearizing system (2.1) at E_0 and restricting attention to infection-related compartments, we obtain the following linearized system for infection dynamics:

$$
\begin{cases}
P_{4t} =\nabla\cdot(d_4(x)\nabla P_{4t}) + f_1(x)\dfrac{\partial F_1}{\partial B}(x, S_0, 0)P_{10} + f_2(x)r_1(x)\dfrac{\partial F_2}{\partial B}(x, V_{10}, 0)P_{10} \\
\qquad + f_3(x)r_2(x)\dfrac{\partial F_3}{\partial B}(x, V_{20}, 0)P_{10} - (\kappa(x)+\sigma_w(x)+\mu(x))P_4, \\
P_{5t} =\nabla\cdot(d_5(x)\nabla P_{5t}) + (1-f_1(x))\dfrac{\partial F_1}{\partial B}(x, S_0, 0)P_{10} \\
\qquad + (1-f_2(x))r_1(x)\dfrac{\partial F_2}{\partial B}(x, V_{10}, 0)P_{10} + (1-f_3(x))r_2(x)\dfrac{\partial F_3}{\partial B}(x, V_{20}, 0)P_{10} \\
\qquad + (1-q(x))\theta_t(x)P_9 - (\sigma_r(x)+\mu(x))P_5 \\
P_{6t} =\nabla\cdot(d_6(x)\nabla P_{6t}) + \kappa(x)P_4 - (\alpha(x)+\theta_a(x)+\mu(x)+\delta_a(x))P_6, \\
P_{7t} =\nabla\cdot(d_7(x)\nabla P_{7t}) + \sigma_w(x)P_4 + \alpha(x)P_6 - (\eta(x)+\theta_s(x)+\tau(x)+\mu(x)+\delta_s(x))P_7, \\
P_{8t} =\nabla\cdot(d_8(x)\nabla P_{8t}) + \sigma_r(x)P_5 + \eta(x)P_7 - (\theta_r(x)+\mu(x)+\delta_r(x))P_8, \\
P_{9t} =\nabla\cdot(d_9(x)\nabla P_{9t}) + \tau(x)P_7 - (\mu(x)+\theta_t(x)+\delta_t(x))P_9, \\
P_{10t} =\nabla\cdot(d_{10}(x)\nabla P_{10t}) + \phi_a(x)P_6 + \phi_s(x)P_7 + \phi_r(x)P_8 + \phi_t(x)P_9 + \Pi_B(x)P_{10} \\
\qquad - \mu_B(x)P_{10},
\end{cases}
\tag{3.1}
$$

for $t > 0, x \in \Omega$, and $\frac{\partial P_i}{\partial \nu} = 0, t > 0, x \in \partial\Omega$, for $i = 4, 5, \ldots, 10$.

Let $(P_4, P_5, \ldots, P_{11}) = e^{\lambda t}(\psi_4(x), \psi_5(x), \ldots, \psi_{10}(x))$. Then, model (3.1) can be rewritten as

$$
\begin{cases}
\lambda\psi_4 =\nabla\cdot(d_4(x)\nabla\psi_4) + f_1(x)\dfrac{\partial F_1}{\partial B}(x, S_0, 0)\psi_{10} + f_2(x)r_1(x)\dfrac{\partial F_2}{\partial B}(x, V_{10}, 0)\psi_{10} \\
\qquad + f_3(x)r_2(x)\dfrac{\partial F_3}{\partial B}(x, V_{20}, 0)\psi_{10} - (\kappa(x)+\sigma_w(x)+\mu(x))\psi_4, \\
\lambda\psi_5 =\nabla\cdot(d_5(x)\nabla\psi_5) + (1-f_1(x))\dfrac{\partial F_1}{\partial B}(x, S_0, 0)\psi_{10} \\
\qquad + (1-f_2(x))r_1(x)\dfrac{\partial F_2}{\partial B}(x, V_{10}, 0)\psi_{10} + (1-f_3(x))r_2(x)\dfrac{\partial F_3}{\partial B}(x, V_{20}, 0)\psi_{10} \\
\qquad + (1-q(x))\theta_t(x)\psi_9 - (\sigma_r(x)+\mu(x))\psi_5, \\
\lambda\psi_6 =\nabla\cdot(d_6(x)\nabla\psi_6) + \kappa(x)\psi_4 - (\alpha(x)+\theta_a(x)+\mu(x)+\delta_a(x))\psi_6, \\
\lambda\psi_7 =\nabla\cdot(d_7(x)\nabla\psi_7) + \sigma_w(x)\psi_4 + \alpha(x)\psi_6 - (\eta(x)+\theta_s(x)+\tau(x)+\mu(x)+\delta_s(x))\psi_7, \\
\lambda\psi_8 =\nabla\cdot(d_8(x)\nabla\psi_8) + \sigma_r(x)\psi_5 + \eta(x)\psi_7 - (\theta_r(x)+\mu(x)+\delta_r(x))\psi_8, \\
\lambda\psi_9 =\nabla\cdot(d_9(x)\nabla\psi_9) + \tau(x)\psi_7 - (\mu(x)+\theta_t(x)+\delta_t(x))\psi_9, \\
\lambda\psi_{10} =\nabla\cdot(d_{10}(x)\nabla\psi_{10}) + \phi_a(x)\psi_6 + \phi_s(x)\psi_7 + \phi_r(x)\psi_8 + \phi_t(x)\psi_9 + \Pi_B(x)\psi_{10} \\
\qquad - \mu_B(x)\psi_{10},
\end{cases}
\tag{3.2}
$$

for $x \in \Omega$, and $\frac{\partial \psi_i}{\partial \nu} = 0, x \in \partial\Omega$, for $i = 4, 5, \ldots, 10$, which is a cooperation system. According to Krein-Rutman theorem, we can assert that model (3.2) admits a

unique principal eigenvalue, denoted as λ_0, associated with a strictly positive eigenfunction $(\phi_4(x), \phi_5(x), \ldots, \phi_{10}(x))$. We introduce $\Psi(t) : C(\overline{\Omega}, \mathbb{R}^7) \to C(\overline{\Omega}, \mathbb{R}^7)$ as the solution semigroup generated by the following model:

$$\begin{cases} P_{4t} = \nabla \cdot (d_4(x)\nabla P_{4t}) - (\kappa(x) + \sigma_w(x) + \mu(x))P_4, \\ P_{5t} = \nabla \cdot (d_5(x)\nabla P_{5t}) + (1 - q(x))\theta_t(x)P_9 - (\sigma_r(x) + \mu(x))P_5, \\ P_{6t} = \nabla \cdot (d_6(x)\nabla P_{6t}) + \kappa(x)P_4 - (\alpha(x) + \theta_a(x) + \mu(x) + \delta_a(x))P_6, \\ P_{7t} = \nabla \cdot (d_7(x)\nabla P_{7t}) + \sigma_w(x)P_4 + \alpha(x)P_6 - (\eta(x) + \theta_s(x) + \tau(x) + \mu(x) + \delta_s(x))P_7, \\ P_{8t} = \nabla \cdot (d_8(x)\nabla P_{8t}) + \sigma_r(x)P_5 + \eta(x)P_7 - (\theta_r(x) + \mu(x) + \delta_r(x))P_8, \\ P_{9t} = \nabla \cdot (d_9(x)\nabla P_{9t}) + \tau(x)P_7 - (\mu(x) + \theta_t(x) + \delta_t(x))P_9, \\ P_{10t} = \nabla \cdot (d_{10}(x)\nabla P_{10t}) + \phi_a(x)P_6 + \phi_s(x)P_7 + \phi_r(x)P_8 + \phi_t(x)P_9 + \Pi_B(x)P_{10} \\ \qquad - \mu_B(x)P_{10}, \end{cases}$$

for $t > 0, x \in \Omega$, $\frac{\partial P_i}{\partial \nu} = 0, i = 4, 5, \ldots, 10, t > 0, x \in \partial\Omega$. Define

$$\mathcal{F}(x) = \begin{pmatrix} 0 & 0 & 0 & 0 & 0 & 0 & J_1(x) \\ 0 & 0 & 0 & 0 & 0 & 0 & J_2(x) \\ 0 & 0 & 0 & 0 & 0 & 0 & 0 \\ 0 & 0 & 0 & 0 & 0 & 0 & 0 \\ 0 & 0 & 0 & 0 & 0 & 0 & 0 \\ 0 & 0 & 0 & 0 & 0 & 0 & 0 \\ 0 & 0 & 0 & 0 & 0 & 0 & 0 \end{pmatrix},$$

where

$$\begin{aligned} J_1(x) =& f_1(x)\frac{\partial F_1}{\partial B}(x, S_0, 0) + f_2(x)r_1(x)\frac{\partial F_2}{\partial B}(x, V_{10}, 0) + f_3(x)r_2(x)\frac{\partial F_3}{\partial B}(x, V_{20}, 0), \\ J_2(x) =& (1 - f_1(x))\frac{\partial F_1}{\partial B}(x, S_0, 0) + (1 - f_2(x))r_1(x)\frac{\partial F_2}{\partial B}(x, V_{10}, 0) \\ &+ (1 - f_3(x))r_2(x)\frac{\partial F_3}{\partial B}(x, V_{20}, 0). \end{aligned}$$

Let $\psi = (\psi_4(x), \psi_5(x), \ldots, \psi_{10}(x))$ denote the spatial distribution of initial infections. As time evolves, $\Psi(t)\psi$ represents the spatiotemporal distribution of those infective numbers. Consequently, the cumulative distribution of new infections can be expressed as $\mathcal{L}(\psi)(x) = \int_0^\infty \mathcal{F}(x)\Psi(t)\psi\, dt$. According to the next generation operator, we derive the basic reproduction number, which is given by the spectral radius of $\mathcal{L}$, i.e., $R_0 = \rho(\mathcal{L})$. This leads to the following lemma:

Lemma 3.1 *The following statements hold:*

1. $R_0 - 1$ *and the principal eigenvalue* λ_0 *are of the same sign.*
2. *The disease-free steady state* E_0 *is locally asymptotically stable when* $R_0 < 1$.
3. *The disease-free steady state* E_0 *is unstable when* $R_0 > 1$.

Theorem 3.2 *When $R_0 < 1$, the disease-free steady state E_0 is globally asymptotically stable.*

Proof Detailed proof is provided in the Appendix B. □

Therefore, when the basic reproduction number $R_0 < 1$ and the disease-free steady state is globally asymptotically stable, it can be concluded that the disease cannot persist in the population and will ultimately fade away.

In the next step, we prove the uniform persistence of model (2.1) and subsequently show that an endemic steady state exists when $R_0 > 1$.

Theorem 3.3 *If $R_0 > 1$, there exists a constant $\delta_1 > 0$ such that the solution of model (2.1) satisfies the following inequality*

$$\lim_{t\to\infty} \|\Phi(t)u_0 - E_0\| > \delta_1, \tag{3.3}$$

which holds uniformly for all $x \in \overline{\Omega}$.

Proof Detailed proof is provided in the Appendix C. □

4 Threshold dynamics of a spatially homogeneous case

In this section, we focus on the stability analysis of the endemic steady state. Since analyzing stability in a fully heterogeneous environment poses considerable challenges, we consider a simplified scenario in which the model parameters are spatially homogeneous, while spatial heterogeneity is retained through the diffusion terms. We further assume that $f_1 = f_2 = f_3 = p$ and define

$$\begin{aligned}
\varrho_1(S) &= \lim_{B\to 0^+} \frac{F_1(S,B)}{B} = \frac{\partial F_1(S,0)}{\partial B},\\
\varrho_2(V_1) &= \lim_{B\to 0^+} \frac{F_2(V_1,B)}{B} = \frac{\partial F_2(V_1,0)}{\partial B},\\
\varrho_3(V_2) &= \lim_{B\to 0^+} \frac{F_3(V_2,B)}{B} = \frac{\partial F_3(V_2,0)}{\partial B}.
\end{aligned}$$

According to the definition of basic reproduction number in infectious disease models, we can deduce that

$$R_0 = \frac{A_1L_1 + A_2L_2}{k_1k_2k_3k_4k_5k_6k_7},$$

where

$$\begin{aligned}
&A_1 = p(\varrho_1 + r_1\varrho_2 + r_2\varrho_3),\ A_2 = (1-p)(\varrho_1 + r_1\varrho_2 + r_2\varrho_3),\\
&k_1 = \kappa + \sigma_w + \mu,\ k_2 = \sigma_r + \mu,\ k_3 = \mu_B - \Pi_B,\ k_4 = \alpha + \theta_a + \mu + \delta_a,\\
&k_5 = \eta + \theta_s + \tau + \mu + \delta_s,\ k_6 = \theta_r + \mu + \delta_r,\ k_7 = \mu + \theta_t + \delta_t,\\
&L_1 = k_2k_5k_6k_7\kappa\phi_a + [k_2k_7(k_6\phi_s + \eta\phi_r) + k_2k_6\tau\phi_t + \tau(1-q)\theta_t\phi_r\sigma_r](\kappa\alpha + k_4\sigma_w),
\end{aligned}$$

$L_2 = k_1 k_4 k_5 k_7 \phi_r \sigma_r$.

Theorem 4.1 *If $R_0 > 1$ and Assumption 2.1 (P2-P4) holds, model (2.1) admits an endemic equilibrium E_1 in the homogeneous case. Then E_1 is globally asymptotically stable in Δ and hence the endemic equilibrium is unique.*

Proof Detailed proof is provided in the Appendix D. □

5 Numerical simulations

To investigate the impact of vaccination, drug resistance, and spatial diffusion on the transmission of cholera in Zimbabwe, we conduct numerical simulations in this section to discuss the effects of these factors on the transmission of the disease. Our numerical simulations are mainly divided into two scenarios: 1) In the one-dimensional spatial scenario, based on the fitting results of Zimbabwe 2023 cholera data (without vaccination), we analyze the impact of model parameters on R_0, the evolutionary competition between the wild strain and the drug-resistant strain in the exposed infected population, the impact of different vaccination parameters on the transmission. In particular, we fit the cholera data in 2024 (with vaccination) and use it to evaluate the effects of vaccination. 2) In the two-dimensional spatial scenario, based on population density data and a two-dimensional map, combined with COMSOL Multiphysics software, we simulate the spatiotemporal transmission of cholera in real geographical space (2023 and 2024 in Zimbabwe), thereby more intuitively reflecting the spatiotemporal characteristics of cholera transmission in Zimbabwe.

The conclusion of this section can be summarized as follows:

P1. Intensifying the treatment of infected individuals with drugs in a short period can indeed control the spread of cholera, but the resulting drug resistance poses a potential risk. This can significantly reduce the effectiveness of existing drugs when cholera breaks out again and also increase the failure rate of existing vaccines.

P2. Combining data simulation with the actual cholera epidemic in Zimbabwe in 2024, the results show that vaccination is an effective way to control cholera outbreaks.

P3. The two-dimensional spatial simulation shows that cholera transmission in Zimbabwe occurs only in a few key areas and does not lead to a nationwide outbreak.

Next, we estimate the model parameters using real data from Zimbabwe, obtained from the World Health Organization World Health Organization (2024). We use a semi-saturated incidence function for the subsequent simulations, defined as $F(x, H(t,x), B(t,x)) = \frac{\beta(x)H(t,x)B(t,x)}{K_B(x)+B(t,x)}$, $H = S, V_1, V_2$, where $\beta(x)$ is the transmission rate and $K_B(x)$ is the semi-saturation constant. Incorporating spatial heterogeneity in the parameters would make parameter estimation extremely challenging due to the increased data requirements and computational complexity. Therefore, we assume all parameters are spatially uniform to simplify the fitting process. Furthermore, we make the rational assumptions that $\theta_a = \theta_s = \theta_r = \theta_t = \theta$, $\delta_a = \delta_s = \delta_r = \delta_t = \delta$, $\sigma_w = \sigma_r = l$, $f_1 = f_2 = f_3 = p$ and $\phi_a = \phi_s = \phi_r = \phi_t = \phi$ in model (2.1) Safi et al. (2013).

5.1 Parameter estimation based on cholera data from Zimbabwe

A cholera outbreak began in Zimbabwe in February 2023, and vaccination efforts were implemented in January 2024. For the unvaccinated scenario, we use cholera infection weekly cases data from weeks 20 to 52 of 2023 in Zimbabwe, whereas for the vaccinated scenario, we use data from weeks 1 to 24 of 2024 World Health Organization (2024).

5.1.1 Model parameter estimation without vaccination in Zimbabwe, 2023

We first fit the model to data from the 2023 cholera outbreak in Zimbabwe World Health Organization (2024), during which no vaccination was administered. Accordingly, we assume $V_1(t,x) = V_2(t,x) \equiv 0$ and set the related vaccination parameters $\psi = \sigma = \omega = \gamma \equiv 0$ in model (2.1). The reported data reflect total cholera cases at the national level, while our model accounts for both time and spatial location. To ensure consistency with the national case data, we integrate the spatial model equations over the entire domain Ω, so that the model describes the overall population and disease dynamics rather than local patterns. This allows for direct comparison with the national case data and facilitates parameter estimation. As a result of this integration, we derive the following equivalent system:

$$
\begin{cases}
\dfrac{d\int_\Omega S(t,x)\,dx}{dt} = \Pi - \dfrac{\beta \int_\Omega S(t,x)\,dx \int_\Omega B(t,x)\,dx}{K_B + \int_\Omega B(t,x)\,dx} - \mu \displaystyle\int_\Omega S(t,x)\,dx, \\
\dfrac{d\int_\Omega E_w(t,x)\,dx}{dt} = p\dfrac{\beta \int_\Omega S(t,x)\,dx \int_\Omega B(t,x)\,dx}{K_B + \int_\Omega B(t,x)\,dx} - (\kappa + l + \mu)\displaystyle\int_\Omega E_w(t,x)\,dx, \\
\dfrac{d\int_\Omega E_r(t,x)\,dx}{dt} = (1-p)\dfrac{\beta \int_\Omega S(t,x)\,dx \int_\Omega B(t,x)\,dx}{K_B + \int_\Omega B(t,x)\,dx} + (1-q)\theta \displaystyle\int_\Omega T(t,x)\,dx \\
\qquad\qquad - (l+\mu)\displaystyle\int_\Omega E_r(t,x)\,dx, \\
\dfrac{d\int_\Omega I_a(t,x)\,dx}{dt} = \kappa \displaystyle\int_\Omega E_w(t,x)\,dx - (\alpha + \theta + \mu + \delta)\int_\Omega I_a(t,x)\,dx, \\
\dfrac{d\int_\Omega I_s(t,x)\,dx}{dt} = l\displaystyle\int_\Omega E_w(t,x)\,dx + \alpha \int_\Omega I_a(t,x)\,dx - (\eta + \theta + \tau \\
\qquad\qquad + \mu + \delta)\displaystyle\int_\Omega I_s(t,x)\,dx, \\
\dfrac{d\int_\Omega I_r(t,x)\,dx}{dt} = l\displaystyle\int_\Omega E_r(t,x)\,dx + \eta \int_\Omega I_s(t,x)\,dx - (\theta + \mu + \delta)\int_\Omega I_r(t,x)\,dx, \\
\dfrac{d\int_\Omega T(t,x)\,dx}{dt} = \tau \displaystyle\int_\Omega I_s(t,x)\,dx - (\mu + \theta + \delta)\int_\Omega T(t,x)\,dx, \\
\dfrac{d\int_\Omega B(t,x)\,dx}{dt} = \phi \displaystyle\int_\Omega I_a(t,x) + I_s(t,x)dx + I_r(t,x)dx + T(t,x)\,dx \\
\qquad\qquad + (\Pi_B - \mu_B)\displaystyle\int_\Omega B(t,x)\,dx.
\end{cases}
\tag{5.1}
$$

Since the cholera outbreak in Zimbabwe was concentrated in specific regions, we assume the initial number of unvaccinated individuals is $S(0) = 2.3 \times 10^6$, which corresponds to the target of vaccinating 2.3 million people in the most affected districts

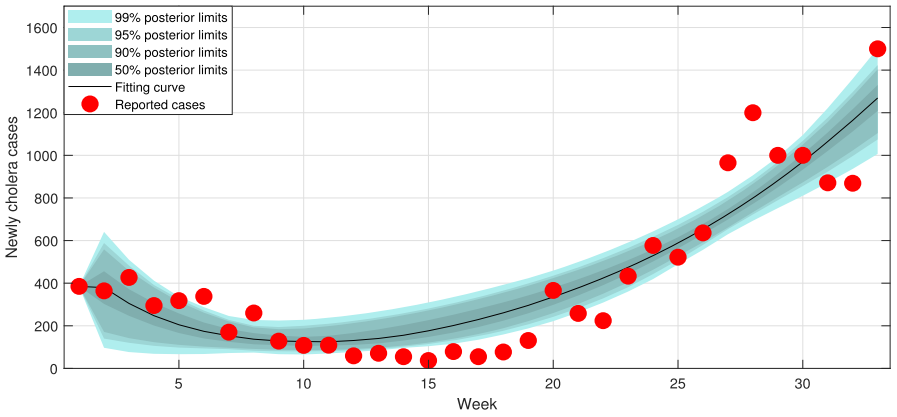

Fig. 2 The fitting curve of the newly cholera cases by model (5.1) in Zimbabwe, 2023.

United Nations Children's Fund (2024). The initial value $I_a(0) = 385$ corresponds to the number of reported cases at the beginning of the outbreak. We assume $I_s(0) = I_r(0) = T(0) = 0$, while the initial values of $E_w(0)$, $E_r(0)$, and $B(0)$ are to be estimated. According to Chitnis et al. (2008); Ilic and Ilic (2023), we assume $\Pi = 800$, $\mu = 0.001$, and $\delta = 0.02$. Based on the above-known parameter values, we fit model (5.1) to the weekly reported cases by Markov Chain Monte Carlo (MCMC). Figure 2 shows that the curve of model (5.1) fits the newly reported cases very well, and we obtain the estimated values of $\beta, K_B, p, q, \kappa, \alpha, l, \theta, \tau, \eta, \phi, \mu_B, \Pi_B, E_w(0), E_r(0)$ and $B(0)$, which are displayed in Figure 3. Their values are listed in Table 2, where **mean** represents the mean value of the estimated parameter value, **std** denotes the standard deviation, **MC_err** represents the error due to MCMC method, **tau** represents the delay acceptance time for MCMC method and **geweke** is an index to evaluate the quality of Markov Chains, the closer the index is to one, the better the Markov Chain.

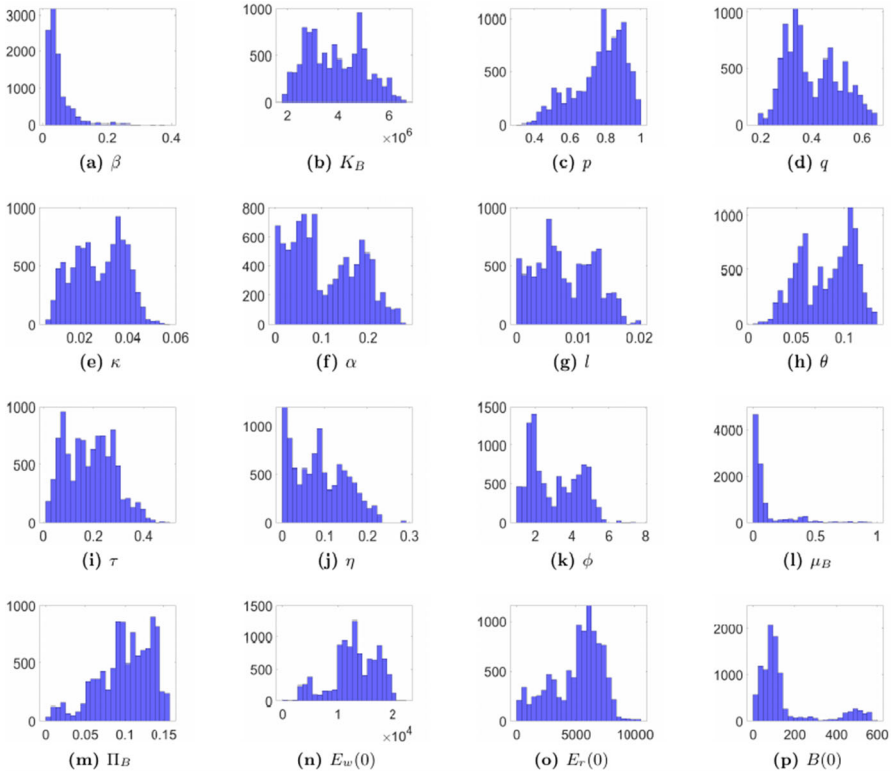

Fig. 3 Estimation of parameters β, K_B, p, q, κ, α l, θ, τ, η, ϕ, μ_B, Π_B, $E_w(0)$, $E_r(0)$ and $B(0)$ in model (5.1) by MCMC.

5.1.2 Model parameter estimation with vaccination in Zimbabwe, 2024

In subsection 5.1.1, we fit the model without vaccination and obtain the values of parameters of model (5.1) in Table 2. Next, we fit the model to reported case data from the 2024 cholera outbreak in Zimbabwe World Health Organization (2024), which involved vaccination efforts. Following the same approach as in subsection 5.1.1, we consider the following model:

Table 2 The parameters of model (5.1) by MCMC

Parameters	mean	std	MC err	tau	geweke
β	0.11116	0.12081	0.025094	2058.6	0.048717
K_B	3.804e+06	1.0284e+06	1.9485e+05	1107.2	0.75076
p	0.73104	0.15873	0.027495	1350	0.47978
q	0.3834	0.12574	0.02449	1309.3	0.5083
κ	0.030096	0.012245	0.0021873	1311.5	0.53417
α	0.12594	0.067273	0.01187	1179.3	0.53192
l	0.007771	0.0044321	0.00074458	881.26	0.89044
θ	0.078289	0.035783	0.0069317	1435.7	0.36888
τ	0.22727	0.1195	0.020767	1305.9	0.44902
η	0.093487	0.065405	0.011544	759.08	0.73443
ϕ	2.8153	1.1218	0.22652	1352.3	0.89475
μ_B	0.24342	0.31812	0.066552	1769	0.039677
Π_B	0.088351	0.035288	0.0066349	976.05	0.27228
$E_w(0)$	12437	5109.2	962.51	1450.9	0.23913
$E_r(0)$	4394.4	2422	422.39	658.91	0.81472
$B(0)$	125.98	114.52	20.59	767.49	0.46516

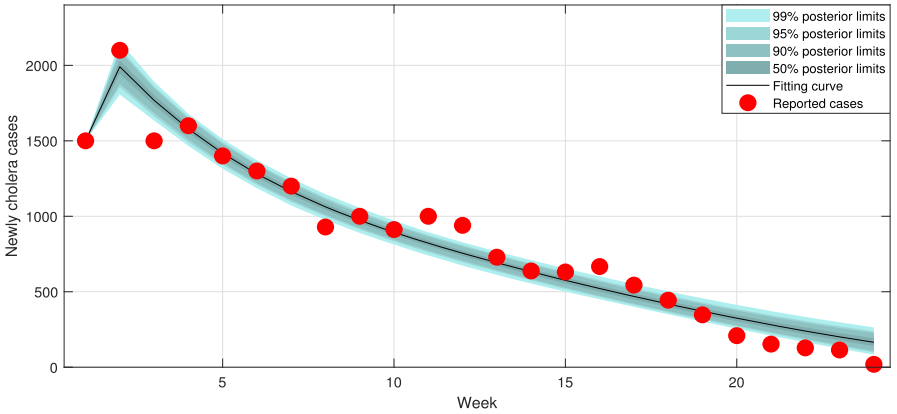

Fig. 4 The fitting curve of the new cholera cases by model in Zimbabwe, 2024.

$$
\begin{cases}
\dfrac{d\int_\Omega S(t,x)\,dx}{dt} = \Pi + \omega\displaystyle\int_\Omega V_1(t,x)\,dx - \dfrac{\beta\int_\Omega (S(t,x)\,dx\int_\Omega B(t,x)\,dx}{K_B+\int_\Omega B(t,x)\,dx} \\
\qquad\qquad - (\psi+\mu)\displaystyle\int_\Omega S(t,x)\,dx, \\
\dfrac{d\int_\Omega V_1(t,x)\,dx}{dt} = \psi\displaystyle\int_\Omega S(t,x)\,dx + \gamma\int_\Omega V_2(t,x)\,dx - r_1\dfrac{\beta\int_\Omega V_1(t,x)\,dx\int_\Omega B(t,x)\,dx}{K_B+\int_\Omega B(t,x)\,dx} \\
\qquad\qquad - (\omega+\sigma+\mu)\displaystyle\int_\Omega V_1(t,x)\,dx, \\
\dfrac{d\int_\Omega V_2(t,x)\,dx}{dt} = \sigma\displaystyle\int_\Omega V_1(t,x)\,dx - r_2\dfrac{\beta\int_\Omega V_2(t,x)\,dx\int_\Omega B(t,x)\,dx}{K_B+\int_\Omega B(t,x)\,dx} \\
\qquad\qquad - (\gamma+\mu)\displaystyle\int_\Omega V_2(t,x)\,dx, \\
\dfrac{d\int_\Omega E_w(t,x)\,dx}{dt} = p\Big(\dfrac{\beta\int_\Omega S(t,x)\,dx\int_\Omega B(t,x)\,dx}{K_B+\int_\Omega B(t,x)\,dx} + r_1\dfrac{\beta\int_\Omega V_1(t,x)\,dx\int_\Omega B(t,x)\,dx}{K_B+\int_\Omega B(t,x)\,dx} \\
\qquad\qquad + r_2\dfrac{\beta\int_\Omega V_2(t,x)\,dx\int_\Omega B(t,x)\,dx}{K_B+\int_\Omega B(t,x)\,dx}\Big) - (\kappa+l+\mu)\displaystyle\int_\Omega E_w(t,x)\,dx, \\
\dfrac{d\int_\Omega E_r(t,x)\,dx}{dt} = (1-p)\Big(\dfrac{\beta\int_\Omega S(t,x)\,dx\int_\Omega B(t,x)\,dx}{K_B+\int_\Omega B(t,x)\,dx} + r_1\dfrac{\beta\int_\Omega V_1(t,x)\,dx\int_\Omega B(t,x)\,dx}{K_B+\int_\Omega B(t,x)\,dx} \\
\qquad\qquad + r_2\dfrac{\beta\int_\Omega V_2(t,x)\,dx\int_\Omega B(t,x)\,dx}{K_B+\int_\Omega B(t,x)\,dx}\Big) + (1-q)\theta\displaystyle\int_\Omega T(t,x)\,dx \\
\qquad\qquad - (l+\mu)\displaystyle\int_\Omega E_r(t,x)\,dx, \\
\dfrac{d\int_\Omega I_a(t,x)\,dx}{dt} = \kappa\displaystyle\int_\Omega E_w(t,x)\,dx - (\alpha+\theta+\mu+\delta)\int_\Omega I_a(t,x)\,dx, \\
\dfrac{d\int_\Omega I_s(t,x)\,dx}{dt} = l\displaystyle\int_\Omega E_w(t,x)\,dx + \alpha\int_\Omega I_a(t,x)\,dx - (\eta+\theta+\tau+\mu+\delta)\int_\Omega I_s(t,x)\,dx, \\
\dfrac{d\int_\Omega I_r(t,x)\,dx}{dt} = l\displaystyle\int_\Omega E_r(t,x)\,dx + \eta\int_\Omega I_s(t,x)\,dx - (\theta+\mu+\delta)\int_\Omega I_r(t,x)\,dx, \\
\dfrac{d\int_\Omega T(t,x)\,dx}{dt} = \tau\displaystyle\int_\Omega I_s(t,x)\,dx - (\mu+\theta+\delta)\int_\Omega T(t,x)\,dx, \\
\dfrac{d\int_\Omega B(t,x)\,dx}{dt} = \phi\displaystyle\int_\Omega I_a(t,x)+I_s(t,x)+I_r(t,x)+T(t,x)\,dx + (\Pi_B-\mu_B)\int_\Omega B(t,x)\,dx.
\end{cases}
\tag{5.2}
$$

Following the same parameter settings as in subsection 5.1.1, we set $\Pi(x) = 800$, $\mu(x) = 0.001$, and $\delta(x) = 0.02$, with the initial value given by $S(0) = 2.3 \times 10^6$. We further set $I_a(0) = 1200$, $I_s(0) = 200$, and $I_r(0) = 100$, whose sum corresponds to the first reported number of cholera cases in the 2024 outbreak. In addition, we assume $T(0) = 50$, while the initial values of $V_1(0)$, $V_2(0)$, $E_w(0)$, $E_r(0)$, and $B(0)$ are to be estimated. Using the parameter values listed in Table 2, namely $\beta = 0.11116$, $\phi = 2.8153$, $\mu_B = 0.24342$, and $\Pi_B = 0.088351$, we fit the model to the reported 2024 cholera case data in Zimbabwe using MCMC. Figure 4 shows that the curve of model (5.2) fits the newly reported cases well, and we obtain the estimated values of $p, q, l, \theta, \tau, \eta, \omega, \psi, \gamma, \sigma, r_1, r_2, \kappa, \alpha, K_B, V_1(0), V_2(0), E_w(0), E_r(0)$ and $B(0)$, which are displayed in Figure 5. Their values are listed in Table 3.

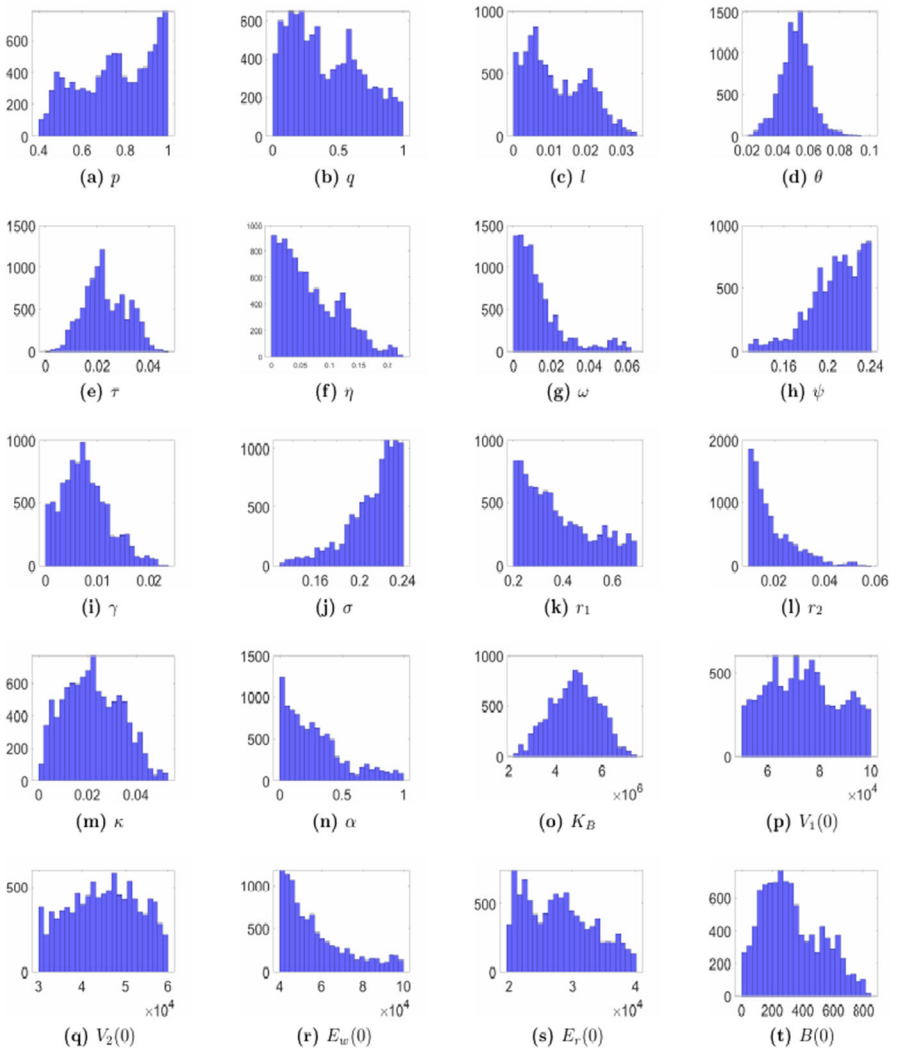

Fig. 5 Estimation of parameters $p, q, l, \theta, \tau, \eta, \omega, \psi, \gamma, \sigma, r_1, r_2, \kappa, \alpha, K_B, V_1(0), V_2(0), E_w(0), E_r(0)$ and $B(0)$ in model (5.2) by MCMC.

5.2 Impact of model parameters on R_0

To better understand cholera transmission dynamics, it is important to assess how the basic reproduction number R_0 responds to key model parameters. This allows us to identify the factors most influencing disease spread. To achieve this, we conducted numerical experiments, varying model parameters systematically. By examining how these changes affect R_0, we gain insights into the roles of spatial heterogeneity, treatment rates, and other factors in cholera transmission. This section presents the results, highlighting the complex relationships between these parameters and R_0.

Table 3 The parameters of model (5.2) by MCMC

Parameters	mean	std	MC err	tau	geweke
p	0.7133	0.16388	0.020709	473.65	0.72378
q	0.43626	0.26353	0.03311	327.44	0.46758
l	0.01457	0.0075926	0.001262	611.29	0.57281
θ	0.054272	0.009838	0.0013368	518.1	0.92613
τ	0.022636	0.0072573	0.0010122	472.59	0.97841
η	0.057452	0.047859	0.0067308	372.52	0.29755
ω	0.013595	0.011325	0.0020987	1364.5	0.49069
ψ	0.20737	0.023863	0.0028207	277.96	0.91118
γ	0.008567	0.0042067	0.00047284	353.79	0.58322
σ	0.2095	0.024217	0.0023509	235.63	0.91928
r_1	0.37639	0.12911	0.017421	756.62	0.79861
r_2	0.020175	0.0082649	0.00099606	342.19	0.70687
κ	0.017603	0.010871	0.0019219	989.38	0.15208
α	0.27831	0.20581	0.024283	328.93	0.7003
K_B	4.6654e+06	9.8973e+05	1.3358e+05	325.7	0.88865
$V_1(0)$	76337	13591	1293.2	178.84	0.88299
$V_2(0)$	44484	7958.3	927.31	242	0.78554
$E_w(0)$	59157	15775	2248.4	530.45	0.79338
$E_r(0)$	28984	5636.7	634.55	342.81	0.7976
$B(0)$	268.35	171.24	30.141	996.55	0.32106

Next, we study the sensitivity of R_0 to model (2.1) parameters under the unvaccinated scenario. We assume that $V_1(t,x) = V_2(t,x) \equiv 0$, $\psi = \sigma = \omega = \gamma \equiv 0$ and $\beta = 0.11116 \times (1 + k\sin(\pi x))$. Additionally, we set $\Pi = 800$, $\mu = 0.001$, and $\delta = 0.02$, with the remaining parameters adopting the values specified in Table 2. Let $d_1 = 0.0007, d_2 = 0, d_3 = 0, d_4 = 0.0006, d_5 = 0.0007, d_6 = 0.0015, d_7 = 0.001, d_8 = 0.0009, d_9 = 0.0008, d_{10} = 0.00085$. As shown in Figure 6(a), R_0 increases with the parameter k. Figure 6(b) illustrates the significant influence of parameter m on the basic reproduction number R_0 when $\beta = 0.11116 \times (1 + k\sin(m\pi x))$ with $m = 1, 2$. These findings underscore the critical role of spatial heterogeneity in cholera transmission. We also evaluate the influence of various parameters on the basic reproduction number R_0 in Figure 6(c-k). Setting $\beta = 0.11116 \times (1 + 0.25\sin(\pi x))$, we observe that R_0 increases with the rise of $\alpha, \kappa, \phi, \sigma_w, \sigma_r$, and τ. Faster disease progression rates (α and κ) and higher transition rates from exposed to bacteria-shedding individuals (σ_w and σ_r) accelerate disease development. A higher bacterial shedding rate (ϕ) increases the concentration of *Vibrio cholerae* in the environment, thereby elevating the risk of infection. Although a higher treatment rate (τ) may temporarily maintain bacterial release before recovery, it generally contributes to shortening the infectious period. In contrast, larger values of η, μ_B, q, and θ reduce R_0 by promoting faster transitions to the recovered state, enhancing bacterial decay in the environment, and shortening the duration of infection. These

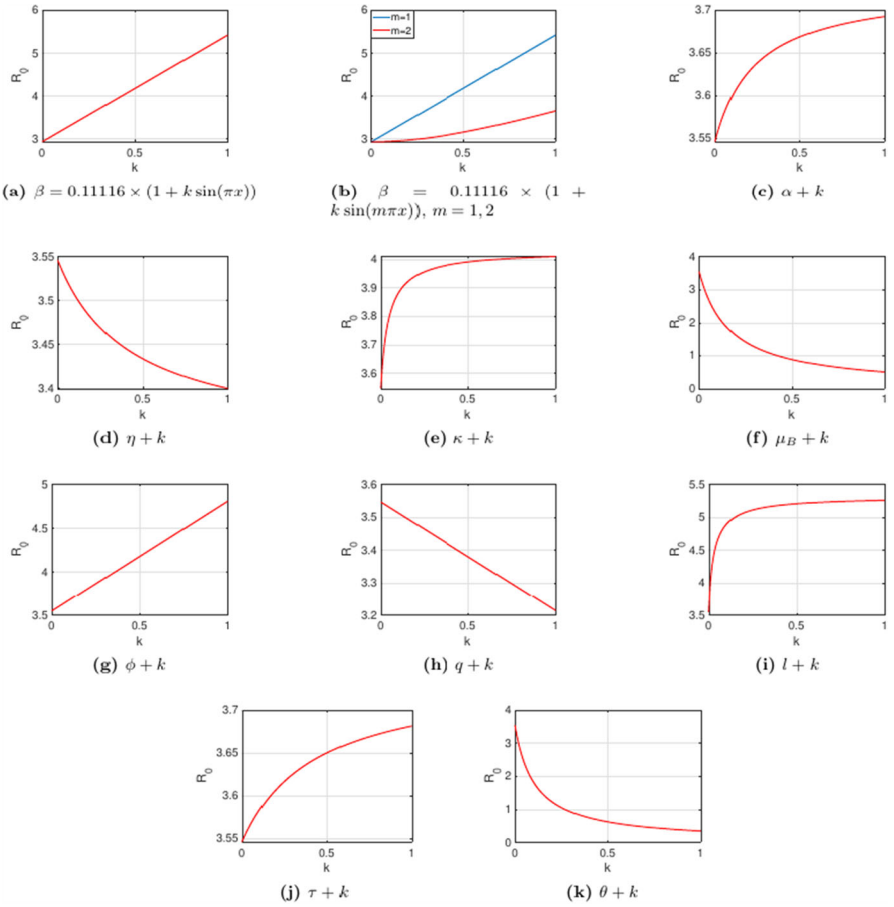

Fig. 6 The impact of parameters on R_0 of model (2.1) without vaccination.

results suggest that cholera control requires an integrated strategy: promptly identifying and isolating cases to shorten the infectious period, improving environmental sanitation, and ensuring access to safe drinking water to reduce exposure risk and suppress disease transmission. Of note, higher rates of treatment also slightly increase transmission rates. In the following section, we will discuss the competitive evolution of two strains to understand this result.

5.3 The competitive evolution of individuals exposed to two strains.

Antibiotics are the primary treatment for cholera. The use of antibiotics, while effective in controlling bacterial infections in the short term, also exerts selective pressure that drives bacterial evolution. Under the influence of antibiotics, the drug-resistant strain of bacteria is more likely to survive and reproduce, gradually becoming dominant. This process is a result of natural selection, wherein the wild strain is progressively

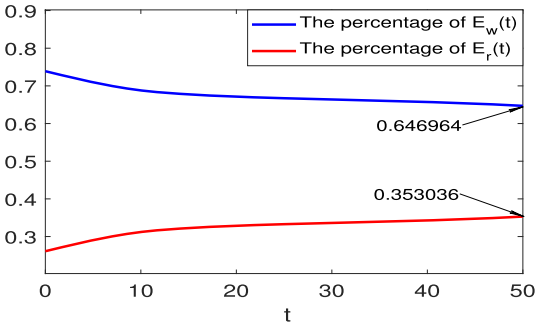

Fig. 7 The competitive evolution of individuals exposed to two strains.

eliminated, and the proportion of the drug-resistant strain increases. The evolution of antibiotic resistance not only complicates treatment but also accelerates the transmission of the drug-resistant, posing a significant global public health challenge.

In this section, we simulate the change in the proportion of individuals infected by two strains in an antibiotic-treated environment, and further analyze the impact of these changes on cholera control strategies. We assume $x \in [0, 1]$. Let $V_1(t, x) = V_2(t, x) \equiv 0$ and $\psi = \sigma = \omega = \gamma \equiv 0$. We set $\Pi = 800$, $\mu = 0.001$ and $\delta = 0.02$, with the remaining parameters adopting the values specified in Table 2. We simulate the competitive evolution of individuals exposed to the wild strain and the drug-resistant strain by extracting the evolution curve at $x = 0.5$. The results show that the proportion of individuals exposed to the drug-resistant strain slightly increases, accounting for 35.3036% at week 50. The proportion of individuals exposed to the wild strain decreases accordingly, accounting for 64.6964% at week 50 in Figure 7. This trend is attributed to the selective pressure exerted by antibiotics. Due to the lower sensitivity of the drug-resistant strain to antibiotics, the use of antibiotics gives them a survival advantage in the environment compared to the wild strain. Therefore, the drug-resistant strain reproduce more effectively, leading to an increasing proportion of exposure to this strain over time. The result indicates that cholera control cannot be achieved solely through treatment efforts, as it will inadvertently increase the risk of future outbreaks. This underscores the critical necessity of pursuing more effective strategies for cholera management and prevention.

5.4 Impact of vaccination on the number of infected individuals

In the previous section, we find that implementation of treatment can potentially result in the exacerbation of drug-resistant strain. In order to mitigate the emergence and transmission of the drug-resistant strain, it is crucial to explore more effective strategies for reducing cholera infections, with vaccination being a key component among them. The vaccine activates the immune system to recognize specific *Vibrio cholerae* antigens, helping to establish immunological memory. This enables the immune system to respond rapidly and efficiently upon subsequent exposure, preventing the onset of infection. Vaccination induces the synthesis of antibodies specific to *Vibrio cholerae* and cholera toxin. These antibodies neutralize the toxin and mitigate its harmful effects on the intestinal mucosa, reducing symptoms such as diarrhea and dehydration. The

vaccine activates the intestinal immune system, particularly through the production of antibodies, which are key to preventing the colonization and spread of *Vibrio cholerae* in the intestinal tract. There are two primary categories of cholera vaccines: oral inactivated vaccines (e.g., Dukoral and Shanchol), which elicit both systemic and mucosal immunity, and oral live attenuated vaccines, which use genetically engineered live *Vibrio cholerae* strains to stimulate the intestinal immune response.

In this section, we mainly discuss the impact of vaccination. We examine how vaccine-related parameters and vaccination strategies influence the number of infections ($I_a + I_s + I_r$). We set $\Pi = 800$, $\mu = 0.001$ and $\delta = 0.02$. The remaining parameters adopt the values specified in Table 3. In Figure 8, we analyze the impact of vaccine-related parameters on the number of infections at $x = 0.5$. When the first dose vaccination coverage rate ψ decreases from 0.20737 to 0.15, the number of infections increases from 18,342.2 to 21,735 (Figure 8(a)). A similar trend is observed when the second dose coverage rate σ decreases from 0.2095 to 0.15, resulting in 20,470.1 infections (Figure 8(b)). Increasing the first dose failure rate ω from 0.013595 to 0.05 raises infections to 21,735 (Figure 8(c)), while increasing the second dose failure rate γ from 0.008567 to 0.02 leads to 20,321.9 infections (Figure 8(d)). Additionally, increasing the contact efficiency of vaccinated individuals, r_1 from 0.37639 to 0.5 and r_2 from 0.020175 to 0.06, results in 19,617.2 and 22,702.7 infections respectively (Figure 8(e-f)). In contrast, adjusting all six parameters ($\psi = 0.245$, $\sigma = 0.245$, $\omega = 0.005$, $\gamma = 0.005$, $r_1 = 0.2$, $r_2 = 0.01$) significantly reduces the number of infections to 13,581.5 (Figure 8(g)). These results indicate that improving vaccine coverage and efficacy, and reducing contact efficiency, play key roles in reducing cholera transmission.

Next, we use partial rank correlation coefficients (PRCC) to investigate the sensitivity of the basic reproduction number R_0 to model parameters. To this end, we adopt the formula for sensitivity index as presented in Wu et al. (2024):

$$\text{Sensitivity index (S.I.)} = \frac{\partial R_0}{\partial(\text{parameter})} \cdot \frac{\text{parameter}}{R_0},$$

$$\frac{\partial R_0}{\partial(\text{parameter})} = \frac{R_0(\text{parameter} + h) - R_0(\text{parameter} - h)}{2h} + O(h^2).$$

The sensitivity indices of R_0 with respect to the parameters ψ, σ, ω, γ, r_1, r_2, l, θ, δ, α, μ, ϕ are calculated as -0.6787, -0.8974, 0.3409, 0.8756, 0.8801, 0.9088, 0.3451, -0.9867, -0.9136, 0.2204, -0.9778, 0.9808 (see Figure 9). Among these, ω, γ, r_1, r_2, l, α, ϕ are positively correlated with R_0, whereas ψ, σ, θ, δ, μ are negatively correlated. The sensitivity analysis indicates that increasing vaccine coverage and efficacy can significantly reduce the basic reproduction number R_0, thereby effectively suppressing disease transmission. These results highlight the critical role of vaccination in disease control Fig 9.

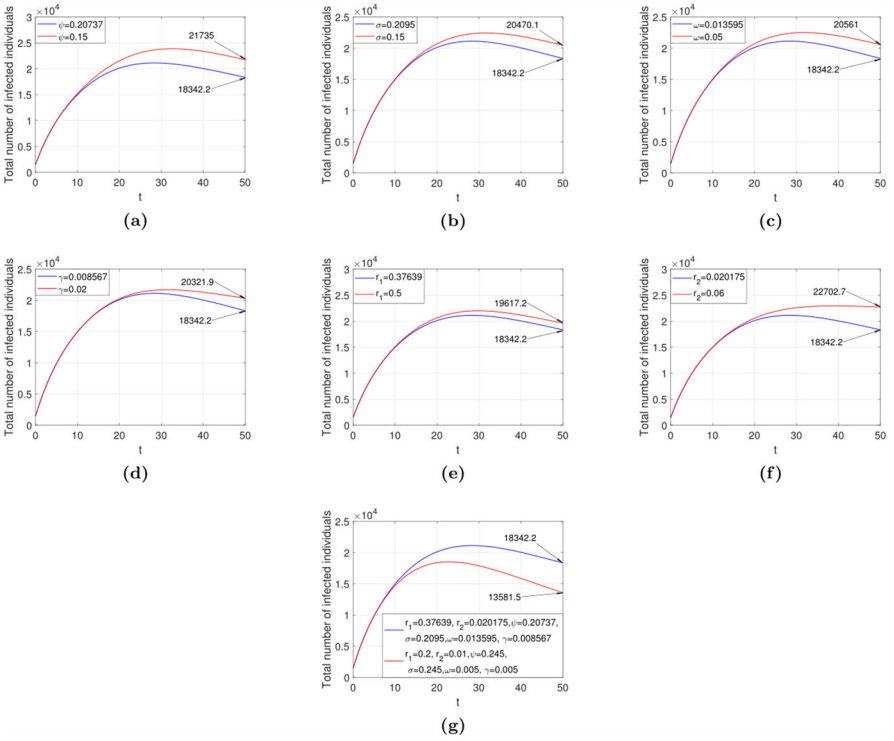

Fig. 8 The impact of vaccine-related parameters on the number of infected individuals.

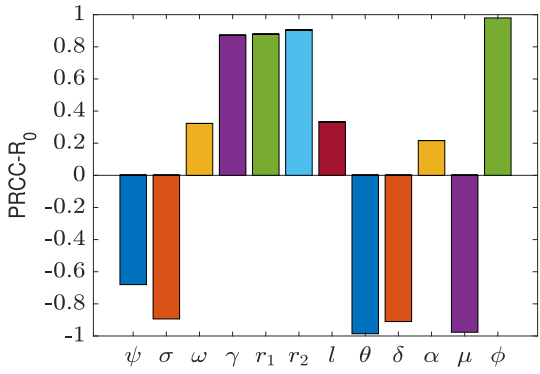

Fig. 9 Sensitivity analysis of R_0 with respect to parameters. We set $\Pi = 800$, $\mu = 0.001$, and $\delta = 0.02$, while the remaining parameters take the values listed in Table 3.

5.5 Comparison of Human- and Environment-Driven Transmission in a Heterogeneous Diffusion Framework

This section explores the relative roles of human movement and environmental bacterial diffusion in shaping the spatial patterns of cholera epidemics, within an idealized one-dimensional space. In biological systems, such as the behavior of infected individuals, spatial diffusion rates often vary due to factors such as environmental conditions,

population density, and movement patterns. This spatial heterogeneity is crucial for understanding the spatial spread of cholera and its dynamic evolution. In the cholera transmission process, the diffusion mechanisms of infected individuals and *Vibrio cholerae* in the environment differ fundamentally: infected individuals can travel over large distances via roads, public transportation, etc., while free *Vibrio cholerae* in water primarily relies on slower processes such as water flow and molecular diffusion, leading to a more limited effective diffusion range. While precise field measurements to determine the absolute diffusion coefficients of both mechanisms are lacking, it is widely accepted that the spatial scale of human movement is significantly larger than that of passive bacterial diffusion. Therefore, in the simulation, we set the baseline diffusion coefficient for human-related compartments to be approximately 10–100 times the diffusion coefficient of the bacteria to reflect this magnitude difference. This setting is not arbitrary, but rather a reasonable simplification based on epidemiological knowledge.

We introduce the following Gaussian-type and arctangent-type diffusion rates:

$$\begin{aligned} &d_i(x) = d_i D(x),\ i = 1, \ldots, 10, \\ &D_1(x) = 2 + \frac{50}{\sqrt{2\pi}} \exp\left(-\frac{(x-30)^2}{8}\right) + \frac{100}{3\sqrt{2\pi}} \exp\left(-\frac{(x-70)^2}{18}\right), \\ &d_{11}(x) = d_{11} D(x),\ \ D_2(x) = 0.1\,[\arctan(x-50) + 2.5] - 0.01. \end{aligned} \tag{5.3}$$

The initial values are as follows:

$$\begin{aligned} &S(0,x) = 2300000,\ E_w(0,x) = 12437,\ E_r(0,x) = 4394.4,\ I_a(0,x) = 385, \\ &I_s(0,x) = 0,\ I_r(0,x) = 0,\ T(0,x) = 0,\ B(0,x) = 125.98. \end{aligned} \tag{5.4}$$

Based on the initial conditions (5.4), Figure 10 illustrates the spatial distributions of infected individuals and *Vibrio cholerae* under the two diffusion mechanisms. The diffusion rate $D_1(x)$ within the interval $x \in [0, 100]$ is modulated by two Gaussian functions, showing a bimodal distribution. The diffusion rate function $D_2(x)$ increases monotonically with x, with a sharp inflection point around $x \approx 50$, where the growth rate is steepest. For values of $x < 50$ and $x > 50$, the increase in the function is more gradual.

Figure 10(a–g) show the steady-state distributions of various components: regions with higher diffusion rates correspond to lower densities of the variables. In Figure 10(g), the steady-state distribution of *Vibrio cholerae* exhibits a similar pattern but, unlike Figure 10(a–f), a clear fluctuation appears near $x = 50$ (highlighted in the figure). This fluctuation can be explained biologically: in low-diffusion areas, bacteria tend to accumulate, while in high-diffusion areas, bacteria spread rapidly. The inflection point represents the boundary between these two states, where the bacteria are neither fully accumulated nor fully diffused, leading to a local fluctuation.

It is important to emphasize that the spatial distribution of *Vibrio cholerae* is primarily driven by the release behavior of infected individuals. Even in areas with the highest bacterial concentration, the density of infected individuals may not be maximal, indicating that the key to new infections lies in human exposure to contaminated

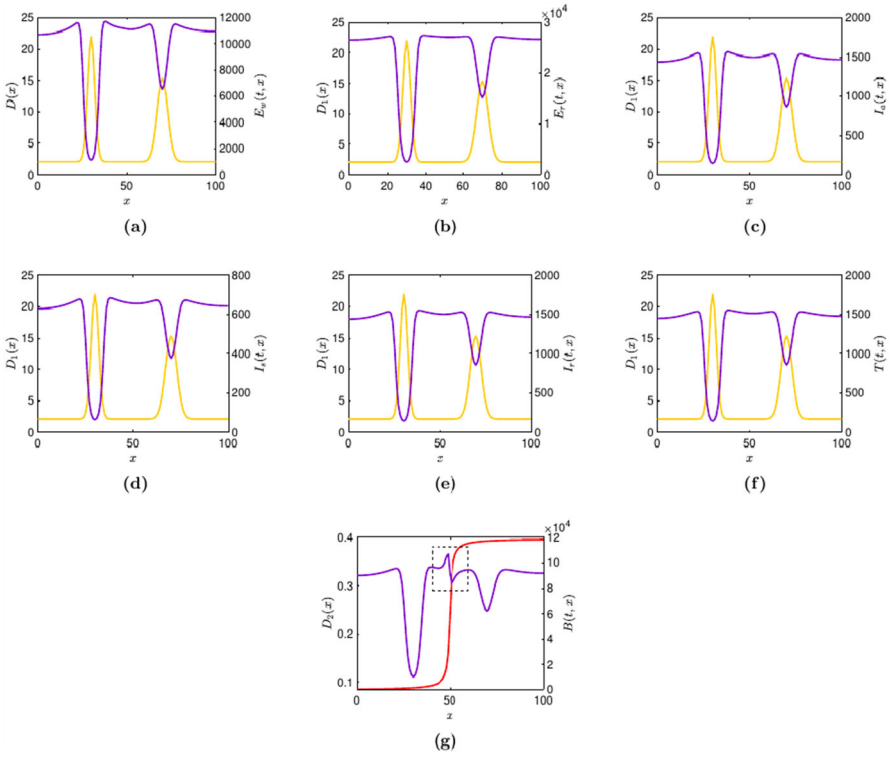

Fig. 10 We set $\Pi = 800$, $\mu = 0.001$, and $\delta = 0.02$, while the remaining parameter values are as listed in Table 2. The purple curves represent the steady-state distributions of the compartments, obtained using the initial conditions specified in (5.4) and diffusion rates: $d_1 = 0.0007$, $d_2 = 0.0007$, $d_3 = 0.0007$, $d_4 = 0.0006$, $d_5 = 0.0007$, $d_6 = 0.0015$, $d_7 = 0.001$, $d_8 = 0.0009$, $d_9 = 0.0008$, and $d_{10} = 0.00085$. The yellow curve shows the spatial distribution of the diffusion rate $D_1(x)$. The red curve shows the spatial distribution of the diffusion rate $D_2(x)$.

environments rather than the diffusion capacity of the bacteria. Under the assumption that long-distance transmission is mainly driven by human movement, our results suggest that the large-scale spatial pattern of the epidemic is primarily controlled by the heterogeneity of human movement, with limited sensitivity to changes in bacterial diffusion rates. This does not negate the crucial role of environmental transmission in sustaining localized epidemics but indicates that, within reasonable parameter ranges, the long-distance spread of cholera is primarily mediated by human activity, while bacterial diffusion mainly affects local dynamics.

Finally, we clarify that the conclusions in this section provide mechanistic insights under idealized assumptions, aimed at revealing the relative roles of human movement and environmental bacterial diffusion in the spatial spread of epidemics, rather than offering a quantitative prediction for a specific outbreak.

5.6 Numerical simulation in a two-dimensional geographic area of Zimbabwe

In the previous section, we focus on the one-dimensional numerical simulation of model (2.1). However, infectious disease transmission typically exhibits pronounced spatial heterogeneity, which necessitates the integration of real-world geographic and population data to assess how spatial structure influences epidemic dynamics. To this end, this section investigates the spatiotemporal spread of cholera in Zimbabwe within a two-dimensional framework that incorporates actual administrative boundaries and population density information.

We assume that the diffusion coefficients for both the human population and *Vibrio cholerae* are constant throughout the computational domain. This assumption is primarily due to the current lack of reliable observational data on long-distance human mobility (e.g., transportation network fluxes) or directional bacterial transport in water bodies (e.g., river flow velocity and direction), which would be required to construct a physically grounded, spatially heterogeneous diffusion function. Nevertheless, despite the uniform and isotropic nature of the diffusion process, the model successfully reproduces realistic transmission patterns-because the initial distribution of susceptible individuals, $S_0(x)$, is directly constructed from real population density data.

Specifically, we use COMSOL Multiphysics to import Zimbabwe's geographic boundaries and population density data from WorldPop (2024). Given the highly uneven population distribution, Figure 11(a) presents a heatmap of $\log_{10}$(population density) to clearly illustrate the spatial pattern of high- and low-density regions (note that $S_0(x)$ is based on the original population density values, not their logarithmic transformation). Subsequently, we grid the map accordingly (see Figure 11(b)), and employ the finite element method to discretize and numerically solve the partial differential equation model. The simulation starts at Week 20 of 2023, corresponding to the time when outbreaks are simultaneously reported in four key regions: Harare, Manicaland Province, Mashonaland West Province, and Matabeleland South Province.

As shown in Figure 12, when $R_0 > 1$, cholera spreads from the initially affected four cities to nearby areas, indicating persistent transmission. However, the disease does not spread across the entire region, remaining relatively localized. This spatially confined pattern is closely linked to Zimbabwe's highly heterogeneous population distribution (see Figure 11(a)): the epidemic persists primarily in densely populated urban and peri-urban areas, while sparsely populated rural regions act as natural transmission barriers that effectively impede further geographic spread of the outbreak. In contrast, Figure 13 shows that after vaccination brings R_0 below 1, the epidemic gradually subsides and is eventually eliminated. The transmission of cholera is closely related to population distribution. In densely populated areas, frequent use of public facilities and shared resources facilitates the occurrence and transmission of cholera. In contrast, in sparsely populated areas, opportunities for transmission are limited, and the risk of cholera outbreaks is relatively low. The gradual reduction and eventual disappearance of cholera infections after vaccination can be attributed to the effective immunization effect of the vaccine. The vaccine has increased the immune coverage of the population, resulting in a significant reduction in the opportunities for transmission

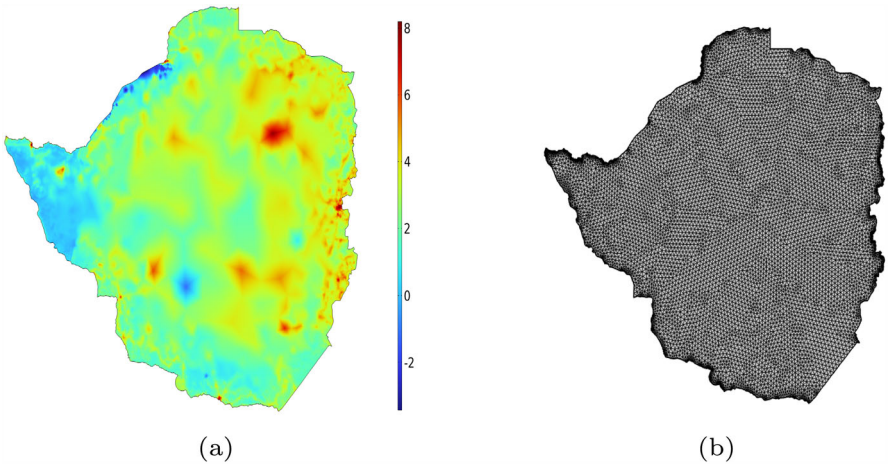

Fig. 11 (a)Heat map of population density in Zimbabwe; (b)Meshed Map of Zimbabwe.

between infected and susceptible individuals. This process promotes the formation of herd immunity, significantly reducing the risk of infection even if some individuals have not been vaccinated. With the continuous vaccination and improvement of public health measures, the transmission chain and routes of cholera are gradually interrupted, ultimately leading to a significant reduction in infection cases and the disappearance of the disease. This mechanism indicates the crucial role of vaccination in controlling the transmission of infectious diseases.

6 Conclusion

Contact with water sources and food contaminated by *Vibrio cholerae* can lead to cholera infections. Infected individuals typically require antibiotic treatment. However, the widespread use of antibiotics leads to the emergence of the drug-resistant strains, which poses a serious challenge to effective cholera control and drive the search for more effective preventive measures, such as vaccination. Recent studies Capone et al. (2015); Wang and Wang (2021) considered the spatial diffusion of cholera, emphasizing the importance of incorporating spatial heterogeneity into disease modeling. To further investigate the spatiotemporal transmission characteristics of cholera, we established a reaction-diffusion model based on the biological characteristics of the disease, taking into account spatial heterogeneity, two strains (wild and drug-resistant), and vaccination strategies.

We derived the basic reproduction number R_0, defined as the spectral radius of the next-generation operator. Based on this threshold parameter, we rigorously analyzed the system's dynamics: when $R_0 < 1$, the disease-free steady state is globally asymptotically stable; when $R_0 > 1$, the disease persists. The introduction of spatial heterogeneity presented significant challenges in establishing the global asymptotic stability of the endemic equilibrium. To address this, under heterogeneous diffusion

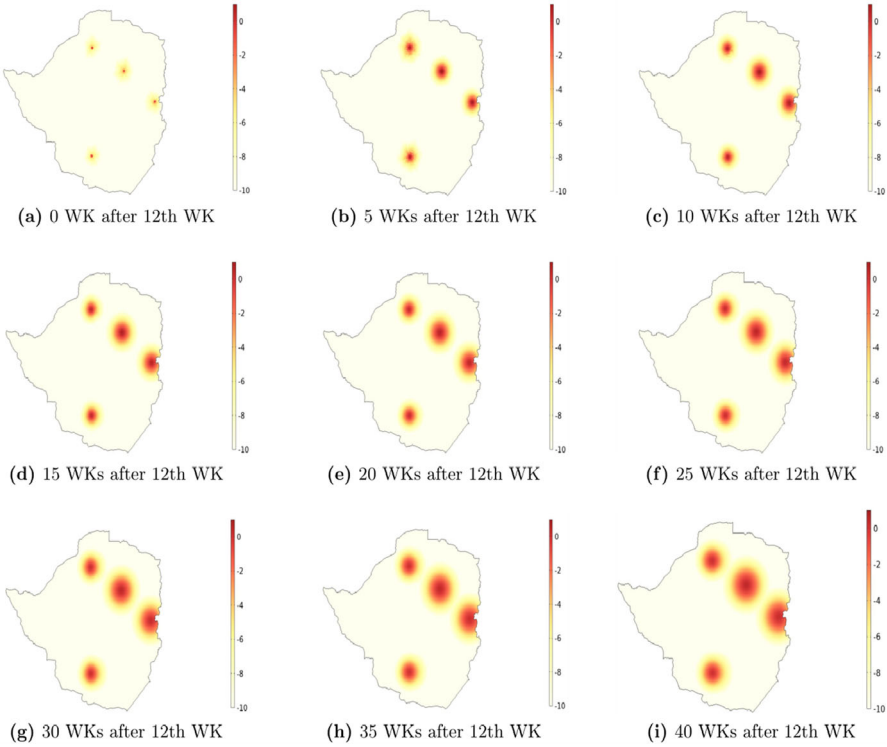

Fig. 12 Evolution of the cholera confirmed case density $\log_{10}(I_a + I_s + I_r)$ for $t = 0, 5, 10, 15, 20, 25, 30, 35, 40$ WKs after 12 WKs of 2023 based on the model (2.1) without vaccination, and the values of the other model parameters are the same as in Table 2.

coefficients and homogeneous parameters, we constructed an appropriate Lyapunov functional and applied LaSalle's invariance principle to prove that the endemic equilibrium is globally asymptotically stable when $R_0 > 1$.

Following the theoretical development of the model, we conducted a series of numerical simulations using a demographic and geographic map from Zimbabwe, along with actual cholera case data. These simulations systematically evaluated the effectiveness of various control strategies and provided new insights and scientific evidence for understanding cholera transmission mechanisms and designing effective interventions. We first fitted the model to empirical case data under the non-vaccination scenario (see Figure 2) and obtained the corresponding parameter estimates (see Table 2), and then fitted the model under the vaccination scenario (see Figure 4) to obtain the corresponding parameter estimates (see Table 3). The model showed good agreement with the data, confirming its applicability. Sensitivity analysis of model parameters with respect to the basic reproduction number R_0 (see Figure 6) identified several key variables that are critical to epidemic control. To explore the risk of antibiotic resistance arising from overuse, we simulated competitive evolution between the wild strain and the drug-resistant strain (see Figure 7). The results indicated that continuous antibiotic use led to the dominance of the drug-resistant strain, thereby

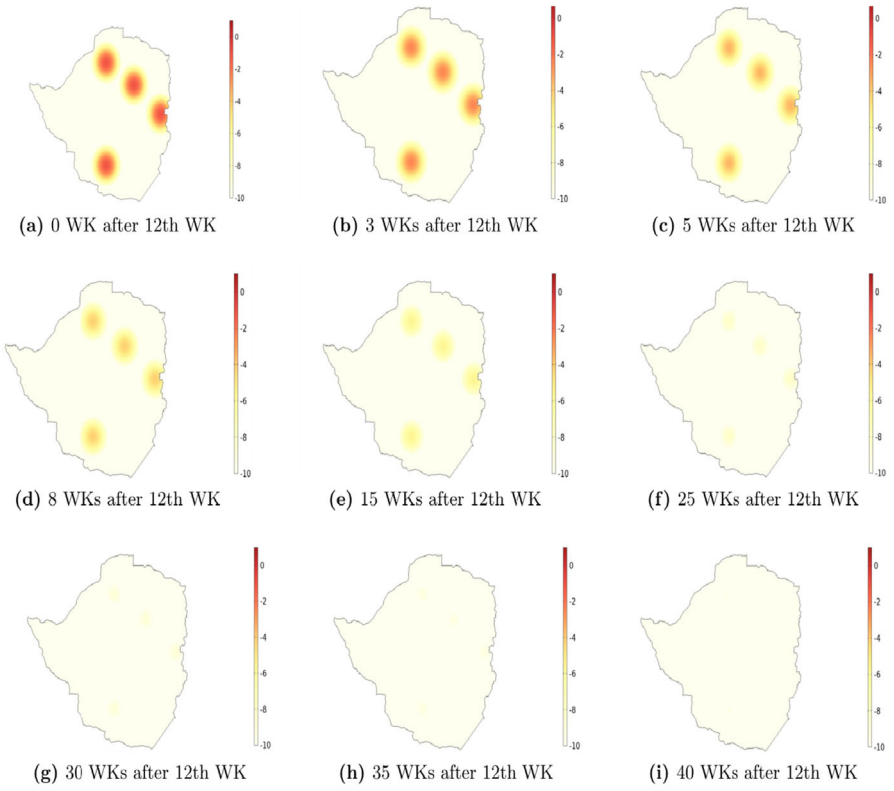

(a) 0 WK after 12th WK (b) 3 WKs after 12th WK (c) 5 WKs after 12th WK

(d) 8 WKs after 12th WK (e) 15 WKs after 12th WK (f) 25 WKs after 12th WK

(g) 30 WKs after 12th WK (h) 35 WKs after 12th WK (i) 40 WKs after 12th WK

Fig. 13 Evolution of the cholera confirmed case density $\log_{10}(I_a + I_s + I_r)$ for $t = 0, 3, 5, 8, 15, 25, 30, 35, 40$ WKs in 2024 based on the model (2.1), and the values of the other model parameters are the same as in Table 3.

increasing the risk of future outbreaks. To further evaluate the impact of vaccination, we conducted simulations adjusting vaccine coverage, failure rate, and efficacy (see Figure 8) and found that increasing both coverage and effectiveness can substantially reduce infection numbers. Next, we performed a sensitivity analysis of R_0 to further examine its relationship with the model parameters (see Figure 9). At the spatial level, we examined the effect of diffusion on disease transmission (see Figure 10). In high diffusion regions, the densities of both infected individuals and *Vibrio cholerae* are lower, but a localized fluctuation in *Vibrio cholerae* density appears near $x = 50$; overall, *Vibrio cholerae* distribution is mainly driven by the movement of infected individuals, while bacterial diffusion has a limited direct effect on infection.

It is worth noting that we employed COMSOL Multiphysics to simulate the spatial evolution of the cholera outbreak in Zimbabwe. In this simulation, real population density data were used to prescribe the initial distribution of the susceptible population $S_0(x)$ (see the $\log_{10}$-scaled heat map in Figure 11(a)), while the diffusion coefficients of both the human population and *Vibrio cholerae* were assumed to be spatially homogeneous constants. Consequently, the localized spatial transmission pattern of

the epidemic, namely, that the outbreak remained largely confined to the four initially affected cities and their surrounding suburban areas, without spreading nationwide (see Figure 12)-can be entirely attributed to the heterogeneity in population distribution shown in Figure 11(a). Sparsely populated rural regions act as natural transmission barriers, effectively limiting the further geographical spread of the epidemic. After the implementation of vaccination, the number of reported cases gradually declined and the epidemic was eventually eliminated (see Figure 13). This outcome highlights the combined effects of population structure and immunization: while population heterogeneity shapes the spatial propagation pattern of the epidemic, vaccination reduces the basic reproduction number R_0 below the epidemic threshold, thereby effectively interrupting the transmission chain.

This study provides theoretical and numerical insights into cholera transmission dynamics, with particular emphasis on the emergence of antibiotic resistance and the role of vaccination in disease control. However, our current study still has some limitations. Owing to the large number of parameters, the complex model structure, and the presence of multiple interactions, the parameter fitting in this study is limited to a single set of reasonably well-fitted values, which may not represent the optimal solution. Conducting a thorough parameter identifiability analysis is essential for evaluating model reliability and predictive performance. We aim to address the issue of parameter identifiability more systematically in future research.

Acknowledgements Research of P.W. was partially supported by the National Nature Science Foundation of China (No. 12201557), the Fundamental Research Funds for the Provincial Universities of Zhejiang (No. GK249909299001-020). X.W.'s research was partially supported by the U.S. National Science Foundation (NSF LEAPS-MPS 2532311). H.W.'s research was partially supported by the Natural Sciences and Engineering Research Council of Canada (Individual Discovery Grant RGPIN-2025-05734) and a Canada Research Chair. The authors are grateful to Jesús Cuevas Maraver in Universidad de Sevilla and Instituto de Matemáticas de la Universidad de Sevilla (IMUS) for his COMSOL Multiphysics code assistance. In addition, P.W. is grateful to his wife for giving birth to a lovely daughter Qiuxun Wu.

Data Availability All data used in this study were obtained from public sources with references provided in the paper.

Declarations

Conflict of interest: The authors declare no conflict of interest.

Appendix A: Existence and Uniqueness of Global Solutions

In this appendix, we commence by proving the existence and uniqueness of global solutions for model (2.1). Let $\mathbb{X} = C(\overline{\Omega}, \mathbb{R}^{10})$ be equipped with the supremum norm $\|\cdot\|_{\mathbb{X}}$, and define $\mathbb{X}^+ = C(\overline{\Omega}, \mathbb{R}^{10}_+)$. Consequently, $(\mathbb{X}, \mathbb{X}^+)$ constitutes an ordered Banach space. We define $o^+ = \max_{x\in\Omega}\{o(x)\}$, $o^- = \min_{x\in\Omega}\{o(x)\}$, where $o(x)$ is any parameter of model (2.1).

Theorem 6.1 *For initial value function* $\phi := (\phi_1, \phi_2, \ldots, \phi_{10}) \in \mathbb{X}^+$, *model (2.1) admits a unique solution* $U(t, \cdot; \phi) = (S(t, \cdot; \phi), V_1(t, \cdot; \phi), V_2(t, \cdot; \phi), E_w(t, \cdot; \phi),$

$E_r(t,\cdot;\phi), I_a(t,\cdot;\phi), I_s(t,\cdot;\phi), I_r(t,\cdot;\phi), T(t,\cdot;\phi), B(t,\cdot;\phi))$. *This solution is defined on* $[0,\infty)$ *and satisfies the initial condition* $U(0,\cdot;\phi)=\phi$.

Proof Define $\pi_1(x)=\psi(x)+\mu(x)$, $\pi_2(x)=\omega(x)+\sigma(x)+\mu(x)$, $\pi_3(x)=\gamma(x)+\mu(x)$, $\pi_4(x)=\kappa(x)+\sigma_w(x)+\mu(x)$, $\pi_5(x)=\sigma_r(x)+\mu(x)$, $\pi_6(x)=\alpha(x)+\theta_a(x)+\mu(x)+\delta_a(x)$, $\pi_7(x)=\eta(x)+\theta_s(x)+\tau(x)+\mu(x)+\delta_s(x)$, $\pi_8(x)=\theta_r(x)+\mu(x)+\delta_r(x)$, $\pi_9(x)=\mu(x)+\theta_t(x)+\delta_t(x)$, $\pi_{10}(x)=-\Pi_B(x)+\mu_B(x)$.

Let $\Gamma_i : C(\overline{\Omega},\mathbb{R})\to C(\overline{\Omega},\mathbb{R})$ denote the C_0 semigroup generated by the operator $\nabla\cdot(d_i(\cdot)\nabla)-\pi_i(\cdot)$ under the Neumann boundary condition, where $i=1,2,\ldots,10$. Then, for $t>0$, $\phi\in C(\overline{\Omega},\mathbb{R})$, we obtain

$$(\Gamma_i(t)\phi)(x)=\int_\Omega T_i(t,x,y)\phi(y)dy,$$

where $T_i(t,x,y)$ denotes the Green's function corresponding to $\nabla\cdot(d_i(\cdot)\nabla)-\pi_i(\cdot)$ under the Neumann boundary condition. By (Smith, 2008, Corollary 7.2.3), we obtain that the semigroup $\Gamma(t):=(\Gamma_1(t),\Gamma_2(t),\ldots,\Gamma_{10}(t))$ exhibits strong positivity and compactness for all $t>0$.

The operator $\nabla\cdot(d_i(\cdot)\nabla)-\pi_i(\cdot)$ under the Neumann boundary condition admits a negative principal eigenvalue, denoted by α_i. Following Ren et al. (2018); Luo et al. (2019), we obtain that there exist some positive constants M_i such that for all $t\geq 0$,

$$\|\Gamma_i(t)\|\leq M_i e^{\alpha_i t}, i=1,2,\ldots,10.$$

Given an initial value function $\phi=(\phi_1(\cdot),\phi_2(\cdot),\ldots,\phi_{10}(\cdot))$ in $\mathbb{X}^+$, we introduce the operator $\mathbb{F}=(\mathbb{F}_1,\mathbb{F}_2,\ldots,\mathbb{F}_{10}):\mathbb{X}^+\to\mathbb{X}$ defined as follows

$$\begin{aligned}
\mathbb{F}_1(\phi)(x)=&\Pi(x)+\omega(x)\phi_2-F_1(x,\phi_1,\phi_{10}),\\
\mathbb{F}_2(\phi)(x)=&\psi(x)\phi_1+\gamma(x)\phi_3-r_1(x)F_2(x,\phi_2,\phi_{10}),\\
\mathbb{F}_3(\phi)(x)=&\sigma(x)\phi_2-r_2(x)F_3(x,\phi_3,\phi_{10}),\\
\mathbb{F}_4(\phi)(x)=&f_1(x)F_1(x,\phi_1,\phi_{10})+f_2(x)r_1(x)F_2(x,\phi_2,\phi_{10})\\
&+f_3(x)r_2(x)F_3(x,\phi_3,\phi_{10}),\\
\mathbb{F}_5(\phi)(x)=&(1-f_1(x))F_1(x,\phi_1,\phi_{10})+(1-f_2(x))r_1(x)F_2(x,\phi_2,\phi_{10})\\
&+(1-f_3(x))r_2(x)F_3(x,\phi_3,\phi_{10})+(1-q(x))\theta_t(x)\phi_9,\\
\mathbb{F}_6(\phi)(x)=&\kappa(x)\phi_4,\\
\mathbb{F}_7(\phi)(x)=&\sigma_w(x)\phi_4+\alpha(x)\phi_6,\\
\mathbb{F}_8(\phi)(x)=&\sigma_r(x)\phi_5+\eta(x)\phi_7,\\
\mathbb{F}_9(\phi)(x)=&\tau(x)\phi_7,\\
\mathbb{F}_{10}(\phi)(x)=&\phi_a(x)\phi_6+\phi_s(x)\phi_7+\phi_r(x)\phi_8+\phi_t(x)\phi_9.
\end{aligned}$$

Consequently, model (2.1) can be reformulated as the following integral equation

$$U(t)=\Gamma(t)\phi+\int_0^t\Gamma(t-s)\mathbb{F}(U(s))ds,$$

where $U(t) = (S(t), V_1(t), V_2(t), E_w(t), E_r(t), I_a(t), I_s(t), I_r(t), T(t), B(t))^T$. Moreover, from (Martin and Smith, 1990, Corollary 4), we verify that it satisfies the subtangential condition. Consequently, we obtain that model (2.1) admits a unique positive solution $(S(t,\cdot;\phi), V_1(t,\cdot;\phi), V_2(t,\cdot;\phi), E_w(t,\cdot;\phi), E_r(t,\cdot;\phi), I_a(t,\cdot;\phi), I_s(t,\cdot;\phi), I_r(t,\cdot;\phi), T(t,\cdot;\phi), B(t,\cdot;\phi))$ defined on $[0, t_0)$, where $0 < t_0 \leq +\infty$.

We now demonstrate that the local solution can be extended to a global solution, i.e., $t_0 = +\infty$. To prove the conclusion by contradiction, we suppose that $t_0 < \infty$. Invoking the theory of abstract functional differential equations as presented in Groeger (2014), we can obtain that $\lim_{t\to t_0} \|U(t,x,\phi)\| = +\infty$. Therefore, it suffices to demonstrate that the solution is bounded on $\Omega \times [0, t_0)$. To achieve this, we introduce $N(t)$ defined as

$$\begin{aligned} N(t) = \int_\Omega & (S(t,x) + V_1(t,x) + V_2(t,x) + E_w(t,x) + E_r(t,x) + I_a(t,x) + I_s(t,x) \\ & + I_r(t,x) + T(t,x))dx. \end{aligned}$$

Based on (Groeger, 2014, Theorem 3.7) and taking into account the homogeneous Neumann boundary condition, we obtain that $\int_\Omega \nabla \cdot (d_i(x)\nabla(\cdot))dx = 0$, for $i = 1, 2, \ldots, 10$. Therefore, the following formula is obtained:

$$\begin{aligned} \frac{d}{dt}N(t) &\leq \int_\Omega \big[\Pi(x) - \mu(x)(S(t,x) + V_1(t,x) + V_2(t,x) + E_w(t,x) + E_r(t,x) \\ &\quad + I_a(t,x) + I_s(t,x) + I_r(t,x) + T(t,x))\big]dx \\ &\leq \Pi^+|\Omega| - \mu^- N(t), \forall t \in [0, t_0), \end{aligned}$$

where $|\Omega|$ denotes the volume of Ω. Applying the comparison principle, we can assert the existence of constants $N_1 > 0$ and $t_1 > 0$ which satisfy $N(t) \leq N_1$, for all $t \in [t_1, t_0)$. As a consequence, we obtain $\int_\Omega u(t,x)dx \leq N_1$, where $u \in \{S, V_1, V_2, E_w, E_r, I_a, I_s, I_r, T\}$. We proceed by defining the function $K(t)$ as $K(t) = \int_\Omega B(t,x)dx$. Subsequently, we derive that

$$\begin{aligned} \frac{d}{dt}K(t) &\leq \int_\Omega \big[\phi_a^+ I_a(t,x) + \phi_s^+ I_s(t,x) + \phi_r^+ I_r(t,x) + \phi_t^+ T(t,x) - \big(\mu_B^- - \Pi_B^+\big)B(t,x)\big]dx \\ &\leq \big(\phi_a^+ + \phi_s^+ + \phi_r^+ + \phi_t^+\big)N_1 - \big(\mu_B^- - \Pi_B^+\big)K(t), \forall t \in [0, t_0). \end{aligned}$$

Similarly, we can obtain the existence of constants $N_2 > 0$ and $t_2 > 0$ which satisfy $K(t) \leq N_2$, for all $t \in [t^*, t_0)$, where $t^* = \max\{t_1, t_2\}$. Let m_j^i denote the eigenvalues of the operator $\nabla \cdot (d_i(\cdot)\nabla) - \pi_i(\cdot)$, subject to the Neumann boundary condition. These eigenvalues correspond to the eigenfunctions $\varphi_j^i(x)$ and satisfy the ordering $m_1^i > m_2^i \geq m_3^i \geq \cdots \geq m_j^i \geq \cdots$, $i = 1, 2, \ldots, 10$. From Guenther and Lee (1996), we can obtain $T_i(x,y,t) = \sum_{j\geq 1} \exp(m_j^i t)\varphi_j^i(x)\varphi_j^i(y)$. Since φ_j^i is uniformly bounded, for all $t > 0$, $x, y \in \overline{\Omega}$, there exists a positive constant c such that $T_i(x,y,t) \leq c\sum_{j\geq 1} \exp(m_j^i t)$. We define $d_i^- := \min_{x\in\overline{\Omega}} d_i(x)$ and $\pi_i^- := \min_{x\in\overline{\Omega}} \pi_i(x)$, $i = 1, 2, \ldots, 10$.

Let ρ_j^i denote the eigenvalues of the operator $\nabla\cdot(d_i^-\nabla)-\pi_i^-$ subject to the Neumann boundary condition, such that $-\pi_i^- = \rho_1^i > \rho_2^i \geq \rho_3^i \geq \cdots \geq \rho_j^i \geq \cdots$. Consequently, $-\rho_j^i$ and $-m_j^i$ represent the j-th eigenvalues of $-\nabla\cdot(d_i^-\nabla)+\pi_i^-$ and $-\nabla\cdot(d_i(\cdot)\nabla)+\pi_i(\cdot)$, respectively, both subject to the Neumann boundary condition. We observe that $d_i^- z^2 \leq d_i(x)z^2$ and $\pi_i^- \leq \pi_i(x)$ hold for all $x\in\Omega$ and $z\in\mathbb{R}$. Consequently, according to (Wang, 2010, Theorem 2.4.7), we can obtain that $-\rho_j^i \leq -m_j^i$ for all $j\in\mathbb{N}$, which, in turn, implies that $\rho_j^i \geq m_j^i$ for all $j\in\mathbb{N}$. Due to ρ_j^i is a decreasing function with respect to $-j^2$, for $t>0, x, y\in\overline{\Omega}, i=1,2,\ldots,10$, we can assert that there exists a constant $c_i>0$ such that $T_i(x,y,t)\leq c\sum_{j\geq 1}\exp(\rho_j^i t)\leq c_i\exp(\rho_1^i t)=c_i\exp(-\pi_i^- t)$. Then, from the first equation of model (2.1), it follows that

$$
\begin{aligned}
S(t,x) &\leq \Gamma_1(t)S(t^*,x)+\int_{t^*}^{t}\Gamma_1(t-s)\big[\Pi(x)+\omega(x)V_1(t,x)\big]\,ds\\
&\leq M_1 e^{\alpha_1(t-t^*)}\|S(t^*,\cdot)\|+\int_{t^*}^{t}\int_{\Omega}T_1(t-s,x,y)\big(\Pi(x)+\omega(x)V_1(t,x)\big)\,dy\,ds\\
&\leq M_1 e^{\alpha_1(t-t^*)}\|S(t^*,\cdot)\|+\int_{t^*}^{t}c_1 e^{-(t-s)\pi_1^-}\big(\Pi^+|\Omega|+\omega^+N_1\big)\,ds\\
&\leq M_1 e^{-\alpha_1 t^*}\|S(t^*,\cdot)\|+\frac{c_1(\Pi^+|\Omega|+\omega^+N_1)}{\pi_1^-},\quad \forall t\in[t^*,t_0).
\end{aligned}
$$

Hence, $\|S(t,\cdot)\|\leq M_1e^{-\alpha_1t^*}\|S(t^*,\cdot)\|+\frac{c_1(\Pi^+|\Omega|+\omega^+N_1)}{\pi_1^-}=:N_3$, $\forall t\in[t^*,t_0)$. Similarly, we obtain $\|V_1(t,\cdot)\|\leq M_2e^{-\alpha_2t^*}\|V_1(t^*,\cdot)\|+\frac{c_2(\psi^++\gamma^+)N_1}{\pi_2^-}=:N_4$, and $\|V_2(t,\cdot)\|\leq M_3e^{-\alpha_3t^*}\|V_2(t^*,\cdot)\|+\frac{c_3\sigma^+N_1}{\pi_3^-}=:N_5$, $\forall t\in[t^*,t_0)$. According to Assumption 2.1 (P3), we obtain that $F_1(x,S,B)\leq\partial_BF_1(x,N_3,0)B$, $F_2(x,V_1,B)\leq\partial_BF_2(x,N_4,0)B$, and $F_3(x,V_2,B)\leq\partial_BF_3(x,N_5,0)B$, for all $x\in\Omega$. Let $F_{1B}^*:=\max_{x\in\overline{\Omega}}\partial_BF_1(x,N_3,0)$, $F_{2B}^*:=\max_{x\in\overline{\Omega}}\partial_BF_2(x,N_4,0)$, and $F_{3B}^*:=\max_{x\in\overline{\Omega}}\partial_BF_3(x,N_5,0)$. Therefore, $\|E_w(t,\cdot)\|\leq M_4e^{-\alpha_4t^*}\|E_w(t^*,\cdot)\|+\frac{c_4(f_1^+F_{1B}^*+f_2^+r_1^+F_{2B}^*+f_3^+r_2^+F_{3B}^*)N_2}{\pi_4^-}=:N_6$, $\forall t\in[t^*,t_0)$. Similarly, we can obtain that

$$
\begin{aligned}
\|E_r(t,\cdot)\|\leq& M_5e^{-\alpha_5t^*}\|E_r(t^*,\cdot)\|+\frac{c_5}{\pi_5^-}\big[((1-f_1^-)F_{1B}^*+(1-f_2^-)r_1^+F_{2B}^*\\
&+(1-f_3^-)r_2^+F_{3B}^*)N_2+(1-q^-)\theta_t^+N_1\big]=:N_7,\\
\|I_a(t,\cdot)\|\leq& M_6e^{-\alpha_6t^*}\|I_a(t^*,\cdot)\|+\frac{c_6\kappa^+N_1}{\pi_6^-}=:N_8,\\
\|I_s(t,\cdot)\|\leq& M_7e^{-\alpha_7t^*}\|I_s(t^*,\cdot)\|+\frac{c_7(\sigma_w^++\alpha^+)N_1}{\pi_7^-}=:N_9,\\
\|I_r(t,\cdot)\|\leq& M_8e^{-\alpha_8t^*}\|I_r(t^*,\cdot)\|+\frac{c_8(\sigma_r^++\eta^+)N_1}{\pi_8^-}=:N_{10},
\end{aligned}
$$

$$\|T(t,\cdot)\| \leq M_9 e^{-\alpha_9 t^*}\|T(t^*,\cdot)\| + \frac{c_9\tau^+ N_1}{\pi_9^-} =: N_{11},$$
$$\|B(t,\cdot)\| \leq M_{10} e^{-\alpha_{10} t^*}\|B(t^*,\cdot)\| + \frac{c_{10}(\phi_a^+ + \phi_s^+ + \phi_r^+ + \phi_t^+)N_1}{\pi_{10}^-} =: N_{12},$$

for $t \in [t^*, t_0)$. Hence, we conclude that S, V_1, V_2, E_w, E_r, I_a, I_s, I_r, T, and B are bounded on $\Omega \times [0, t_0)$, which leads a contradiction. Therefore, we conclude that $t_0 = +\infty$. □

According to Theorem 6.1, we can obtain the following corollary on the boundedness of solutions on $[0, \infty)$.

Corollary 6.2 *For each solution* $U(t,\cdot;\phi) = (S(t,\cdot;\phi), V_1(t,\cdot;\phi), V_2(t,\cdot;\phi), E_w(t,\cdot;\phi), E_r(t,\cdot;\phi), I_a(t,\cdot;\phi), I_s(t,\cdot;\phi), I_r(t,\cdot;\phi), T(t,\cdot;\phi), B(t,\cdot;\phi))$ *of model (2.1) with initial value function* $\phi \in \mathbb{X}^+$, *there exist positive constants* M_S, M_{V_1}, M_{V_2}, M_{E_w}, M_{E_r}, M_{I_a}, M_{I_s}, M_{I_r}, M_T, *and* M_B *independent of the initial value such that*

$$\begin{aligned}
&\limsup_{t\to\infty}\|S(t,\cdot)\| \leq M_S, && \limsup_{t\to\infty}\|V_1(t,\cdot)\| \leq M_{V_1}, && \limsup_{t\to\infty}\|V_2(t,\cdot)\| \leq M_{V_2},\\
&\limsup_{t\to\infty}\|E_w(t,\cdot)\| \leq M_{E_w}, && \limsup_{t\to\infty}\|E_r(t,\cdot)\| \leq M_{E_r}, && \limsup_{t\to\infty}\|I_a(t,\cdot)\| \leq M_{I_a},\\
&\limsup_{t\to\infty}\|I_s(t,\cdot)\| \leq M_{I_s}, && \limsup_{t\to\infty}\|I_r(t,\cdot)\| \leq M_{I_r}, && \limsup_{t\to\infty}\|T(t,\cdot)\| \leq M_T,\\
&\limsup_{t\to\infty}\|B(t,\cdot)\| \leq M_B.
\end{aligned} \tag{6.1}$$

Moreover, the solution semiflow $\Phi_t : \mathbb{X}^+ \to \mathbb{X}^+$ *exhibits point dissipativity and possesses a global attractor.*

Proof According to Theorem 6.1 and replacing t_0 by $+\infty$, we can know that

$$M_S = \frac{c_1(\Pi^+|\Omega| + \omega^+ N_1)}{\psi^- + \mu^-}, M_{V_1} = \frac{c_2(\psi^+ + \gamma^+)N_1}{\omega^- + \sigma^- + \mu^-}, M_{V_2} = \frac{c_3\sigma^+ N_1}{\gamma^- + \mu^-},$$
$$M_{E_w} = \frac{c_4(f_1^+ F_{1B}^* + f_2^+ r_1^+ F_{2B}^* + f_3^+ r_2^+ F_{3B}^*)N_2}{\kappa^- + \sigma_w^- + \mu^-},$$
$$M_{E_r} = \frac{c_5[((1-f_1^-)F_{1B}^* + (1-f_2^-)r_1^+ F_{2B}^* + (1-f_3^-)r_2^+ F_{3B}^*)N_2 + (1-q^-)\theta_t^+ N_1]}{\sigma_r^- + \mu^-},$$
$$M_{I_a} = \frac{c_6\kappa^+ N_1}{\alpha^- + \theta_a^- + \mu^- + \delta_a^-}, M_{I_s} = \frac{c_7(\sigma_w^+ + \alpha^+)N_1}{\eta^- + \theta_s^- + \tau^- + \mu^- + \delta_s^-}, M_{I_r} = \frac{c_8(\sigma_r^+ + \eta^+)N_1}{\theta_r^- + \mu^- + \delta_r^-},$$
$$M_T = \frac{c_9\tau^+ N_1}{\theta_t^- + \mu^- + \delta_t^-}, M_B = \frac{c_{10}(\phi_a^+ + \phi_s^+ + \phi_r^+ + \phi_t^+)N_1}{\mu_B^- - \Pi_B^+},$$

which satisfy (6.1). Consequently, it can be deduced that model (2.1) exhibits point dissipativity. Furthermore, by (Wu, 2012, Theorem 2.2.6), the solution semiflow Φ_t

is compact for any $t > 0$. Thus, according to (Hale, 2010, Theorem 3.4.8), we can conclude that Φ_t possesses a global compact attractor. This completes the proof. □

Moreover, we obtain the invariant set of model (2.1) is

$$\begin{aligned}\Delta = \Big\{ & (S, V_1, V_2, E_w, E_r, I_a, I_s, I_r, T, B) \in \mathbb{X}^+ : \forall x \in \overline{\Omega}, \int_\Omega (S(\cdot,x) + V_1(\cdot,x) \\ & + V_2(\cdot,x) + E_w(\cdot,x) + E_r(\cdot,x) + I_a(\cdot,x) + I_s(\cdot,x) + I_r(\cdot,x) + T(\cdot,x))\,dx \\ & \le \frac{\Pi^+|\Omega|}{\mu}, \int_\Omega B(\cdot,x)\,dx \le \frac{(\phi_a^+ + \phi_s^+ + \phi_r^+ + \phi_t^+)N_1}{\mu_B^- - \Pi_B^+} \Big\}. \end{aligned} \tag{6.2}$$

In what follows, we consider only solutions with initial values inside the region Δ.

Appendix B: Proof of Theorem 3.2

Proof of Theorem 3.2 By Lemma 3.1, there exists a positive constant δ such that $\lambda_0 + \delta < 0$. According to the comparison principle, it implies the existence of a time $t_1 > 0$ such that for all $t \ge t_1$, and $x \in \overline{\Omega}$, $S(t,x) \le S_0 + \delta$, $V_1(t,x) \le V_{10} + \delta$ and $V_2(t,x) \le V_{20} + \delta$ hold. Therefore, we obtain the following model:

$$\begin{cases} \dfrac{\partial E_w}{\partial t} = \nabla\cdot(d_4(x)\nabla E_w) + f_1(x)\dfrac{\partial F_1}{\partial B}(x, S_0+\delta, 0)B + f_2(x)r_1(x)\dfrac{\partial F_2}{\partial B}(x, V_{10}+\delta, 0)B \\ \qquad\qquad + f_3(x)r_2(x)\dfrac{\partial F_3}{\partial B}(x, V_{20}+\delta, 0)B - (\kappa(x) + \sigma_w(x) + \mu(x))E_w, \\ \dfrac{\partial E_r}{\partial t} = \nabla\cdot(d_5(x)\nabla E_r) + (1-f_1(x))\dfrac{\partial F_1}{\partial B}(x, S_0+\delta, 0)B \\ \qquad\qquad + (1-f_2(x))r_1(x)\dfrac{\partial F_2}{\partial B}(x, V_{10}+\delta, 0)B + (1-f_3(x))r_2(x)\dfrac{\partial F_3}{\partial B}(x, V_{20}+\delta, 0)B \\ \qquad\qquad + (1-q(x))\theta_t(x)T - (\sigma_r(x) + \mu(x))E_r, \\ \dfrac{\partial I_a}{\partial t} = \nabla\cdot(d_6(x)\nabla I_a) + \kappa(x)E_w - (\alpha(x) + \theta_a(x) + \mu(x) + \delta_a(x))I_a, \\ \dfrac{\partial I_s}{\partial t} = \nabla\cdot(d_7(x)\nabla I_s) + \sigma_w(x)E_w + \alpha(x)I_a - (\eta(x) + \theta_s(x) + \tau(x) + \mu(x) + \delta_s(x))I_s, \\ \dfrac{\partial I_r}{\partial t} = \nabla\cdot(d_8(x)\nabla I_r) + \sigma_r(x)E_r + \eta(x)I_s - (\theta_r(x) + \mu(x) + \delta_r(x))I_r, \\ \dfrac{\partial T}{\partial t} = \nabla\cdot(d_9(x)\nabla T) + \tau(x)I_s - (\mu(x) + \theta_t(x) + \delta_t(x))T, \\ \dfrac{\partial B}{\partial t} = \nabla\cdot(d_{10}(x)\nabla B) + \phi_a(x)I_a + \phi_s(x)I_s + \phi_r(x)I_r + \phi_t(x)T + \Pi_B(x)B - \mu_B(x)B, \end{cases}$$

for $t > t_1$, $x \in \Omega$. We consider the assumption that $b(\overline{\phi_4}(x), \overline{\phi_5}(x), \ldots, \overline{\phi_{10}}(x)) \ge (E_w(t_1,x), E_r(t_1,x), I_a(t_1,x), I_s(t_1,x), I_r(t_1,x), T(t_1,x), B(t_1,x))$, where $(\overline{\phi_4}(x), \overline{\phi_5}(x), \ldots, \overline{\phi_{10}}(x))$ denotes the eigenfunction corresponding to the principal eigenvalue $\lambda_0 + \delta < 0$. Consequently, for all $t \ge t_1$, by applying the comparison principle, we can deduce that

$$\begin{aligned} & (E_w(t,x), E_r(t,x), I_a(t,x), I_s(t,x), I_r(t,x), T(t,x), B(t,x)) \\ \le & b(\overline{\phi_4}(x), \overline{\phi_5}(x), \ldots, \overline{\phi_{10}}(x))e^{(\lambda_0+\delta)(t-t_1)} \end{aligned}$$

Therefore, $\lim_{t\to\infty}(E_w(t,x), E_r(t,x), I_a(t,x), I_s(t,x), I_r(t,x), T(t,x), B(t,x)) = (0,0,0,0,0,0,0)$ and $S(t,x)$, $V_1(t,x)$, $V_2(t,x)$ is asymptotic to the solutions of the following model:

$$\begin{cases} \dfrac{\partial \hat{S}(t,x)}{\partial t} = \nabla\cdot(d_1(x)\nabla\hat{S}(t,x)) + \Pi(x) + \omega(x)\hat{V}_1(t,x) - (\psi(x)+\mu(x))\hat{S}(t,x), \\ \dfrac{\partial \hat{V}_1(t,x)}{\partial t} = \nabla\cdot(d_2(x)\nabla\hat{V}_1(t,x)) + \psi(x)\hat{S}(t,x) + \gamma(x)\hat{V}_2(t,x) - (\omega(x)+\sigma(x) \\ \qquad\qquad + \mu(x))\hat{V}_1(t,x), \\ \dfrac{\partial \hat{V}_2(t,x)}{\partial t} = \nabla\cdot(d_3(x)\nabla\hat{V}_2(t,x)) + \sigma(x)\hat{V}_1(t,x) - (\gamma(x)+\mu(x))\hat{V}_2(t,x), \end{cases}$$

for $t > 0, x \in \Omega$, and $\frac{\partial \hat{S}(t,x)}{\partial \nu} = \frac{\partial \hat{V}_1(t,x)}{\partial \nu} = \frac{\partial \hat{V}_2(t,x)}{\partial \nu} = 0$, $t > 0$, $x \in \partial\Omega$. Thus, according to the theory of asymptotically autonomous semiflows, we obtain that $\lim_{t\to\infty}(S(t,x), V_1(t,x), V_2(t,x)) = (S_0, V_{10}, V_{20})$. By the comparison principle, we derive

$$\begin{aligned} &\limsup_{t\to\infty} S(t,\cdot) \le \limsup_{t\to\infty}\hat{S}(t,\cdot) = S_0(\cdot), \\ &\limsup_{t\to\infty} V_1(t,\cdot) \le \limsup_{t\to\infty}\hat{V}_1(t,\cdot) = V_{10}(\cdot), \\ &\limsup_{t\to\infty} V_2(t,\cdot) \le \limsup_{t\to\infty}\hat{V}_2(t,\cdot) = V_{20}(\cdot), \end{aligned}$$

uniformly in $\overline{\Omega}$. □

Appendix C: Proof of Theorem 3.3

Proof of Theorem 3.3 We first define the sets

$$\begin{aligned} \mathbb{X}_0 =& \{u_0 \in \mathbb{X} : \|S^0\| \le M_S, \|V_1^0\| \le M_{V_1}, \|V_2^0\| \le M_{V_2}, \|E_w^0\| \le M_{E_w}, \|E_r^0\| \le M_{E_r}, \\ & \|I_a^0\| \le M_{I_a}, \|I_s^0\| \le M_{I_s}, \|I_r^0\| \le M_{I_a}, \|T^0\| \le M_T, \|B^0\| \le M_B\},\ P := \mathbb{X}^+ \cap \mathbb{X}_0, \\ P_0 :=& \{u_0 \in P : E_w^0 \ne 0, E_r^0 \ne 0, I_a^0 \ne 0, I_s^0 \ne 0, I_r^0 \ne 0, T^0 \ne 0, B^0 \ne 0\}, \\ \partial P_0 :=& \{u_0 \in P : E_w^0 = 0 \text{ or } E_r^0 = 0 \text{ or } I_a^0 = 0 \text{ or } I_s^0 = 0 \text{ or } I_r^0 = 0 \text{ or } T^0 = 0 \text{ or } B^0 = 0\}, \end{aligned}$$

where $u_0 = (S^0, V_1^0, V_2^0, E_w^0, E_r^0, I_a^0, I_s^0, I_r^0, T^0, B^0)^T$. To establish the validity of our theorem, we proceed by demonstrating the following three claims:

Claim 1. The semiflow $\Phi(t)$ satisfies that $\Phi(t)P_0 \subset P_0$ for all $t \ge 0$. This claim follows as a direct consequence of the strong maximum principle. Let U_∂ denote the maximal positive invariant set of $\Phi(t)$ within ∂P_0, defined as $U_\partial := \{u_0 \in P : \Phi(t)u_0 \in \partial P_0\}$. It can be verified that $U_\partial = \{u_0 \in P : E_w^0 = E_r^0 = I_a^0 = I_s^0 = I_r^0 = T^0 = B^0 = 0\}$. Let $\omega(u_0)$ represent the omega limit set of u_0 in P. We define $\overline{U}_\partial$ as $\overline{U}_\partial := \bigcup_{u_0\in U_\partial}\omega(u_0)$.

Claim 2. $\overline{U}_\partial$ constitutes a singleton set, with its sole element being E_0, i.e., $\overline{U}_\partial = \{E_0\}$.

In fact, for any $u_0 \in U_\partial$, the definition of U_∂ implies that $E_w(t,x) = E_r(t,x) = I_a(t,x) = I_s(t,x) = I_r(t,x) = T(t,x) = B(t,x) = 0$, for all $t \geq 0$ and $x \in \overline{\Omega}$. Consequently, upon substituting these values into model (2.1), we derive

$$\begin{cases} \dfrac{\partial S(t,x)}{\partial t} = \nabla \cdot (d_1(x)\nabla S(t,x)) + \Pi(x) + \omega(x)V_1(t,x) - (\psi(x) + \mu(x))S(t,x), \\ \dfrac{\partial V_1(t,x)}{\partial t} = \nabla \cdot (d_2(x)\nabla V_1(t,x)) + \psi(x)S(t,x) + \gamma(x)V_2(t,x) - (\omega(x) + \sigma(x) \\ \qquad\qquad + \mu(x))V_1(t,x), \\ \dfrac{\partial V_2(t,x)}{\partial t} = \nabla \cdot (d_3(x)\nabla V_2(t,x)) + \sigma(x)V_1(t,x) - (\gamma(x) + \mu(x))V_2(t,x), \end{cases}$$

for $t > 0$, $x \in \Omega$, and $\frac{\partial S(t,x)}{\partial \nu} = \frac{\partial V_1(t,x)}{\partial \nu} = \frac{\partial V_2(t,x)}{\partial \nu} = 0$, for $t > 0$, $x \in \partial\Omega$. Consequently, we can obtain that $\overline{U}_\partial = \{E_0\}$. Furthermore, it can be deduced that $\{E_0\}$ constitutes an isolated and compact invariant set for $\Phi(t)$ when restricted in U_∂.

Claim 3. There exists a constant $\delta_1 > 0$, which is independent of u_0, such that $\limsup_{t\to\infty} \|\Phi(t)u_0 - E_0\| > \delta_1$. Proceeding by contradiction, we suppose that for any $\hat{\delta}_1 > 0$, there exists $\hat{u}_0 = (\hat{S}^0, \hat{V}_1^0, \hat{V}_2^0, \hat{E}_w^0, \hat{E}_r^0, \hat{I}_a^0, \hat{I}_s^0, \hat{I}_r^0, \hat{T}^0, \hat{B}^0)$ such that

$$\limsup_{t\to\infty} \|\Phi(t)\hat{u}_0 - E_0\| \leq \hat{\delta}_1, \tag{6.3}$$

where $\Phi(t)\hat{u}_0 = (\hat{S}^0(t,\cdot), \hat{V}_1^0(t,\cdot), \hat{V}_2^0(t,\cdot), \hat{E}_w^0(t,\cdot), \hat{E}_r^0(t,\cdot), \hat{I}_a^0(t,\cdot), \hat{I}_s^0(t,\cdot), \hat{I}_r^0(t,\cdot), \hat{T}^0(t,\cdot), \hat{B}^0(t,\cdot))$. Take a $\delta_2 > 0$ small enough. We define $k_1(\delta_2)$ as the principal eigenvalue of the following eigenvalue problem:

$$\begin{cases} k\psi_4 = \nabla \cdot (d_4(x)\nabla\psi_4) + f_1(x)\dfrac{\partial F_1}{\partial B}(x, S_0, 0)\psi_{10} + f_2(x)r_1(x)\dfrac{\partial F_2}{\partial B}(x, V_{10}, 0)\psi_{10} \\ \qquad + f_3(x)r_2(x)\dfrac{\partial F_3}{\partial B}(x, V_{20}, 0)\psi_{10} - (\kappa(x) + \sigma_w(x) + \mu(x))\psi_4, \\ k\psi_5 = \nabla \cdot (d_5(x)\nabla\psi_5) + (1 - f_1(x))\dfrac{\partial F_1}{\partial B}(x, S_0, 0)\psi_{10} \\ \qquad + (1 - f_2(x))r_1(x)\dfrac{\partial F_2}{\partial B}(x, V_{10}, 0)\psi_{10} + (1 - f_3(x))r_2(x)\dfrac{\partial F_3}{\partial B}(x, V_{20}, 0)\psi_{10} \\ \qquad + (1 - q(x))\theta_t(x)\psi_9 - (\sigma_r(x) + \mu(x))\psi_5, \\ k\psi_6 = \nabla \cdot (d_6(x)\nabla\psi_6) + \kappa(x)\psi_4 - (\alpha(x) + \theta_a(x) + \mu(x) + \delta_a(x))\psi_6, \\ k\psi_7 = \nabla \cdot (d_7(x)\nabla\psi_7) + \sigma_w(x)\psi_4 + \alpha(x)\psi_6 - (\eta(x) + \theta_s(x) + \tau(x) + \mu(x) + \delta_s(x))\psi_7, \\ k\psi_8 = \nabla \cdot (d_8(x)\nabla\psi_8) + \sigma_r(x)\psi_5 + \eta(x)\psi_7 - (\theta_r(x) + \mu(x) + \delta_r(x))\psi_8, \\ k\psi_9 = \nabla \cdot (d_9(x)\nabla\psi_9) + \tau(x)\psi_7 - (\mu(x) + \theta_t(x) + \delta_t(x))\psi_9, \\ k\psi_{10} = \nabla \cdot (d_{10}(x)\nabla\psi_{10}) + \phi_a(x)\psi_6 + \phi_s(x)\psi_7 + \phi_r(x)\psi_8 + \phi_t(x)\psi_9 + \Pi_B(x)\psi_{10} \\ \qquad - \mu_B(x)\psi_{10}, \end{cases} \tag{6.4}$$

for $x \in \Omega$, and $\frac{\partial \psi_i}{\partial \nu} = 0$, $x \in \partial\Omega$, $i = 4, 5, \ldots, 10$. $(\psi_4, \psi_5, \ldots, \psi_{10})^T$ denote the corresponding positive eigenfunction. Since $R_0 > 1$, by Lemma 3.1, we have $k_1 < 0$, where k_1 is the eigenvalue of (6.4). Observe that $k_1(\delta_2) \to k_1$ as $\delta_2 \to 0$. Consequently, we can select a sufficiently small δ_2 such that $k_1(\delta_2) < 0$. Given the arbitrariness of $\hat{\delta}_1$, we assume $\hat{\delta}_1 = \delta_2$. There exists a point $t_0^* > 0$ such that for any $t \geq t_0^*$, the following inequalities hold in $\overline{\Omega}$:

$$\hat{S}(t,\cdot) \geq S_0(\cdot) - \delta_2,\ \hat{V}_1(t,\cdot) \geq V_{10}(\cdot) - \delta_2,\ \hat{V}_2(t,\cdot) \geq V_{20}(\cdot) - \delta_2,\ \hat{E}_w(t,\cdot) \leq \delta_2,$$
$$\hat{E}_r(t,\cdot) \leq \delta_2,\ \hat{I}_a(t,\cdot) \leq \delta_2,\ \hat{I}_s(t,\cdot) \leq \delta_2,\ \hat{I}_r(t,\cdot) \leq \delta_2,\ \hat{B}(t,\cdot) \leq \delta_2.$$

Consequently, according to Assumption 2.1 (P3), we deduce

$$\begin{aligned}
&F_1(x, \hat{S}, \hat{B}) \geq F_1(x, S_0 - \delta_2, \hat{B}) \geq \partial_{\hat{B}} F_1(x, S_0 - \delta_2, \delta_2)\hat{B},\\
&F_2(x, \hat{V}_1, \hat{B}) \geq F_2(x, V_{10} - \delta_2, \hat{B}) \geq \partial_{\hat{B}} F_2(x, V_{10} - \delta_2, \delta_2)\hat{B},\\
&F_3(x, \hat{V}_2, \hat{B}) \geq F_3(x, V_{20} - \delta_2, \hat{B}) \geq \partial_{\hat{B}} F_3(x, V_{20} - \delta_2, \delta_2)\hat{B},
\end{aligned}$$

for $t \geq t_0^*$, $x \in \Omega$.

According to Theorem 6.1 and the strong maximum principle, we deduce $(\hat{E}_w(t,\cdot), \hat{E}_r(t,\cdot), \hat{V}_2(t,\cdot), \hat{E}_w(t,\cdot), \hat{E}_r(t,\cdot), \hat{I}_a(t,\cdot), \hat{I}_s(t,\cdot), \hat{I}_r(t,\cdot), \hat{T}(t,\cdot), \hat{B}(t,\cdot))^T \in \mathrm{Int}(\mathbb{X}^+)$, where $\mathrm{Int}(\mathbb{X}^+)$ denotes the interior of $\mathbb{X}^+$. Consequently, there exists a sufficiently small constant $\rho_0 > 0$ such that $\hat{E}_w(t_0^*,\cdot) \geq \rho_0\psi_4$, $\hat{E}_r(t_0^*,\cdot) \geq \rho_0\psi_5$, $\hat{I}_a(t_0^*,\cdot) \geq \rho_0\psi_6$, $\hat{I}_s(t_0^*,\cdot) \geq \rho_0\psi_7$, $\hat{I}_r(t_0^*,\cdot) \geq \rho_0\psi_8$, $\hat{T}(t_0^*,\cdot) \geq \rho_0\psi_9$, $\hat{B}(t_0^*,\cdot) \geq \rho_0\psi_{10}$. Furthermore, it can be demonstrated that $(\hat{E}_w(t,\cdot), \hat{E}_r(t,\cdot), \hat{I}_a(t,\cdot), \hat{I}_s(t,\cdot), \hat{I}_r(t,\cdot), \hat{T}(t,\cdot), \hat{B}(t,\cdot))^T$ constitutes a super-solution of the following model:

$$
\begin{cases}
\dfrac{\partial \tilde{E}_w(t,x)}{\partial t} =& \nabla\cdot(d_4(x)\nabla\tilde{E}_w(t,x)) + f_1(x)\partial_{\tilde{B}}F_1(x, S_0-\delta_2, \delta_2)\tilde{B} \\
& + f_2(x)r_1(x)\partial_{\tilde{B}}F_2(x, V_{10}-\delta_2, \delta_2)\tilde{B} + f_3(x)r_2(x)\partial_{\tilde{B}}F_2(x, V_{20}-\delta_2, \delta_2)\tilde{B} \\
& - (\kappa(x)+\sigma_w(x)+\mu(x))\tilde{E}_w(t,x), \\
\dfrac{\partial \tilde{E}_r(t,x)}{\partial t} =& \nabla\cdot(d_5(x)\nabla\tilde{E}_r(t,x)) + (1-f_1(x))\partial_{\tilde{B}}F_1(x, S_0-\delta_2, \delta_2)\tilde{B} \\
& + (1-f_2(x))r_1(x)\partial_{\tilde{B}}F_2(x, V_{10}-\delta_2, \delta_2)\tilde{B} \\
& + (1-f_3(x))r_2(x)\partial_{\tilde{B}}F_3(x, V_{20}-\delta_2, \delta_2)\tilde{B} + (1-q(x))\theta_t(x)\tilde{T}(t,x) \\
& - (\sigma_r(x)+\mu(x))\tilde{E}_r(t,x), \\
\dfrac{\partial \tilde{I}_a(t,x)}{\partial t} =& \nabla\cdot(d_6(x)\nabla\tilde{I}_a(t,x)) + \kappa(x)\tilde{E}_w(t,x) - (\alpha(x)+\theta_a(x)+\mu(x) \\
& + \delta_a(x))\tilde{I}_a(t,x), \\
\dfrac{\partial \tilde{I}_s(t,x)}{\partial t} =& \nabla\cdot(d_7(x)\nabla\tilde{I}_s(t,x)) + \sigma_w(x)\tilde{E}_w(t,x) + \alpha(x)\tilde{I}_a(t,x) \\
& - (\eta(x)+\theta_s(x)+\tau(x)+\mu(x)+\delta_s(x))\tilde{I}_s(t,x) \\
\dfrac{\partial \tilde{I}_r(t,x)}{\partial t} =& \nabla\cdot(d_8(x)\nabla\tilde{I}_r(t,x)) + \sigma_r(x)\tilde{E}_r(t,x) + \eta(x)\tilde{I}_s(t,x) \\
& - (\theta_r(x)+\mu(x)+\delta_r(x))\tilde{I}_r(t,x), \\
\dfrac{\partial \tilde{T}(t,x)}{\partial t} =& \nabla\cdot(d_9(x)\nabla\tilde{T}(t,x)) + \tau(x)\tilde{I}_s(t,x) - (\mu(x)+\theta_t(x)+\delta_t(x))\tilde{T}(t,x), \\
\dfrac{\partial \tilde{B}(t,x)}{\partial t} =& \nabla\cdot(d_{10}(x)\nabla\tilde{B}(t,x)) + \phi_a(x)\tilde{I}_a(t,x) + \phi_s(x)\tilde{I}_s(t,x) + \phi_r(x)\tilde{I}_r(t,x) \\
& + \phi_t(x)\tilde{T}(t,x) + \Pi_B(x)\tilde{B}(t,x) - \mu_B(x)\tilde{B}(t,x), \\
\dfrac{\partial \tilde{E}_w(t,x)}{\partial \nu} =& \dfrac{\partial \tilde{E}_r(t,x)}{\partial \nu} = \dfrac{\partial \tilde{I}_a(t,x)}{\partial \nu} = \dfrac{\partial \tilde{I}_s(t,x)}{\partial \nu} = \dfrac{\partial \tilde{I}_r(t,x)}{\partial \nu} = \dfrac{\partial \tilde{T}(t,x)}{\partial \nu} = \dfrac{\partial \tilde{B}(t,x)}{\partial \nu} = 0,
\end{cases}
$$

for $t > t_0^*$, $x \in \Omega$. For $x \in \Omega$, $\tilde{E}_w(t_0^*, x) = \rho_0\psi_4(x)$, $\tilde{E}_r(t_0^*, x) = \rho_0\psi_5(x)$, $\tilde{I}_a(t_0^*, x) = \rho_0\psi_6(x)$, $\tilde{I}_s(t_0^*, x) = \rho_0\psi_7(x)$, $\tilde{I}_r(t_0^*, x) = \rho_0\psi_8(x)$, $\tilde{T}(t_0^*, x) = \rho_0\psi_9(x)$, and $\tilde{B}(t_0^*, x) = \rho_0\psi_{10}(x)$.

We observe that $(\rho_0 e^{-k_1(\delta_2)(t-t_0^*)}\psi_4, \ldots, \rho_0 e^{-k_1(\delta_2)(t-t_0^*)}\psi_{10})^T$ constitutes a solution to the aforementioned model. Since $k_1(\delta_2) < 0$, we have

$$
\begin{aligned}
&\tilde{E}_w(t,\cdot) \geq \rho_0 e^{-k_1(\delta_2)(t-t_0^*)}\psi_4(\cdot) \to \infty, \quad \tilde{E}_r(t,\cdot) \geq \rho_0 e^{-k_1(\delta_2)(t-t_0^*)}\psi_5(\cdot) \to \infty, \\
&\tilde{I}_a(t,\cdot) \geq \rho_0 e^{-k_1(\delta_2)(t-t_0^*)}\psi_6(\cdot) \to \infty, \quad \tilde{I}_s(t,\cdot) \geq \rho_0 e^{-k_1(\delta_2)(t-t_0^*)}\psi_7(\cdot) \to \infty, \\
&\tilde{I}_r(t,\cdot) \geq \rho_0 e^{-k_1(\delta_2)(t-t_0^*)}\psi_8(\cdot) \to \infty, \quad \tilde{T}(t,\cdot) \geq \rho_0 e^{-k_1(\delta_2)(t-t_0^*)}\psi_9(\cdot) \to \infty, \\
&\tilde{B}(t,\cdot) \geq \rho_0 e^{-k_1(\delta_2)(t-t_0^*)}\psi_{10}(\cdot) \to \infty,
\end{aligned}
$$

as $t \to \infty$, which leads to a contradiction with (6.3) and validates Claim 3. This claim establishes that $\{E_0\}$ constitutes an isolated invariant set for $\Phi(t)$ when restricted in P, and $W^S(\{E_0\}) \cap P_0 = \varnothing$, where $W^S(\{E_0\})$ denotes the stable set of $\{E_0\}$ with respect to $\Phi(t)$. According to Claims 1-3 and (Zhao, 2017, Theorem 1.3.1), we can establish that $\Phi(t)$ exhibits uniform persistence with respect to $(P, \partial P_0)$. This consequentially

validates the assertion in (3.3). Furthermore, by applying (Magal and Zhao, 2005, Theorem 4.7), we can deduce that model (2.1) admits at least one endemic steady state. This completes the proof. □

Appendix D: Proof of Theorem 4.1

Proof of Theorem 4.1 First, we prove the existence of the endemic equilibrium. If model (2.1) has an endemic equilibrium $E_1=(S^*, V_1^*, V_2^*, E_w^*, E_r^*, I_a^*, I_s^*, I_r^*, T^*, B^*)$ when $R_0 > 1$ in the homogeneous case, then it satisfies the following equations:

$$
\begin{aligned}
S^* &= \frac{\Pi + \omega V_1^* - F_1(S^*, B^*)}{\psi + \mu}, \ V_1^* = \frac{\psi S^* + \gamma V_2^* - r_1 F_2(V_1^*, B^*)}{\omega+\sigma+\mu},\\
V_2^* &= \frac{\sigma V_1^* - r_2 F_3(V_2^*, B^*)}{\gamma + \mu}, \ E_w^* = \frac{p(F_1(S^*, B^*) + r_1 F_2(V_1^*, B^*) + r_2 F_3(V_2^*, B^*))}{k_1},\\
E_r^* &= \frac{(1-p)(F_1(S^*, B^*) + r_1 F_2(V_1^*, B^*) + r_2 F_3(V_2^*, B^*))}{k_1}\\
&\quad + \frac{[\tau(1-q)\theta_t(\kappa\alpha + k_4\sigma_w)](F_1(S^*, B^*) + r_1 F_2(V_1^*, B^*) + r_2 F_3(V_2^*, B^*))p}{k_1 k_2 k_4 k_5 k_7},\\
I_a^* &= \frac{\kappa p(F_1(S^*, B^*) + r_1 F_2(V_1^*, B^*) + r_2 F_3(V_2^*, B^*))}{k_1 k_4},\\
I_s^* &= \frac{(\kappa\alpha + k_4\sigma_w)(F_1(S^*, B^*) + r_1 F_2(V_1^*, B^*) + r_2 F_3(V_2^*, B^*))p}{k_1 k_4 k_5},\\
I_r^* &= \frac{\sigma_r E_r^*}{k_6} + \frac{\eta(\kappa\alpha + k_4\sigma_w)(F_1(S^*, B^*) + r_1 F_2(V_1^*, B^*) + r_2 F_3(V_2^*, B^*))p}{k_1 k_4 k_5 k_6},\\
T^* &= \frac{\tau(\kappa\alpha + k_4\sigma_w)(F_1(S^*, B^*) + r_1 F_2(V_1^*, B^*) + r_2 F_3(V_2^*, B^*))p}{k_1 k_4 k_5 k_7},\\
B^* &= \frac{\phi_a I_a^* + \phi_s I_s^* + \phi_r I_r^* + \phi_t T^*}{k_3}.
\end{aligned}
$$

Then we can obtain

$$
\frac{[L_1 p + L_2(1-p)](F_1(S^*, B^*) + r_1 F_2(V_1^*, B^*) + r_1 F_3(V_2^*, B^*))}{k_1 k_2 k_4 k_5 k_6 k_7} = k_3 B^*.
$$

Let

$$
f(B) = \frac{[L_1 p + L_2(1-p)](F_1(S, B) + r_1 F_2(V_1, B) + r_2 F_3(V_2, B))}{k_1 k_2 k_3 k_4 k_5 k_6 k_7} - B.
$$

It is obvious that $f(0) = 0$ and

$$
f'(B) = \frac{[L_1 p + L_2(1-p)](\partial_B F_1(S, B) + r_1 \partial_B F_2(V_1, B) + r_2 \partial_B F_3(V_2, B))}{k_1 k_2 k_3 k_4 k_5 k_6 k_7} - 1,
$$

and thus we obtain that $f'(0) = R_0 - 1 > 0$. According to Assumption 2.1 (P4), we know that

$$f''(B) = \frac{[L_1 p + L_2(1-p)](\partial_B^2 F_1(S, B) + r_1 \partial_B^2 F_2(V_1, B) + r_1 \partial_B^2 F_3(V_2, B))}{k_1 k_2 k_3 k_4 k_5 k_6 k_7} < 0,$$

then $f'(B)$ is monotonically decreasing. According to Assumption 2.1 (P3), we deduce that $\lim_{B\to\infty} f'(B) = -1$. Hence, there exists a constant $B_0 \in (0, \infty)$ such that $f'(B_0) = 0$. It follows that $f(B)$ is monotonically increasing for $B \in [0, B_0)$ and monotonically decreasing for $B \in [B_0, \infty)$. Invoking Assumption 2.1 (P3), we can conclude that $f(B) \to -\infty$ as $B \to \infty$. Given these considerations, we can assert the existence of a unique B^*, where $B^* > B_0 > 0$, such that $f(B^*) = 0$. This establishes the existence of the endemic equilibrium.

Next, we show the global attractivity of the endemic equilibrium. Let $W(t) = \int_\Omega V(t, x)\, dx$ and

$$\begin{aligned} V(t,x) =& S^* g\left(\frac{S}{S^*}\right) + V_1^* g\left(\frac{V_1}{V_1^*}\right) + V_2^* g\left(\frac{V_2}{V_2^*}\right) + c_1 E_w^* g\left(\frac{E_w}{E_w^*}\right) + c_2 E_r^* g\left(\frac{E_r}{E_r^*}\right) \\ &+ c_3 I_a^* g\left(\frac{I_a}{I_a^*}\right) + c_4 I_s^* g\left(\frac{I_s}{I_s^*}\right) + c_5 I_r^* g\left(\frac{I_r}{I_r^*}\right) + c_6 T^* g\left(\frac{T}{T^*}\right) \\ &+ c_7 B^* g\left(\frac{B}{B^*}\right), \end{aligned}$$

where $g(x) = x - 1 - lnx$ for $x > 0$. The constants $c_1, \ldots, c_7$ satisfy the following equations:

$$\begin{cases} c_1 p + c_2(1-p) = 1, \\ -c_1 k_1 + c_3 \kappa + c_4 \sigma_w = 0, \\ -c_2 k_2 + c_5 \sigma_r = 0, \\ -c_3 k_4 + c_4 \alpha + c_7 \phi_a = 0, \\ -c_4 k_5 + c_5 \eta + c_6 \tau + c_7 \phi_s = 0, \\ -c_5 k_6 + c_7 \phi_r = 0, \\ -c_6 k_7 + c_7 \phi_t + c_2(1-q)\theta_t = 0. \end{cases}$$

Then, we can obtain that

$$\begin{aligned} c_1 &= \frac{k_2 k_5 k_6 k_7 \phi_a \kappa + [k_2 k_7 (k_6 \phi_s + \eta \phi_r) + (1-q)\theta_t \phi_r \sigma_r \tau + k_2 k_6 \phi_t \tau](\kappa \alpha + k_4 \sigma_w)}{A}, \\ c_2 &= \frac{\sigma_r \phi_r k_1 k_4 k_5 k_7}{A}, c_3 = \frac{k_1 k_2 k_5 k_6 k_7 \phi_a + [k_2 k_7 (k_6 \phi_s + \eta \phi_r) + (1-q)\theta_t \phi_r \sigma_r \tau + k_2 k_6 \phi_t \tau] k_1 \alpha}{A}, \\ c_4 &= \frac{k_1 k_4 [k_2 k_7 (k_6 \phi_s + \eta \phi_r) + (1-q)\theta_t \phi_r \sigma_r \tau + k_2 k_6 \phi_t \tau]}{A}, c_5 = \frac{\phi_r k_1 k_2 k_4 k_5 k_7}{A}, \\ c_6 &= \frac{[(1-q)\theta_t \phi_r \sigma_r + k_2 k_6 \phi_t] k_1 k_4 k_5}{A}, c_7 = \frac{k_1 k_2 k_4 k_5 k_6 k_7}{A}, \end{aligned}$$

where $A = k_2k_5k_6k_7\phi_a\kappa\, p + [k_2k_7(k_6\phi_s + \eta\phi_r) + (1-q)\theta_t\phi_r\sigma_r\tau + k_2k_6\phi_t\tau](\kappa\alpha + k_4\sigma_w)\, p + \sigma_r\phi_r k_1k_4k_5k_7(1-p)$.

$$
\begin{aligned}
\frac{dW}{dt} =& \int_\Omega \left(1 - \frac{S^*}{S}\right)\nabla\cdot(d_1(x)\nabla S(t,x)) + \left(\Pi - \Pi\frac{S^*}{S} - \omega V_1\frac{S^*}{S} - \mu S + \psi S^*\right.\\
&\left. + \mu S^* + F_1(S,B)\frac{S^*}{S}\right)dx + \int_\Omega \left(1 - \frac{V_1^*}{V_1}\right)\nabla\cdot(d_2(x)\nabla V_1(t,x))\\
&+ \left(-\mu V_1 - \psi S\frac{V_1^*}{V_1} - \gamma V_2\frac{V_1^*}{V_1} + r_1F_2(V_1^*,B^*)\frac{V_1^*}{V_1} + \omega V_1^* + \sigma V_1^* + \mu V_1^*\right)dx\\
&+ \int_\Omega \left(1 - \frac{V_2^*}{V_2}\right)\nabla\cdot(d_3(x)\nabla V_2(t,x)) + \left(-\mu V_2 - \sigma V_1\frac{V_2^*}{V_2} + r_2F_3(V_2^*,B^*)\frac{V_2^*}{V_2}\right.\\
&\left. + \gamma V_2^* + \mu V_2^*\right)dx + c_1\int_\Omega \left(1 - \frac{E_w^*}{E_w}\right)\nabla\cdot(d_4(x)\nabla E_w(t,x))\\
&+ \left(-pF_1(S,B)\frac{E_w^*}{E_w} - r_1pF_2(V_1,B)\frac{E_w^*}{E_w} - r_2pF_3(V_2,B)\frac{E_w^*}{E_w} + k_1E_w^*\right)dx\\
&+ c_2\int_\Omega \left(1 - \frac{E_r^*}{E_r}\right)\nabla\cdot(d_5(x)\nabla E_r(t,x)) + \left(-(1-p)F_1(S,B)\frac{E_r^*}{E_r}\right.\\
&- (1-p)r_1F_2(V_1,B)\frac{E_r^*}{E_r} - (1-p)r_2F_3(V_2,B)\frac{E_r^*}{E_r} - (1-q)\theta_t\frac{E_r^*}{E_r}\\
&\left. + k_2E_r^*\right)dx + \int_\Omega c_3\left(1 - \frac{I_a^*}{I_a}\right)\nabla\cdot(d_6(x)\nabla I_a(t,x)) + c_3\left(-\kappa E_w\frac{I_a^*}{I_a} + k_4I_a^*\right)dx\\
&+ c_4\int_\Omega \left(1 - \frac{I_s^*}{I_s}\right)\nabla\cdot(d_7(x)\nabla I_s(t,x)) + \left(-\sigma_wE_w\frac{I_s^*}{I_s} - \alpha I_a\frac{I_s^*}{I_s} + k_5I_s^*\right)dx\\
&+ c_5\int_\Omega \left(1 - \frac{I_s^*}{I_r}\right)\nabla\cdot(d_8(x)\nabla I_r(t,x)) + \left(\sigma_rE_r\frac{I_r^*}{I_r} - \eta I_s\frac{I_r^*}{I_r} + k_6I_r^*\right)dx\\
&+ c_6\int_\Omega \left(1 - \frac{T^*}{T}\right)\nabla\cdot(d_9(x)\nabla T(t,x)) + \left(-\tau I_s\frac{T^*}{T} + k_7T^*\right)dx\\
&+ c_7\int_\Omega \left(1 - \frac{B^*}{B}\right)\nabla\cdot(d_{10}(x)\nabla B(t,x)) + \left(\Pi_BB - \mu_BB - \phi_aI_a\frac{B^*}{B}\right.\\
&\left. - \phi_sI_s\frac{B^*}{B} - \phi_rI_r\frac{B^*}{B} - \phi_tT\frac{B^*}{B} - \Pi_BB^* - \mu_BB^*\right)dx.
\end{aligned}
$$

Under the homogeneous Neumann boundary condition, it follows that

$$
\int_\Omega \nabla\cdot(d_i(x)\nabla u)\,dx = 0, \quad -\frac{u^*}{u}\int_\Omega \nabla\cdot(d_i(x)\nabla u)dx = -u^*\int_\Omega d_i(x)\frac{\|\nabla u\|^2}{u^2}\,dx \le 0.
$$

According to $\psi S^* = -\gamma V_2^* + r_1F_2(V_1^*,B^*) + \omega V_1^* + \sigma V_1^* + \mu V_1^*$, $\sigma V_1^* = \gamma V_2^* + \mu V_2^* + r_2F_3(V_2^*,B^*)$, and $\Pi = -\omega V_1^* + F_1(S^*,B^*) + \psi S^* + \mu S^*$, we obtain

$$
\begin{aligned}
\frac{dW}{dt} =& \int_\Omega \mu S^*\left(2 - \frac{S^*}{S} - \frac{S}{S^*}\right)dx + \int_\Omega \omega V_1^*\left(2 - \frac{S^*V_1}{SV_1^*} - \frac{SV_1^*}{S^*V_1}\right)dx\\
&+ \int_\Omega \gamma V_2^*\left(2 - \frac{V_1V_2^*}{V_1^*V_2} - \frac{V_1^*V_2}{V_1V_2^*}\right)dx + \int_\Omega \mu V_1^*\left(3 - \frac{S^*}{S} - \frac{SV_1^*}{S^*V_1} - \frac{V_1}{V_1^*}\right)dx
\end{aligned}
$$

$$+\int_\Omega \mu V_2^*\left(4-\frac{S^*}{S}-\frac{SV_1^*}{S^*V_1}-\frac{V_2}{V_2^*}-\frac{V_1V_2^*}{V_1^*V_2}\right)dx-S^*\int_\Omega d_1(x)\frac{\|\nabla S\|^2}{S^2}\,dx$$
$$-V_1^*\int_\Omega d_2(x)\frac{\|\nabla V_1\|^2}{V_1^2}\,dx-V_2^*\int_\Omega d_3(x)\frac{\|\nabla V_2\|^2}{V_2^2}\,dx-c_1E_w^*\int_\Omega d_4(x)\frac{\|\nabla E_w\|^2}{E_w^2}\,dx$$
$$-c_2E_r^*\int_\Omega d_5(x)\frac{\|\nabla E_r\|^2}{E_r^2}\,dx-c_3I_a^*\int_\Omega d_6(x)\frac{\|\nabla I_a\|^2}{I_a^2}\,dx-c_4I_s^*\int_\Omega d_7(x)\frac{\|\nabla I_s\|^2}{I_s^2}\,dx$$
$$-c_5I_r^*\int_\Omega d_8(x)\frac{\|\nabla I_r\|^2}{I_r^2}\,dx-c_6T^*\int_\Omega d_9(x)\frac{\|\nabla T\|^2}{T^2}\,dx-c_7B^*\int_\Omega d_{10}(x)\frac{\|\nabla B\|^2}{B^2}\,dx$$
$$+\frac{k_2k_5k_6k_7\phi_a\kappa p}{A}F_1(S^*,B^*)\int_\Omega\left(5-\frac{S^*}{S}-\frac{I_a^*E_w}{I_aE_w^*}-\frac{F_1(S^*,B^*)SB}{F_1(S,B)S^*B^*}-\frac{F_1(S,B)E_w^*}{F_1(S^*,B^*)E_w}\right.$$
$$\left.-\frac{B^*I_a}{BI_a^*}\right)dx+\frac{k_2k_5k_6k_7\phi_a\kappa p}{A}r_1F_2(V_1^*,B^*)\int_\Omega\left(6-\frac{S^*}{S}-\frac{I_a^*E_w}{I_aE_w^*}-\frac{V_1^*S}{V_1S^*}\right.$$
$$\left.-\frac{F_2(V_1^*,B^*)V_1B}{F_2(V_1,B)V_1^*B^*}-\frac{F_2(V_1,B)E_w^*}{F_2(V_1^*,B^*)E_w}-\frac{B^*I_a}{BI_a^*}\right)dx+\frac{k_2k_5k_6k_7\phi_a\kappa p}{A}r_2F_3(V_2^*,B^*)$$
$$\int_\Omega\left(7-\frac{S^*}{S}-\frac{I_a^*E_w}{I_aE_w^*}-\frac{V_1^*S}{V_1S^*}-\frac{V_1V_2^*}{V_1^*V_2}-\frac{F_3(V_2^*,B^*)V_2B}{F_3(V_2,B)V_2^*B^*}-\frac{F_3(V_2,B)E_w^*}{F_3(V_2^*,B^*)E_w}\right.$$
$$\left.-\frac{B^*I_a}{BI_a^*}\right)dx+\frac{k_2k_6k_7\phi_sk_4\sigma_wp}{A}F_1(S^*,B^*)\int_\Omega\left(5-\frac{S^*}{S}-\frac{F_1(S^*,B^*)SB}{F_1(S,B)S^*B^*}\right.$$
$$\left.-\frac{F_1(S,B)E_w^*}{F_1(S^*,B^*)E_w}-\frac{E_wI_s^*}{E_w^*I_s}-\frac{B^*I_s}{BI_s^*}\right)dx+\frac{k_2k_6k_7\phi_sk_4\sigma_wp}{A}r_1F_2(V_1^*,B^*)\int_\Omega\left(6\right.$$
$$\left.-\frac{S^*}{S}-\frac{V_1^*S}{V_1S^*}-\frac{F_2(V_1^*,B^*)V_1B}{F_2(V_1,B)V_1^*B^*}-\frac{F_2(V_1,B)E_w^*}{F_2(V_1^*,B^*)E_w}-\frac{E_wI_s^*}{E_w^*I_s}-\frac{B^*I_s}{BI_s^*}\right)dx$$
$$+\frac{k_2k_6k_7\phi_sk_4\sigma_wp}{A}r_2F_3(V_2^*,B^*)\int_\Omega\left(7-\frac{S^*}{S}-\frac{V_1^*S}{V_1S^*}-\frac{V_1V_2^*}{V_1^*V_2}-\frac{F_3(V_2^*,B^*)V_2B}{F_3(V_2,B)V_2^*B^*}\right.$$
$$\left.-\frac{F_3(V_2,B)E_w^*}{F_3(V_2^*,B^*)E_w}-\frac{E_wI_s^*}{E_w^*I_s}-\frac{B^*I_s}{BI_s^*}\right)dx+\frac{\sigma_r\phi_rk_1k_4k_5k_7(1-p)}{A}F_1(S^*,B^*)$$
$$\int_\Omega\left(5-\frac{S^*}{S}-\frac{I_r^*E_r}{I_rE_r^*}-\frac{F_1(S^*,B^*)SB}{F_1(S,B)S^*B^*}-\frac{F_1(S,B)E_r^*}{F_1(S^*,B^*)E_r}-\frac{B^*I_r}{BI_r^*}\right)dx$$
$$+\frac{\sigma_r\phi_rk_1k_4k_5k_7(1-p)}{A}r_1F_2(V_1^*,B^*)\int_\Omega\left(6-\frac{S^*}{S}-\frac{V_1^*S}{V_1S^*}-\frac{I_r^*E_r}{I_rE_r^*}-\frac{F_2(V_1^*,B^*)V_1B}{F_2(V_1,B)V_1^*B^*}\right.$$
$$\left.-\frac{F_2(V_1,B)E_r^*}{F_2(V_1^*,B^*)E_r}-\frac{B^*I_r}{BI_r^*}\right)dx+\frac{\sigma_r\phi_rk_1k_4k_5k_7(1-p)}{A}r_2F_3(V_2^*,B^*)\int_\Omega\left(7-\frac{S^*}{S}\right.$$
$$\left.-\frac{V_1^*S}{V_1S^*}-\frac{V_1V_2^*}{V_1^*V_2}-\frac{I_r^*E_r}{I_rE_r^*}-\frac{F_3(V_2^*,B^*)V_2B}{F_3(V_2,B)V_2^*B^*}-\frac{F_3(V_2,B)E_r^*}{F_3(V_2^*,B^*)E_r}-\frac{B^*I_r}{BI_r^*}\right)dx$$
$$+\frac{k_2k_6k_7\phi_s\kappa\alpha p}{A}F_1(S^*,B^*)\int_\Omega\left(6-\frac{S^*}{S}-\frac{I_a^*E_w}{I_aE_w^*}-\frac{F_1(S^*,B^*)SB}{F_1(S,B)S^*B^*}-\frac{F_1(S,B)E_w^*}{F_1(S^*,B^*)E_w}\right.$$
$$\left.-\frac{B^*I_s}{BI_s^*}-\frac{I_s^*I_a}{I_sI_a^*}\right)dx+\frac{k_2k_6k_7\phi_s\kappa\alpha p}{A}r_1F_2(V_1^*,B^*)\int_\Omega\left(7-\frac{S^*}{S}-\frac{I_a^*E_w}{I_aE_w^*}-\frac{V_1^*S}{V_1S^*}\right.$$
$$\left.-\frac{F_2(V_1^*,B^*)V_1B}{F_2(V_1,B)V_1^*B^*}-\frac{F_2(V_1,B)E_w^*}{F_2(V_1^*,B^*)E_w}-\frac{B^*I_s}{BI_s^*}-\frac{I_s^*I_a}{I_sI_a^*}\right)dx+\frac{k_2k_6k_7\phi_s\kappa\alpha p}{A}$$
$$r_2F_3(V_2^*,B^*)\int_\Omega\left(8-\frac{S^*}{S}-\frac{I_a^*E_w}{I_aE_w^*}-\frac{V_1^*S}{V_1S^*}-\frac{V_1V_2^*}{V_1^*V_2}-\frac{F_3(V_2^*,B^*)V_2B}{F_3(V_2,B)V_2^*B^*}\right.$$
$$\left.-\frac{F_3(V_2,B)E_w^*}{F_3(V_2^*,B^*)E_w}-\frac{B^*I_s}{BI_s^*}-\frac{I_s^*I_a}{I_sI_a^*}\right)dx+\frac{k_2k_7\eta\phi_rk_4\sigma_wp}{A}F_1(S^*,B^*)\int_\Omega\left(6-\frac{S^*}{S}\right.$$

$$- \frac{F_1(S^*, B^*)SB}{F_1(S, B)S^*B^*} - \frac{F_1(S, B)E_w^*}{F_1(S^*, B^*)E_w} - \frac{E_w I_s^*}{E_w^* I_s} - \frac{B^* I_r}{B I_r^*} - \frac{I_r^* I_s}{I_r I_s^*}\Big) dx + \frac{k_2 k_7 \eta \phi_r k_4 \sigma_w p}{A}$$

$$r_1 F_2(V_1^*, B^*) \int_\Omega \Big(7 - \frac{S^*}{S} - \frac{V_1^* S}{V_1 S^*} - \frac{F_2(V_1^*, B^*)V_1 B}{F_2(V_1, B)V_1^* B^*} - \frac{F_2(V_1, B)E_w^*}{F_2(V_1^*, B^*)E_w} - \frac{E_w I_s^*}{E_w^* I_s}$$

$$- \frac{B^* I_r}{B I_r^*} - \frac{I_r^* I_s}{I_r I_s^*}\Big) dx + \frac{k_2 k_7 \eta \phi_r k_4 \sigma_w p}{A} r_2 F_3(V_2^*, B^*) \int_\Omega \Big(8 - \frac{S^*}{S} - \frac{V_1^* S}{V_1 S^*} - \frac{V_1 V_2^*}{V_1^* V_2}$$

$$- \frac{F_3(V_2^*, B^*)V_2 B}{F_3(V_2, B)V_2^* B^*} - \frac{F_3(V_2, B)E_w^*}{F_3(V_2^*, B^*)E_w} - \frac{E_w I_s^*}{E_w^* I_s} - \frac{B^* I_r}{B I_r^*} - \frac{I_r^* I_s}{I_r I_s^*}\Big) dx$$

$$+ \frac{k_2 k_6 \phi_t \tau k_4 \sigma_w p}{A} F_1(S^*, B^*) \int_\Omega \Big(6 - \frac{S^*}{S} - \frac{F_1(S^*, B^*)SB}{F_1(S, B)S^*B^*} - \frac{F_1(S, B)E_w^*}{F_1(S^*, B^*)E_w}$$

$$- \frac{E_w I_s^*}{E_w^* I_s} - \frac{T^* I_s}{T I_s^*} - \frac{B^* T}{B T^*}\Big) dx + \frac{k_2 k_6 \phi_t \tau k_4 \sigma_w p}{A} r_1 F_2(V_1^*, B^*) \int_\Omega \Big(7 - \frac{S^*}{S} - \frac{V_1^* S}{V_1 S^*}$$

$$- \frac{F_2(V_1^*, B^*)V_1 B}{F_2(V_1, B)V_1^* B^*} - \frac{F_2(V_1, B)E_w^*}{F_2(V_1^*, B^*)E_w} - \frac{E_w I_s^*}{E_w^* I_s} - \frac{T^* I_s}{T I_s^*} - \frac{B^* T}{B T^*}\Big) dx + \frac{k_2 k_6 \phi_t \tau k_4 \sigma_w p}{A}$$

$$r_2 F_3(V_2^*, B^*) \int_\Omega \Big(8 - \frac{S^*}{S} - \frac{V_1^* S}{V_1 S^*} - \frac{V_1 V_2^*}{V_1^* V_2} - \frac{F_3(V_2^*, B^*)V_2 B}{F_3(V_2, B)V_2^* B^*} - \frac{F_3(V_2, B)E_w^*}{F_3(V_2^*, B^*)E_w}$$

$$- \frac{E_w I_s^*}{E_w^* I_s} - \frac{T^* I_s}{T I_s^*} - \frac{B^* T}{B T^*}\Big) dx + \frac{k_2 k_7 \eta \phi_r \kappa \alpha p}{A} F_1(S^*, B^*) \int_\Omega \Big(7 - \frac{S^*}{S} - \frac{I_a^* E_w}{I_a E_w^*}$$

$$- \frac{F_1(S^*, B^*)SB}{F_1(S, B)S^*B^*} - \frac{F_1(S, B)E_w^*}{F_1(S^*, B^*)E_w} - \frac{I_s^* I_a}{I_s I_a^*} - \frac{B^* I_r}{B I_r^*} - \frac{I_r^* I_s}{I_r I_s^*}\Big) dx + \frac{k_2 k_7 \eta \phi_r \kappa \alpha p}{A}$$

$$r_1 F_2(V_1^*, B^*) \int_\Omega \Big(8 - \frac{S^*}{S} - \frac{I_a^* E_w}{I_a E_w^*} - \frac{V_1^* S}{V_1 S^*} - \frac{F_2(V_1^*, B^*)V_1 B}{F_2(V_1, B)V_1^* B^*} - \frac{F_2(V_1, B)E_w^*}{F_2(V_1^*, B^*)E_w}$$

$$- \frac{I_s^* I_a}{I_s I_a^*} - \frac{B^* I_r}{B I_r^*} - \frac{I_r^* I_s}{I_r I_s^*}\Big) dx + \frac{k_2 k_7 \eta \phi_r \kappa \alpha p}{A} r_2 F_3(V_2^*, B^*) \int_\Omega \Big(9 - \frac{S^*}{S} - \frac{I_a^* E_w}{I_a E_w^*}$$

$$- \frac{V_1^* S}{V_1 S^*} - \frac{V_1 V_2^*}{V_1^* V_2} - \frac{F_3(V_2^*, B^*)V_2 B}{F_3(V_2, B)V_2^* B^*} - \frac{F_3(V_2, B)E_w^*}{F_3(V_2^*, B^*)E_w} - \frac{I_s^* I_a}{I_s I_a^*} - \frac{B^* I_r}{B I_r^*} - \frac{I_r^* I_s}{I_r I_s^*}\Big) dx$$

$$+ \frac{k_2 k_6 \phi_t \tau \kappa \alpha p}{A} F_1(S^*, B^*) \int_\Omega \Big(7 - \frac{S^*}{S} - \frac{I_a^* E_w}{I_a E_w^*} - \frac{F_1(S^*, B^*)SB}{F_1(S, B)S^*B^*} - \frac{F_1(S, B)E_w^*}{F_1(S^*, B^*)E_w}$$

$$- \frac{I_s^* I_a}{I_s I_a^*} - \frac{T^* I_s}{T I_s^*} - \frac{B^* T}{B T^*}\Big) dx + \frac{k_2 k_6 \phi_t \tau \kappa \alpha p}{A} r_1 F_2(V_1^*, B^*) \int_\Omega \Big(8 - \frac{S^*}{S} - \frac{I_a^* E_w}{I_a E_w^*}$$

$$- \frac{V_1^* S}{V_1 S^*} - \frac{F_2(V_1^*, B^*)V_1 B}{F_2(V_1, B)V_1^* B^*} - \frac{F_2(V_1, B)E_w^*}{F_2(V_1^*, B^*)E_w} - \frac{I_s^* I_a}{I_s I_a^*} - \frac{T^* I_s}{T I_s^*} - \frac{B^* T}{B T^*}\Big) dx$$

$$+ \frac{k_2 k_6 \phi_t \tau \kappa \alpha p}{A} r_2 F_3(V_2^*, B^*) \int_\Omega \Big(9 - \frac{S^*}{S} - \frac{I_a^* E_w}{I_a E_w^*} - \frac{V_1^* S}{V_1 S^*} - \frac{V_1 V_2^*}{V_1^* V_2}$$

$$- \frac{F_3(V_2^*, B^*)V_2 B}{F_3(V_2, B)V_2^* B^*} - \frac{F_3(V_2, B)E_w^*}{F_3(V_2^*, B^*)E_w} - \frac{I_s^* I_a}{I_s I_a^*} - \frac{T^* I_s}{T I_s^*} - \frac{B^* T}{B T^*}\Big) dx$$

$$+ \frac{(1-q)\theta_t \phi_r \sigma_r \tau k_4 \sigma_w p}{A} \int_\Omega F_1(S^*, B^*) \Big(8 - \frac{S^*}{S} - \frac{F_1(S^*, B^*)SB}{F_1(S, B)S^*B^*} - \frac{F_1(S, B)E_w^*}{F_1(S^*, B^*)E_w}$$

$$- \frac{E_w I_s^*}{E_w^* I_s} - \frac{T^* I_s}{T I_s^*} - \frac{T E_r^*}{T^* E_r} - \frac{E_r I_r^*}{E_r^* I_r} - \frac{B^* I_r}{B I_r^*}\Big) dx + \frac{(1-q)\theta_t \phi_r \sigma_r \tau k_4 \sigma_w p}{A}$$

$$r_1 F_2(V_1^*, B^*) \int_\Omega \Big(9 - \frac{S^*}{S} - \frac{V_1^* S}{V_1 S^*} - \frac{F_2(V_1^*, B^*)V_1 B}{F_2(V_1, B)V_1^* B^*} - \frac{F_2(V_1, B)E_w^*}{F_2(V_1^*, B^*)E_w} - \frac{E_w I_s^*}{E_w^* I_s}$$

$$- \frac{T^* I_s}{T I_s^*} - \frac{T E_r^*}{T^* E_r} - \frac{E_r I_r^*}{E_r^* I_r} - \frac{B^* I_r}{B I_r^*}\Big) dx + \frac{(1-q)\theta_t \phi_r \sigma_r \tau k_4 \sigma_w p}{A} r_2 F_3(V_2^*, B^*)$$

$$\int_\Omega \Bigg(10-\frac{S^*}{S}-\frac{V_1^*S}{V_1S^*}-\frac{V_1V_2^*}{V_1^*V_2}-\frac{F_3(V_2^*,B^*)V_2B}{F_3(V_2,B)V_2^*B^*}-\frac{F_3(V_2,B)E_w^*}{F_3(V_2^*,B^*)E_w}-\frac{E_wI_s^*}{E_w^*I_s}$$
$$-\frac{T^*I_s}{TI_s^*}-\frac{TE_r^*}{T^*E_r}-\frac{E_rI_r^*}{E_r^*I_r}-\frac{B^*I_r}{BI_r^*}\Bigg)dx+\frac{(1-q)\theta_t\phi_r\sigma_r\tau\kappa\alpha p}{A}F_1(S^*,B^*)\int_\Omega\Bigg(9$$
$$-\frac{S^*}{S}-\frac{I_a^*E_w}{I_aE_w^*}-\frac{F_1(S^*,B^*)SB}{F_1(S,B)S^*B^*}-\frac{F_1(S,B)E_w^*}{F_1(S^*,B^*)E_w}-\frac{I_s^*I_a}{I_sI_a^*}-\frac{T^*I_s}{TI_s^*}-\frac{TE_r^*}{T^*E_r}-\frac{E_rI_r^*}{E_r^*I_r}$$
$$-\frac{B^*I_r}{BI_r^*}\Bigg)dx+\frac{(1-q)\theta_t\phi_r\sigma_r\tau\kappa\alpha p}{A}r_1F_2(V_1^*,B^*)\int_\Omega\Bigg(10-\frac{S^*}{S}-\frac{I_a^*E_w}{I_aE_w^*}-\frac{V_1^*S}{V_1S^*}$$
$$-\frac{F_2(V_1^*,B^*)V_1B}{F_2(V_1,B)V_1^*B^*}-\frac{F_2(V_1,B)E_w^*}{F_2(V_1^*,B^*)E_w}-\frac{I_s^*I_a}{I_sI_a^*}-\frac{T^*I_s}{TI_s^*}-\frac{TE_r^*}{T^*E_r}-\frac{E_rI_r^*}{E_r^*I_r}-\frac{B^*I_r}{BI_r^*}\Bigg)dx$$
$$+\frac{(1-q)\theta_t\phi_r\sigma_r\tau\kappa\alpha p}{A}r_2F_3(V_2^*,B^*)\int_\Omega\Bigg(11-\frac{S^*}{S}-\frac{I_a^*E_w}{I_aE_w^*}-\frac{V_1^*S}{V_1S^*}-\frac{V_1V_2^*}{V_1^*V_2}$$
$$-\frac{F_3(V_2^*,B^*)V_2B}{F_3(V_2,B)V_2^*B^*}-\frac{F_3(V_2,B)E_w^*}{F_3(V_2^*,B^*)E_w}-\frac{I_s^*I_a}{I_sI_a^*}-\frac{T^*I_s}{TI_s^*}-\frac{TE_r^*}{T^*E_r}-\frac{E_rI_r^*}{E_r^*I_r}-\frac{B^*I_r}{BI_r^*}\Bigg)dx$$
$$+\int_\Omega F_1(S^*,B^*)\Bigg(1-\frac{F_1(S^*,B^*)S}{F_1(S,B)S^*}\Bigg)\Bigg(\frac{F_1(S,B)S^*}{F_1(S^*,B^*)S}-\frac{B}{B^*}\Bigg)dx$$
$$+\int_\Omega r_1F_2(V_1^*,B^*)\Bigg(1-\frac{F_2(V_1^*,B^*)V_1}{F_2(V_1,B)V_1^*}\Bigg)\Bigg(\frac{F_2(V_1,B)V_1^*}{F_2(V_1^*,B^*)V_1}-\frac{B}{B^*}\Bigg)dx$$
$$+\int_\Omega r_2F_3(V_2^*,B^*)\Bigg(1-\frac{F_3(V_2^*,B^*)V_2}{F_3(V_2,B)V_2^*}\Bigg)\Bigg(\frac{F_3(V_2,B)V_2^*}{F_3(V_2^*,B^*)V_2}-\frac{B}{B^*}\Bigg)dx.$$

We obtain that

$2-u_1-u_2=-g(u_1)-g(u_2)$, where $u_1=\frac{S^*}{S}$, $u_2=\frac{S}{S^*}$ or $u_1=\frac{S^*V_1}{SV_1^*}$, $u_2=\frac{SV_1^*}{S^*V_1}$ or $u_1=\frac{V_1V_2^*}{V_1^*V_2}$, $u_2=\frac{V_1^*V_2}{V_1V_2^*}$.

$3-u_1-u_2-u_3=-g(u_1)-g(u_2)-g(u_3)$, where $u_1=\frac{S^*}{S}$, $u_2=\frac{SV_1^*}{S^*V_1}$, $u_3=\frac{V_1}{V_1^*}$.

$4-u_1-u_2-u_3-u_4=-g(u_1)-g(u_2)-g(u_3)-g(u_4)$, where $u_1=\frac{S^*}{S}$, $u_2=\frac{SV_1^*}{S^*V_1}$, $u_3=\frac{V_2}{V_2^*}$, $u_4=\frac{V_1V_2^*}{V_1^*V_2}$.

$5-u_1-u_2-u_3-u_4-u_5=-g(u_1)-g(u_2)-g(u_3)-g(u_4)-g(u_5)$, where $u_1=\frac{S^*}{S}$, $u_2=\frac{I_a^*E_w}{I_aE_w^*}$, $u_3=\frac{F_1(S^*,B^*)SB}{F_1(S,B)S^*B^*}$, $u_4=\frac{F_1(S,B)E_w^*}{F_1(S^*,B^*)E_w}$, $u_5=\frac{B^*I_a}{BI_a^*}$ or $u_1=\frac{S^*}{S}$, $u_2=\frac{F_1(S^*,B^*)SB}{F_1(S,B)S^*B^*}$, $u_3=\frac{F_1(S,B)E_w^*}{F_1(S^*,B^*)E_w}$, $u_4=\frac{E_wI_s^*}{E_w^*I_s}$, $u_5=\frac{B^*I_s}{BI_s^*}$ or $u_1=\frac{S^*}{S}$, $u_2=\frac{I_r^*E_r}{I_rE_r^*}$, $u_3=\frac{F_1(S^*,B^*)SB}{F_1(S,B)S^*B^*}$, $u_4=\frac{F_1(S,B)E_r^*}{F_1(S^*,B^*)E_r}$, $u_5=\frac{B^*I_r}{BI_r^*}$.

$6-u_1-u_2-u_3-u_4-u_5-u_6=-g(u_1)-g(u_2)-g(u_3)-g(u_4)-g(u_5)-g(u_6)$, where $u_1=\frac{S^*}{S}$, $u_2=\frac{I_a^*E_w}{I_aE_w^*}$, $u_3=\frac{V_1^*S}{V_1S^*}$, $u_4=\frac{F_2(V_1^*,B^*)V_1B}{F_2(V_1,B)V_1^*B^*}$, $u_5=\frac{F_2(V_1,B)E_w^*}{F_2(V_1^*,B^*)E_w}$, $u_6=\frac{B^*I_a}{BI_a^*}$ or $u_1=\frac{S^*}{S}$, $u_2=\frac{V_1^*S}{V_1S^*}$, $u_3=\frac{F_2(V_1^*,B^*)V_1B}{F_2(V_1,B)V_1^*B^*}$, $u_4=\frac{F_2(V_1,B)E_w^*}{F_2(V_1^*,B^*)E_w}$, $u_5=\frac{E_wI_s^*}{E_w^*I_s}$, $u_6=\frac{B^*I_s}{BI_s^*}$ or $u_1=\frac{S^*}{S}$, $u_2=\frac{V_1^*S}{V_1S^*}$, $u_3=\frac{I_r^*E_r}{I_rE_r^*}$, $u_4=\frac{F_2(V_1^*,B^*)V_1B}{F_2(V_1,B)V_1^*B^*}$, $u_5=\frac{F_2(V_1,B)E_r^*}{F_2(V_1^*,B^*)E_r}$, $u_6=\frac{B^*I_r}{BI_r^*}$ or $u_1=\frac{S^*}{S}$, $u_2=\frac{I_a^*E_w}{I_aE_w^*}$, $u_3=\frac{F_1(S^*,B^*)SB}{F_1(S,B)S^*B^*}$, $u_4=\frac{F_1(S,B)E_w^*}{F_1(S^*,B^*)E_w}$, $u_5=\frac{B^*I_s}{BI_s^*}$, $u_6=\frac{I_s^*I_a}{I_sI_a^*}$ or $u_1=\frac{S^*}{S}$, $u_2=\frac{F_1(S^*,B^*)SB}{F_1(S,B)S^*B^*}$, $u_3=\frac{F_1(S,B)E_w^*}{F_1(S^*,B^*)E_w}$, $u_4=\frac{E_wI_s^*}{E_w^*I_s}$, $u_5=\frac{B^*I_r}{BI_r^*}$, $u_6=\frac{I_r^*I_s}{I_rI_s^*}$, or $u_1=\frac{S^*}{S}$, $u_2=\frac{F_1(S^*,B^*)SB}{F_1(S,B)S^*B^*}$, $u_3=\frac{F_1(S,B)E_w^*}{F_1(S^*,B^*)E_w}$, $u_4=\frac{E_wI_s^*}{E_w^*I_s}$, $u_5=\frac{T^*I_s}{TI_s^*}$, $u_6=\frac{B^*T}{BT^*}$.

$7-u_1-u_2-u_3-u_4-u_5-u_6-u_7=-g(u_1)-g(u_2)-g(u_3)-g(u_4)-g(u_5)-g(u_6)-g(u_7)$, where $u_1=\frac{S^*}{S}$, $u_2=\frac{I_a^*E_w}{I_aE_w^*}$, $u_3=\frac{V_1^*S}{V_1S^*}$, $u_4=\frac{V_1V_2^*}{V_1^*V_2}$, $u_5=\frac{F_3(V_2^*,B^*)V_2B}{F_3(V_2,B)V_2^*B^*}$, $u_6=\frac{F_3(V_2,B)E_w^*}{F_3(V_2^*,B^*)E_w}$, $u_7=\frac{B^*I_a}{BI_a^*}$ or $u_1=\frac{S^*}{S}$, $u_2=\frac{V_1^*S}{V_1S^*}$, $u_3=\frac{V_1V_2^*}{V_1^*V_2}$. $u_4=\frac{F_3(V_2^*,B^*)V_2B}{F_3(V_2,B)V_2^*B^*}$, $u_5=\frac{F_3(V_2,B)E_w^*}{F_3(V_2^*,B^*)E_w}$, $u_6=\frac{E_wI_s^*}{E_w^*I_s}$, $u_7=\frac{B^*I_s}{BI_s^*}$ or $u_1=\frac{S^*}{S}$, $u_2=\frac{V_1^*S}{V_1S^*}$, $u_3=\frac{V_1V_2^*}{V_1^*V_2}$, $u_4=\frac{I_r^*E_r}{I_rE_r^*}$, $u_5=\frac{F_3(V_2^*,B^*)V_2B}{F_3(V_2,B)V_2^*B^*}$, $u_6=\frac{F_3(V_2,B)E_r^*}{F_3(V_2^*,B^*)E_r}$, $u_7=\frac{B^*I_r}{BI_r^*}$ or $u_1=\frac{S^*}{S}$, $u_2=\frac{I_a^*E_w}{I_aE_w^*}$, $u_3=\frac{V_1^*S}{V_1S^*}$, $u_4=\frac{F_2(V_1^*,B^*)V_1B}{F_2(V_1,B)V_1^*B^*}$, $u_5=\frac{F_2(V_1,B)E_w^*}{F_2(V_1^*,B^*)E_w}$, $u_6=\frac{B^*I_s}{BI_s^*}$, $u_7=\frac{I_s^*I_a}{I_sI_a^*}$ or $u_1=\frac{S^*}{S}$, $u_2=\frac{V_1^*S}{V_1S^*}$, $u_3=\frac{F_2(V_1^*,B^*)V_1B}{F_2(V_1,B)V_1^*B^*}$, $u_4=\frac{F_2(V_1,B)E_w^*}{F_2(V_1^*,B^*)E_w}$, $u_5=\frac{E_wI_s^*}{E_w^*I_s}$, $u_6=\frac{B^*I_r}{BI_r^*}$, $u_7=\frac{I_r^*I_s}{I_rI_s^*}$ or $u_1=\frac{S^*}{S}$, $u_2=\frac{V_1^*S}{V_1S^*}$, $u_3=\frac{F_2(V_1^*,B^*)V_1B}{F_2(V_1,B)V_1^*B^*}$, $u_4=\frac{F_2(V_1,B)E_w^*}{F_2(V_1^*,B^*)E_w}$, $u_5=\frac{E_wI_s^*}{E_w^*I_s}$, $u_6=\frac{T^*I_s}{TI_s^*}$, $u_7=\frac{B^*T}{BT^*}$ or $u_1=\frac{S^*}{S}$, $u_2=\frac{I_a^*E_w}{I_aE_w^*}$, $u_3=\frac{F_1(S^*,B^*)SB}{F_1(S,B)S^*B^*}$, $u_4=\frac{F_1(S,B)E_w^*}{F_1(S^*,B^*)E_w}$, $u_5=\frac{I_s^*I_a}{I_sI_a^*}$, $u_6=\frac{I_r^*I_s}{I_rI_s^*}$ or $u_1=\frac{S^*}{S}$, $u_2=\frac{I_a^*E_w}{I_aE_w^*}$, $u_3=\frac{F_1(S^*,B^*)SB}{F_1(S,B)S^*B^*}$, $u_4=\frac{F_1(S,B)E_w^*}{F_1(S^*,B^*)E_w}$, $u_5=\frac{I_s^*I_a}{I_sI_a^*}$, $u_6=\frac{T^*I_s}{TI_s^*}$, $u_7=\frac{B^*T}{BT^*}$.

$8-u_1-u_2-u_3-u_4-u_5-u_6-u_7-u_8=-g(u_1)-g(u_2)-g(u_3)-g(u_4)-g(u_5)-g(u_6)-g(u_7)-g(u_8)$, where $u_1=\frac{S^*}{S}$, $u_2=\frac{I_a^*E_w}{I_aE_w^*}$, $u_3=\frac{V_1^*S}{V_1S^*}$, $u_4=\frac{V_1V_2^*}{V_1^*V_2}$, $u_5=\frac{F_3(V_2^*,B^*)V_2B}{F_3(V_2,B)V_2^*B^*}$, $u_6=\frac{F_3(V_2,B)E_w^*}{F_3(V_2^*,B^*)E_w}$, $u_7=\frac{B^*I_s}{BI_s^*}$, $u_8=\frac{I_s^*I_a}{I_sI_a^*}$ or $u_1=\frac{S^*}{S}$, $u_2=\frac{V_1^*S}{V_1S^*}$, $u_3=\frac{V_1V_2^*}{V_1^*V_2}$, $u_4=\frac{F_3(V_2^*,B^*)V_2B}{F_3(V_2,B)V_2^*B^*}$, $u_5=\frac{F_3(V_2,B)E_w^*}{F_3(V_2^*,B^*)E_w}$, $u_6=\frac{E_wI_s^*}{E_w^*I_s}$, $u_7=\frac{B^*I_r}{BI_r^*}$, $u_8=\frac{I_r^*I_s}{I_rI_s^*}$ or $u_1=\frac{S^*}{S}$, $u_2=\frac{V_1^*S}{V_1S^*}$, $u_3=\frac{V_1V_2^*}{V_1^*V_2}$, $u_4=\frac{F_3(V_2^*,B^*)V_2B}{F_3(V_2,B)V_2^*B^*}$, $u_5=\frac{F_3(V_2,B)E_w^*}{F_3(V_2^*,B^*)E_w}$, $u_6=\frac{E_wI_s^*}{E_w^*I_s}$, $u_7=\frac{T^*I_s}{TI_s^*}$, $u_8=\frac{B^*T}{BT^*}$ or $u_1=\frac{S^*}{S}$, $u_2=\frac{I_a^*E_w}{I_aE_w^*}$, $u_3=\frac{V_1^*S}{V_1S^*}$, $u_4=\frac{F_2(V_1^*,B^*)V_1B}{F_2(V_1,B)V_1^*B^*}$, $u_5=\frac{F_2(V_1,B)E_w^*}{F_2(V_1^*,B^*)E_w}$, $u_6=\frac{I_s^*I_a}{I_sI_a^*}$, $u_7=\frac{B^*I_r}{BI_r^*}$, $u_8=\frac{I_r^*I_s}{I_rI_s^*}$ or $u_1=\frac{S^*}{S}$, $u_2=\frac{I_a^*E_w}{I_aE_w^*}$, $u_3=\frac{V_1^*S}{V_1S^*}$, $u_4=\frac{F_2(V_1^*,B^*)V_1B}{F_2(V_1,B)V_1^*B^*}$, $u_5=\frac{F_2(V_1,B)E_w^*}{F_2(V_1^*,B^*)E_w}$, $u_6=\frac{I_s^*I_a}{I_sI_a^*}$, $u_7=\frac{T^*I_s}{TI_s^*}$, $u_8=\frac{B^*T}{BT^*}$ or $u_1=\frac{S^*}{S}$, $u_2=\frac{F_1(S^*,B^*)SB}{F_1(S,B)S^*B^*}$, $u_3=\frac{F_1(S,B)E_w^*}{F_1(S^*,B^*)E_w}$, $u_4=\frac{E_wI_s^*}{E_w^*I_s}$, $u_5=\frac{T^*I_s}{TI_s^*}$, $u_6=\frac{TE_r^*}{T^*E_r}$, $u_7=\frac{E_rI_r^*}{E_r^*I_r}$, $u_8=\frac{B^*I_r}{BI_r^*}$.

$9-u_1-u_2-u_3-u_4-u_5-u_6-u_7-u_8-u_9=-g(u_1)-g(u_2)-g(u_3)-g(u_4)-g(u_5)-g(u_6)-g(u_7)-g(u_8)-g(u_9)$, where $u_1=\frac{S^*}{S}$, $u_2=\frac{I_a^*E_w}{I_aE_w^*}$, $u_3=\frac{V_1^*S}{V_1S^*}$, $u_4=\frac{V_1V_2^*}{V_1^*V_2}$, $u_5=\frac{F_3(V_2^*,B^*)V_2B}{F_3(V_2,B)V_2^*B^*}$, $u_6=\frac{F_3(V_2,B)E_w^*}{F_3(V_2^*,B^*)E_w}$, $u_7=\frac{I_s^*I_a}{I_sI_a^*}$, $u_8=\frac{B^*I_r}{BI_r^*}$, $u_9=\frac{I_r^*I_s}{I_rI_s^*}$ or $u_1=\frac{S^*}{S}$, $u_2=\frac{I_a^*E_w}{I_aE_w^*}$, $u_3=\frac{V_1^*S}{V_1S^*}$, $u_4=\frac{V_1V_2^*}{V_1^*V_2}$, $u_5=\frac{F_3(V_2^*,B^*)V_2B}{F_3(V_2,B)V_2^*B^*}$, $u_6=\frac{F_3(V_2,B)E_w^*}{F_3(V_2^*,B^*)E_w}$, $u_7=\frac{I_s^*I_a}{I_sI_a^*}$, $u_8=\frac{T^*I_s}{TI_s^*}$, $u_9=\frac{B^*T}{BT^*}$ or $u_1=\frac{S^*}{S}$, $u_2=\frac{V_1^*S}{V_1S^*}$, $u_3=\frac{F_2(V_1^*,B^*)V_1B}{F_2(V_1,B)V_1^*B^*}$, $u_4=\frac{F_2(V_1,B)E_w^*}{F_2(V_1^*,B^*)E_w}$, $u_5=\frac{E_wI_s^*}{E_w^*I_s}$, $u_6=\frac{T^*I_s}{TI_s^*}$, $u_7=\frac{TE_r^*}{T^*E_r}$, $u_8=\frac{E_rI_r^*}{E_r^*I_r}$, $u_9=\frac{B^*I_r}{BI_r^*}$ or $u_1=\frac{S^*}{S}$, $u_2=\frac{I_a^*E_w}{I_aE_w^*}$, $u_3=\frac{F_1(S^*,B^*)SB}{F_1(S,B)S^*B^*}$, $u_4=\frac{F_1(S,B)E_w^*}{F_1(S^*,B^*)E_w}$, $u_5=\frac{I_s^*I_a}{I_sI_a^*}$, $u_6=\frac{T^*I_s}{TI_s^*}$, $u_7=\frac{TE_r^*}{T^*E_r}$, $u_8=\frac{E_rI_r^*}{E_r^*I_r}$, $u_9=\frac{B^*I_r}{BI_r^*}$.

$10-u_1-u_2-u_3-u_4-u_5-u_6-u_7-u_8-u_9-u_{10}=-g(u_1)-g(u_2)-g(u_3)-g(u_4)-g(u_5)-g(u_6)-g(u_7)-g(u_8)-g(u_9)-g(u_{10})$, where $u_1=\frac{S^*}{S}$, $u_2=\frac{I_a^*E_w}{I_aE_w^*}$, $u_3=\frac{V_1^*S}{V_1S^*}$, $u_4=\frac{F_2(V_1^*,B^*)V_1B}{F_2(V_1,B)V_1^*B^*}$, $u_5=\frac{F_2(V_1,B)E_w^*}{F_2(V_1^*,B^*)E_w}$, $u_6=\frac{I_s^*I_a}{I_sI_a^*}$, $u_7=\frac{T^*I_s}{TI_s^*}$, $u_8=\frac{TE_r^*}{T^*E_r}$,

$u_9 = \frac{E_r I_r^*}{E_r^* I_r}, u_{10} = \frac{B^* I_r}{B I_r^*}$ or $u_1 = \frac{S^*}{S}, u_2 = \frac{V_1^* S}{V_1 S^*}, u_3 = \frac{V_1 V_2^*}{V_1^* V_2}, u_4 = \frac{F_3(V_2^*, B^*) V_2 B}{F_3(V_2, B) V_2^* B^*}, u_5 = \frac{F_3(V_2, B) E_w^*}{F_3(V_2^*, B^*) E_w}, u_6 = \frac{E_w I_s^*}{E_w^* I_s}, u_7 = \frac{T^* I_s}{T I_s^*}, u_8 = \frac{T E_r^*}{T^* E_r}, u_9 = \frac{E_r I_r^*}{E_r^* I_r}, u_{10} = \frac{B^* I_r}{B I_r^*}$.

$11 - u_1 - u_2 - u_3 - u_4 - u_5 - u_6 - u_7 - u_8 - u_9 - u_{10} = -g(u_1) - g(u_2) - g(u_3) - g(u_4) - g(u_5) - g(u_6) - g(u_7) - g(u_8) - g(u_9) - g(u_{10}) - g(u_{11})$, where $u_1 = \frac{S^*}{S}, u_2 = \frac{I_a^* E_w}{I_a E_w^*}, u_3 = \frac{V_1^* S}{V_1 S^*}, u_4 = \frac{V_1 V_2^*}{V_1^* V_2}, u_5 = \frac{F_3(V_2^*, B^*) V_2 B}{F_3(V_2, B) V_2^* B^*}, u_6 = \frac{F_3(V_2, B) E_w^*}{F_3(V_2^*, B^*) E_w}, u_7 = \frac{I_s^* I_a}{I_s I_a^*}, u_8 = \frac{T^* I_s}{T I_s^*}, u_9 = \frac{T E_r^*}{T^* E_r}, u_{10} = \frac{E_r I_r^*}{E_r^* I_r}, u_{11} = \frac{B^* I_r}{B I_r^*}$.

Using the fact that $-g(\cdot) \leq 0$, and (Shu et al., 2020, Theorem 5.6), we can obtain that

$$\int_\Omega F_1(S^*, B^*)\left(1 - \frac{F_1(S^*, B^*)S}{F_1(S, B)S^*}\right)\left(\frac{F_1(S, B)S^*}{F_1(S^*, B^*)S} - \frac{B}{B^*}\right) dx \leq 0,$$

$$\int_\Omega r_1 F_2(V_1^*, B^*)\left(1 - \frac{F_2(V_1^*, B^*)V_1}{F_2(V_1, B)V_1^*}\right)\left(\frac{F_2(V_1, B)V_1^*}{F_2(V_1^*, B^*)V_1} - \frac{B}{B^*}\right) dx \leq 0,$$

$$\int_\Omega r_2 F_3(V_2^*, B^*)\left(1 - \frac{F_3(V_2^*, B^*)V_2}{F_3(V_2, B)V_2^*}\right)\left(\frac{F_3(V_2, B)V_2^*}{F_3(V_2^*, B^*)V_2} - \frac{B}{B^*}\right) dx \leq 0.$$

Therefore, it follows that $\frac{dW}{dt} \leq 0$. We define K as the largest invariant subset of $\{(S, V_1, V_2, E_w, E_r, I_a, I_s, I_r, T, B) \in \Delta : W'(t) = 0\}$. Then, from LaSalle's invariance principle Henry (1981), we conclude that the ω-limit sets of the solution are contained in K. $W'(t) = 0$ implies that $S = S^*$, $V_1 = V_1^*$, $V_2 = V_2^*$, $E_w = E_w^*$, $E_r = E_r^*$, $I_a = I_a^*$, $I_s = I_s^*$, $I_r = I_r^*$, $T = T^*$, $B = B^*$. Therefore, by (Djilali et al., 2023, Theorem 6.1), E_1 is unique and globally attractive. This completes the proof. □

References

Brauer F, Shuai ZS, Van Den Driessche P (2013) Dynamics of an age-of-infection cholera model. Math Biosci Eng 10(5&6):1335–49

Cai LM, Fan GX, Yang CY, Wang J (2020) Modeling and analyzing cholera transmission dynamics with vaccination age. J Frankl Inst 357(12):8008–8034

Capasso V, Paveri-Fontana SL (1979) A mathematical model for the 1973 cholera epidemic in the European Mediterranean region. Rev Epidemiol Sante Publique 27(2):121–132

Capone F, De Cataldis V, De Luca R (2015) Influence of diffusion on the stability of equilibria in a reaction–diffusion system modeling cholera dynamic. J Math Biol 71:1107–1131

Carfora MF, Torcicollo I (2022) Identification of epidemiological models: the case study of Yemen cholera outbreak. Appl Anal 101(10):3744–3754

Chatterjee P, Kanungo S, Bhattacharya SK, Dutta S (2020) Mapping cholera outbreaks and antibiotic resistant Vibrio cholerae in India: An assessment of existing data and a scoping review of the literature. Vaccine 38:A93–A104

Chitnis N, Hyman JM, Cushing JM (2008) Determining important parameters in the spread of malaria through the sensitivity analysis of a mathematical model. Bull Math Biol 70:1272–1296

Codeço CT (2001) Endemic and epidemic dynamics of cholera: the role of the aquatic reservoir. BMC Infect Dis 1:1–14

Djilali S, Chen YM, Bentout S (2023) Asymptotic analysis of SIR epidemic model with nonlocal diffusion and generalized nonlinear incidence functional. Math Meth Appl Sci 46(5):6279–6301

Dubey B, Dubey P, Dubey US (2015) Dynamics of an SIR model with nonlinear incidence and treatment rate. Appl Appl Math 10(2):718–737

Faruque SM, Albert MJ, Mekalanos JJ (1998) Epidemiology, genetics, and ecology of toxigenic Vibrio cholerae. Microbiol Mol Biol Rev 62(4):1301–1314
Groeger J (2014) Divergence theorems and the supersphere. J Geom Phys 77:13–29
Guenther RB, Lee JW (1996) Partial differential equations of mathematical physics and integral equations. Courier Corporation
Hale JK (2010) Asymptotic behavior of dissipative systems. American Mathematical Soc
Harris JB, LaRocque RC, Charles RC, Mazumder RN, Khan AI, Bardhan PK (2010) Cholera's western front. Lancet 376(9757):1961–1965
Henry D (1981) Geometric theory of semilinear parabolic equations. Lecture notes in mathematics, vol 840. Springer, New York
Ilic I, Ilic M (2023) Global patterns of trends in cholera mortality. Trop Med Infect Dis 8(3):169
Joh RI, Wang H, Wesis H, Weitz JS (2009) Dynamics of indirectly transmitted infectious diseases with immunological thrshold. Bull Math Biol 71:845–862
Kong JD, Davis W, Li X, Wang H (2014) Stability and sensitivity analysis of the iSIR model for indirectly transmitted infectious diseases with immunological threshold. SIAM J Appl Math 74(5):1418–1441
Kunkle DE, Bina XR, Bina JE (2017) The Vibrio cholerae VexGH RND efflux system maintains cellular homeostasis by effluxing vibriobactin. MBio 8(3):e00126-17
Li XG, Cai LM, Murshed M, Wang J (2023) Dynamical analysis of an age-structured dengue model with asymptomatic infection. J Math Anal Appl 524(2):127127
Luo JH, Wang J, Wang H (2017) Seasonal forcing and exponential in cholera dynamics. Dis Con Dyn Syst Series B 22:2261–2290
Luo YT, Zhang L, Zheng TT, Teng ZD (2019) Analysis of a diffusive virus infection model with humoral immunity, cell-to-cell transmission and nonlinear incidence. Physica A 535:122415
Magal P, Zhao XQ (2005) Global attractors and steady states for uniformly persistent dynamical systems. SIAM J Math Anal 37(1):251–275
Mandal S, Mandal MD, Pal NK (2011) Cholera: a great global concern. Asian Pac J Trop Med 4(7):573–580
Martin RH, Smith HL (1990) Abstract functional-differential equations and reaction–diffusion systems. Trans Am Math Soc 321(1):1–44
Mukandavire Z, Liao S, Wang J, Gaff H, Smith DL, Morris JG Jr (2011) Estimating the reproductive numbers for the 2008–2009 cholera outbreaks in Zimbabwe. Proc Natl Acad Sci 108(21):8767–8772
Qadri F, Bhuiyan TR, Sack DA, Svennerholm AM (2013) Immune responses and protection in children in developing countries induced by oral vaccines. Vaccine 31(3):452–460
Ren XZ, Tian YN, Liu LL, Liu XN (2018) A reaction–diffusion within-host HIV model with cell-to-cell transmission. J Math Biol 76(7):1831–72
Safi MA, Melesse DY, Gumel AB (2013) Dynamics analysis of a multi-strain cholera model with an imperfect vaccine. Bull Math Biol 75:1104–1137
Sampath S, Khedr A, Qamar S, Tekin A, Singh R, Green R, Kashyap R (2021) Pandemics throughout the history. Cureus 13(9)
Shu HY, Ma ZW, Wang XS (2021) Threshold dynamics of a nonlocal and delayed cholera model in a spatially heterogeneous environment. J Math Biol 83(4):41
Shu HY, Ma ZW, Wang XS, Wang L (2020) Viral diffusion and cell-to-cell transmission: mathematical analysis and simulation study. J Math Pures Appl 137:290–313
Smith HL (2008) Monotone dynamical systems: an introduction to the theory of competitive and cooperative systems, 41st edn. American Mathematical Soc
Song CW, Xu R (2022) A note on the global stability of a multi-strain cholera model with an imperfect vaccine. Appl Math Lett 134:108326
Tuite AR, Tien J, Eisenberg M, Earn DJD, Ma JL, Fisman DN (2011) Cholera epidemic in Haiti, 2010: using a transmission model to explain spatial spread of disease and identify optimal control interventions. Ann Intern Med 154(9):593–601
Tuite AR, Tien J, Eisenberg M, Earn DJD, Ma JL, Fisman DN (2019) Genomic plasticity associated with antimicrobial resistance in Vibrio cholerae. Proc Natl Acad Sci 116(13):6226–6231
United Nations Children's Fund, Zimbabwe launches cholera vaccination to curb the spread, Available from:https://www.unicef.org/zimbabwe/press-releases/zimbabwe-launches-cholera-vaccination-curb-spread. (Accessed August 2024)
Upadhyay RK, Pal AK, Kumari S, Roy P (2019) Dynamics of an SEIR epidemic model with nonlinear incidence and treatment rates. Nonlinear Dyn 96(4):2351–2368

Wang JL, Wu XQ (2023) Dynamics and profiles of a diffusive cholera model with bacterial hyperinfectivity and distinct dispersal rates. J Differ Equ 35(2):1205–1241
Wang M (2010) Nonlinear Elliptic Equations. Science Press, Beijing
Wang JL, Wang J (2021) Analysis of a reaction–diffusion cholera model with distinct dispersal rates in the human population. J Dyn Differ Equ 33(1):549–575
Wang XY, Posny D, Wang J (2016) A reaction-convection-diffusion model for cholera spatial dynamics. Discrete Contin Dyn Syst Ser B 21:2785–2809
Wang XY, Wang FB (2019) Impact of bacterial hyperinfectivity on cholera epidemics in a spatially heterogeneous environment. J Math Anal Appl 480(2):123407
Wang W, Wang XT, Wang H (2024) Spatial dynamics of a generalized cholera model with nonlocal time delay in a heterogeneous environment. J Differ Equ 405:103–150
World Health Organization, Global Cholera and Acute Watery Diarrhoea (AWD) Dashboard, Available from: https://who-global-cholera-and-awd-dashboard-1-who.hub.arcgis.com/. (Accessed August 2024)
WorldPop, Available from: https://hub.worldpop.org/. (Accessed August 2024)
Wu JH (2012) Theory and applications of partial functional differential equations. Springer Science & Business Media, p 119
Wu P, Salmaniw Y, Wang X (2024) Threshold dynamics of a reaction–advection–diffusion schistosomiasis epidemic model with seasonality and spatial heterogeneity. J Math Biol 88(6):76
Zhao XQ (2017) Dynamical systems in population biology, 2nd edn. Springer, New York